UNIVERSITY OF HAWAII
LIBRARY

# *The*
# PHILOSOPHICAL MAGAZINE

FIRST PUBLISHED IN 1798

L. 43 SEVENTH SERIES No. 342 July, 1952

## *A Journal of Theoretical Experimental and Applied Physics*

EDITOR
PROFESSOR N. F. MOTT, M.A., D.Sc., F.R.S.

EDITORIAL BOARD
SIR LAWRENCE BRAGG, O.B.E., M.C., M.A., D.Sc., F.R.S.
SIR GEORGE THOMSON, M.A., D.Sc., F.R.S.
PROFESSOR A. M. TYNDALL, C.B.E., D.Sc., F.R.S.

PRICE 15s. 0d.
Annual Subscription £8 0s. 0d. payable in advance

AND PUBLISHED BY TAYLOR & FRANCIS LTD., RED LION COURT, FLEET ST., LONDON, E.C.4.

# ADVANCES IN PHYSICS

## A QUARTERLY SUPPLEMENT OF THE PHILOSOPHICAL MAGAZINE

**On 1st January, 1952, the first number of this new Quarterly Supplement to the Philosophical Magazine was published. The aim of this Supplement will be to give those interested in physics comprehensive and authoritative accounts of recent important developments. It is felt by the Editor that in view of the rapid advances in many branches of physics, scientists will welcome a journal devoted to articles of this type.**

**VOLUME 1** **JULY 1952** **NUMBER 3**

The whole part is devoted to one paper:

### THE MATHEMATICAL THEORY OF STATIONARY DISLOCATIONS

By
F. R. N. NABARRO
*Department of Metallurgy, The University of Birmingham*

**PRICE** *per part* **15/-** *plus postage* **PRICE** *per annum* **£2 15s. 0d.** *post free*

*Editor:* PROFESSOR N. F. MOTT, M.A., D.Sc., F.R.S.
*Editorial Board:* SIR GEORGE THOMSON, M.A., D.Sc., F.R.S.
PROFESSOR A. M. TYNDALL, C.B.E., D.Sc., F.R.S.
SIR LAWRENCE BRAGG, O.B.E., M.C., M.A., D.Sc., F.R.S.

*Printed and Published by*
TAYLOR & FRANCIS, LTD., RED LION COURT, FLEET ST., LONDON, E.C.4

# LXVIII. *Experiments on Separation of Boundary Layers on Probes in Front of Blunt-Nosed Bodies in a Supersonic Air Stream*

By W. A. Mair
Fluid Motion Laboratory, University of Manchester*

[Received March 12, 1952]

## Summary

If a blunt-nosed body of revolution is fitted with a slender probe at the nose and placed in a supersonic air stream, there is an interaction between the shock wave in front of the body and the boundary layer on the probe. Schlieren photographs of this type of flow were taken for bodies of revolution with hemispherical and flat noses and various lengths of probe, at a Mach number of 1·96. Measurements of pressure distribution were also made on the hemispherical-nosed body for one length of probe.

With a probe length of about $1\frac{1}{2}$ body diameters, the boundary layer separates near the nose of the probe and a nearly conical dead-air region is formed. With this type of flow, which occurs with both shapes of body, the drag is considerably less than it is without a probe. For greater probe lengths the boundary layer separates behind the nose of the probe, and the shape of the dead-air region and shock-wave pattern depend on whether the boundary layer is laminar or turbulent at the point of separation. For smaller probe lengths the conical flow is still found with the hemispherical-nosed body, but with the flat-nosed body there is a regular oscillation between widely different types of flow. In the present experiments the oscillation had a frequency of about 6 000 cycles per second, and the sequence of events during a cycle was traced by taking a number of flash photographs at random time intervals. A detailed discussion of the relations between different phases of the oscillation is given. This throws some light on the general problem of the interaction of shock waves and boundary layers.

Schlieren photographs were also taken of the corresponding two-dimensional flow, using a thin plate clamped between two thicker flat-nosed plates. The flows for various protruding lengths of the thin plate were in general similar to those found with the bodies of revolution, except that the unsteady flows found for a range of plate lengths did not have the regular oscillatory form that was found in the experiments with the flat-nosed body of revolution.

## § 1. Introduction

If a blunt body is mounted on a flat plate and fixed in a uniform air stream of *low velocity* with the flat plate parallel to the undisturbed stream, the boundary layer on the plate separates in front of the body and a weak standing eddy is formed in the corner. This is shown, for example, in a photograph by W. S. Farren, reproduced by Goldstein (1938). The separation of the boundary layer is caused by the rise of pressure as the air approaches the blunt body. When separation has occurred, the presence of the dead-air region increases the positive pressure gradient at a given point in the boundary layer before the separation, so causing the separation point to move further upstream. The final equilibrium position of the separation point depends on the shape of the blunt body and the state of the boundary layer on the plate.

---

* Communicated by the Author.

Lighthill (1951) has pointed out that when the undisturbed stream has a supersonic velocity, the processes causing the boundary layer on the plate to separate are essentially the same as at low speeds. The rise of pressure at the bow shock wave in front of the blunt body causes separation of the boundary layer on the plate. The resulting distortion of the streamlines outside the boundary layer then produces a positive pressure gradient on the plate, and the separation point moves upstream until an equilibrium is reached. In the fully developed flow the shock-wave pattern is altered considerably by the presence of the dead-air region downstream of the separation point.

A similar effect occurs in axially symmetrical flow when a slender probe is fixed in front of a blunt-nosed body of revolution. When the flow is supersonic, the dead-air region is in some cases approximately conical and there is then a conical shock wave in front of it.

The experiments described in the present paper were made primarily to investigate the axially symmetrical case in supersonic flow. Schlieren photographs were taken for various lengths of probe, using bodies with hemispherical and flat noses. Measurements of pressure distribution were also made on a hemispherical-nosed body with one length of probe. Some further photographs were taken to investigate the flow in the two-dimensional case, using a thin flat plate projecting from the front of a thicker plate with a flat nose.

## § 2. NOTATION

| | |
|---|---|
| $C_D$ | drag coefficient. |
| $d$ | diameter of body of revolution. |
| $D$ | drag force. |
| $H$ | stagnation pressure in undisturbed stream. |
| $K=l/d$ or $l/t$. | |
| $l$ | length of probe or protruding thin plate (see figs. 1 and 3). |
| $p$ | pressure at point on body. |
| $p_1$ | static pressure in undisturbed stream. |
| $s$ | distance along surface of body, measured downstream from centre of probe. |
| $t$ | thickness of blunt plate (see fig. 3). |
| $U$ | velocity of undisturbed stream. |
| $x$ | distance downstream from shoulder of hemispherical-nosed body (see fig. 2). |

| | |
|---|---|
| $\alpha$ | semi-apex angle of conical shock wave. |
| $\beta$ | semi-apex angle of conical dead-air region. |
| $\theta$ | angle defining position of point on hemispherical nose (see fig. 2). |
| $\rho$ | density of air in undisturbed stream. |

## § 3. EXPERIMENTAL DETAILS

The experiments were made in the intermittent supersonic wind tunnel described in a paper by Bardsley and Mair (1951). The working section was 12·7 cm high and 10·2 cm wide and the Mach number was 1·96. The stagnation pressure was approximately atmospheric and the Reynolds number in the working section was about $1{\cdot}3 \times 10^5$ per cm. A silica-gel drier was used at the intake to the tunnel, and the absolute humidity was always below 0·0005.

Fig. 1

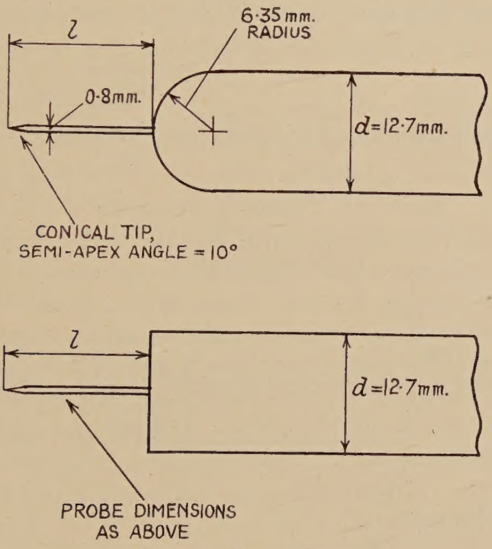

Bodies of revolution.

Schlieren photographs were taken, using the two bodies of revolution shown in fig. 1. The bodies were made of steel, turned to a smooth finish, with an axial hole at the front into which the probe could be pushed, the projecting length $l$ being easily adjustable. The bodies were mounted at zero incidence on the centre line of the wind tunnel.

Most of the photographs were taken with the conical-nosed probe shown in fig. 1, but for a few of the earlier photographs a blunt-nosed probe was used. All the results given in the paper (except fig. 13 (*b*) [figs. 13 *a–e*, Plate XL]) refer to the conical-nosed probe.

To investigate the flow when the boundary layer on the probe was turbulent, some experiments were also made using a long probe with a wire ring fixed to it at a point about 50 mm from the nose of the probe.

The pressure measurements were made with the body shown in fig. 2. The pressure holes were 0·4 mm in diameter and were placed approximately at $\theta=15$, 30, 40, 50, 60, 70, 80 and 90 degrees, and at $x/d=0{\cdot}125$, 0·25, 0·5 and 1·0. The conical-nosed probe was the same as that used for the photographs, and measurements were only made for one length of probe ($l/d=1{\cdot}44$). The body was made with all the pressure holes connected to the central hole, as shown in fig. 2. The pressure holes were then blocked with Durofix, and the pressures were measured by clearing one hole at a time with a small drill.

Fig. 2

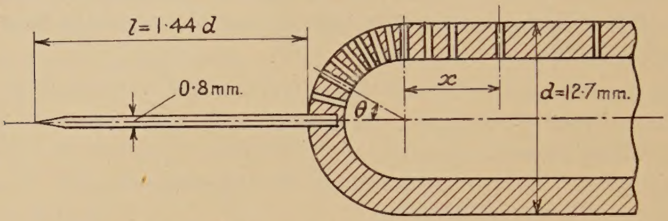

Hemispherical-nosed body with pressure holes.

Fig. 3

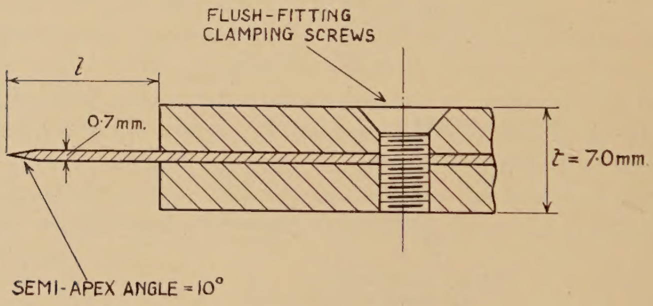

Two-dimensional plates.

The plates used for the two-dimensional experiments are shown in fig. 3. The thin plate was made of spring steel and was clamped between the two thicker steel plates. Schlieren photographs were taken for a range of protruding lengths of the thin plate, up to the maximum allowed by considerations of strength. The load on the thin plate may be very large during starting and stopping of the tunnel, because the flow is then not symmetrical, and it is possible for the pressure on one side of the thin plate to be momentarily equal to that behind a normal shock wave, while on the other side of the plate the pressure is much lower.

The schlieren apparatus was a conventional one, using two concave mirrors of 150 cm focal length and 12·7 cm diameter. The knife edges were always either vertical or horizontal (the stream being horizontal).

The arrangement used for each photograph can easily be seen by considering the appearance of the shock waves. The sensitivity of the system was adjusted to suit the conditions ; it was not the same in all cases. A Mullard LSD.2 flash-tube was used for photography, except in one case (fig. 11, Plate XL) where a long exposure was required. Measurements described by Chesterman (1951) show that for most purposes the flash given by this type of tube may be considered to have an effective duration of about 3 $\mu$sec ($3\times 10^{-6}$ sec) but there is an ‘ afterglow ’ period of about 20 to 30 $\mu$sec, during which the light intensity is comparatively small (less than 5% of the peak intensity). The afterglow does not have any significant effect on the photographs, except in cases where a strong, nearly stationary disturbance occurs in the flow at the appropriate time after the main flash. Some cases of this kind are discussed later.

The unsteady flows that occurred in some cases were investigated by taking six or more separate photographs, using the short-duration flash. When the unsteadiness was of high frequency it could only be detected by this method, because when observed on the screen the flow appeared to be quite steady.

A few shadowgraphs were also taken, using the ‘ focused shadowgraph ’ technique. This method has the advantage that the normal schlieren apparatus can be used with very little alteration, and with the arrangement used here it is not necessary to darken the room. The second knife-edge or slit is removed from the schlieren system, and the positions of the second mirror and object lens are adjusted until a source of light placed at a point $P$, say, between the wind tunnel and the second mirror, produces a sharply focused image on the screen. The focused shadowgraph produced on the screen when the tunnel is running is then exactly the same as the ordinary shadowgraph that would be produced by placing a screen at the point $P$. The distance from the centre of the working section to the point $P$ can be altered by using the focusing adjustment on the camera. This distance was about 20 cm in these experiments.

## § 4. Bodies of Revolution

In the discussion of the results, the exposed length of the probe will be denoted by $l$, the diameter of the body of revolution by $d$, and the ratio $l/d$ by $K$ (see fig. 1). In all the photographs the flow is from left to right.

Figures 4 ($a$) and ($b$) (Plate XXXVI) show the flow past the two shapes of body without a probe. As found by Holder and Chinneck (1952), there is a separation of the boundary layer on the flat-nosed body, with an oblique shock wave starting at the point of re-attachment, but on the hemispherical-nosed body no such separation can be seen. Where the bow shock wave meets the sides of the tunnel there is a curved line in the photograph, near the right-hand side. The line appears *double*, either because of interaction between the bow wave and the boundary layers on the sides of the tunnel, or because the bodies were not exactly in the centre of the tunnel. These curved lines also appear in many of the other photographs, with the probe in position.

With the probe in position, the type of flow depends on the value of $K$, as shown in table 1.

Table 1. Bodies of Revolution. Approximate Values of $K$ for Different Types of Flow

| | *Hemispherical Nose* | *Flat Nose* |
|---|---|---|
| Probe entirely behind bow shock wave on body | $<0{\cdot}18$ | $<0{\cdot}44$ |
| Modified bow wave (see fig. 14, Plate XXXVI) | 0·18 to 0·3 | 0·44 to 0·6 |
| Oscillating flow (see figs. 12 and 13, Plates XXXIX and XL) | Not observed | 0·7 to 1·3 |
| Separation at point of probe, with conical dead-air region | 0·3 to 1·3 | 1·3 to 1·5 |
| Separation at shoulder of probe, with conical dead-air region | 1·3 to 1·65 | 1·5 to 2·1 |
| Separation downstream of shoulder of probe | $>1{\cdot}65$ | $>2{\cdot}1$ |

### (a) *Flow with Separation Downstream of Shoulder of Probe*

For large values of $K$ the flow was unsteady, with irregular oscillations which contained components of low frequency (of the order 10 cycles per second), so that the unsteadiness could be observed on a screen. Figures 5 (*a*) to (*d*) [figs. 5 *a–f*, Plate XXXVII] show photographs for $K \approx 6$. The two photographs given for each shape of body are typical of the extremes that were found in a large number of photographs; the extent of the dead-air region varied between these extremes.

It is believed that the unsteadiness of the flow shown in figs. 5 (*a*) to (*d*) is caused by movement of the transition point in the boundary layer on the probe. The movements of the transition point are probably caused by intermittent turbulence in the air stream, arising from large scale disturbances at the entry to the wind tunnel. It is reasonable to suppose that the ‘ bursts ’ of turbulence might be separated by large enough time intervals to explain the observed low frequency of the oscillations.

It is known from other experiments on shock-wave boundary-layer interaction, e.g. those of Liepmann and others (1951), that the extent of the ‘ upstream influence ’ of the shock wave is considerably greater in a laminar boundary layer than in a turbulent one. This suggests that in figs. 5 (*a*) and (*c*) the boundary layer on the probe is probably laminar at the position of separation, while in figs. 5 (*b*) and (*d*) it is probably turbulent. Further evidence for this is provided by figs. 5 (*e*) and (*f*), which show the flow for the same value of $K$ with a thin wire ring fixed to the probe at a point about 50 mm from its nose. Since the Reynolds number, based on the distance from the nose of the probe to the wire, was about $0{\cdot}65 \times 10^6$, it is almost certain that the boundary layer was turbulent on the downstream side of the wire. With the wire in place the flow was nearly steady, and it can be seen that figs. 5 (*e*) and (*f*) show a close resemblance to figs. 5 (*b*) and (*d*). This shows that the boundary layer is turbulent at the position of separation in figs. 5 (*b*) and (*d*). Moreover in fig. 5 (*d*) the boundary layer can be seen as a dark line on the lower side of the probe. The thickness of this line is a further indication that the boundary layer became turbulent before separation in that case.

The photographs given in fig. 5 show that in all cases a shock wave starts at a point near the shoulder of the body, indicating that the streamlines passing along the edge of the dead-air region are deflected outwards near the shoulder. The effect appears to be more pronounced with the hemispherical nose than with the flat one, especially when the boundary layer on the probe is laminar.

When the probe length was reduced the flow remained similar to that discussed above, provided that separation still occurred downstream of the shoulder on the conical-nosed probe (see table 1). Figure 6 (*a*) [figs. 6 *a–e*, Plate XXXVIII] ($K=2{\cdot}4$) and fig. 6 (*b*) ($K=3{\cdot}2$) show typical photographs for the two shapes of body. In both these cases the boundary layer on the probe was probably laminar at the point of separation ; the flow was still unsteady and in other photographs with about the same probe length the separation occurred nearer the body and the boundary layer was turbulent at the point of separation.

Figure 6 (*c*) is a shadowgraph showing the flow past the flat-nosed body with $K=3{\cdot}2$. In this photograph a sharply defined light line can be seen at the edge of the dead-air region, extending for about 10 probe diameters downstream of the separation point. (This may not be visible in the reproduction.) The presence of the line indicates that the boundary layer remained laminar for this distance after separation ; further downstream the edge of the dead-air region is less well defined and the flow was probably turbulent. Similar effects could be seen in some of the other shadowgraphs (not reproduced here), for both shapes of body, including some for values of $K$ up to about 5.

The ‘ gap ’ in the shock wave from the shoulder of the body, shown in the upper half of fig. 6 (*c*), indicates a transient state in the unsteady flow. The existence of this ‘ gap ’ shows that, although observation on a screen indicated an apparent frequency of oscillation of the order of 10 cycles per second, components of much higher frequency must also have been present in the oscillation.

In figs. 5 (*a*) and (*c*) and 6 (*a*), (*b*) and (*c*), where the boundary layer on the probe is laminar, the conical shock wave starting near the separation point has a semi-apex angle of about 25°. This is considerably less than the Mach angle ($30{\cdot}7°$), showing that the separation point must have been moving rapidly upstream when these photographs were taken. The velocity of upstream movement, calculated from the shock-wave angle, is about 40% of the velocity of sound. The upstream movement of the separation point probably also explains the concave shape of the meridian section of the dead-air region. The section of the dead-air region would be slightly concave, however, even for steady flow with constant pressure in the dead-air region. This is because immediately after the separation point, where the diameter of the dead-air region is not much greater than that of the probe, the flow is of two-dimensional type, and the angle of deflection for a given rise of pressure is less than it is further downstream, where the diameter of the dead-air region is greater and the flow is of axially symmetrical type.

In figs. 5 (*b*) and (*d*), where the boundary layer on the probe is turbulent, the shock-wave angles agree fairly well with the values calculated from the slope of the dead-air region, indicating that the separation point is nearly stationary.

Figures 6 (*d*) and (*e*) show two cases in which the separation point is probably moving downstream. The values of $K$ are the same as for figs. 6 (*a*) and (*b*) (2·4 and 3·2), but now in each case the dead-air region has a *convex* meridian section and the shock wave from the separation point is inclined to the stream at an angle greater than that calculated from the slope of the dead-air region. An attempt was made to investigate the statistical distribution of the various types of flow as shown in the photographs. This was not very successful, because it was difficult to distinguish between nearly steady flow with a turbulent boundary layer, as in fig. 5 (*d*), and flow with the separation point moving downstream, as in fig. 6 (*e*). It was possible to show, however, that upstream movement of the separation point occurred more frequently than downstream movement. This shows that the separation point moves more slowly upstream than downstream.

### (b) *Conical Flow with Separation at Shoulder or Point of Probe*

For the flat-nosed body of revolution the unsteady flow discussed above, with separation of the boundary layer occurring downstream of the shoulder on the conical-nosed probe, was recorded for values of $K$ down to 2·3. For $K=1·9$ or less the separation occurred at the shoulder of the probe, the dead-air region was nearly conical, and the flow was much steadier. Thus for this shape of body the change from one type of flow to the other occurs when $K$ is about 2·1.

For the hemispherical-nosed body the change occurs when $K$ is about 1·65. For this value of $K$ two photographs were obtained in consecutive runs of the tunnel; in one the separation occurred at the shoulder of the probe, while in the other it occurred downstream of the shoulder. The difference between the critical values of $K$ for the two shapes of body illustrates the greater ‘ upstream influence ’ of the flat-nosed body.

Figures 7 (*a*) ($K=1·44$) and 7 (*b*) ($K=1·91$) (Plate XXXVI) are typical photographs of the flow with the boundary layer separating at the shoulder of the conical-nosed probe. When the separation occurred at this point the flow was nearly steady, as shown by the close similarity between photographs taken with the same body and probe length at different times. The dead-air region is very nearly conical, because the separation point is stationary and because (for the range of $K$ giving this type of flow) the apex angle of the dead-air region does not differ greatly from that of the conical nose of the probe. Thus a truly conical flow can exist, satisfying the conditions for constant pressure in the dead-air region.

As the probe length is progressively reduced, the separation point remains at the shoulder of the probe for the values of $K$ shown in table 1. This behaviour is what would be expected from consideration of the pressure distribution on the conical-nosed probe. When separation does not occur until after the shoulder, there is a region of constant pressure on the conical surface: this is followed by a rapid fall of pressure at the shoulder and then a *rise* of pressure after the shoulder. It is this rise of pressure that causes the separation point to remain fixed at the shoulder for a range of values of $K$. The separation point moves rapidly forward to the tip of the probe, as soon as $K$ has decreased so far that the separation can no longer remain at the shoulder.

With the hemispherical-nosed body, separation occurs at the point of the probe for values of $K$ between about 0·3 and 1·3 (table 1). The flow is then steady, with a conical dead-air region, and is similar to that found when the separation occurs at the shoulder. Figure 8 (Plate XXXVIII) shows a typical example for a fairly short probe ($K=0{\cdot}71$).

With the flat-nosed body, steady flow with separation at the point of the probe only occurs for a small range of $K$ (table 1). When $K$ is greater than about 1·5 the separation occurs at the shoulder or further back, while when $K$ is less than about 1·3 regular oscillations occur between widely different types of flow. This oscillating flow is discussed later.

Figure 9 shows the relation between the semi-apex angles $\alpha$ and $\beta$ of the conical shock wave and the dead-air region. The points are derived from all the photographs showing nearly steady conical flow, with separation at the shoulder or point of the probe. The curve in fig. 9 is a theoretical one, plotted from Kopal's tables (1947). Most of the points lie fairly near the theoretical curve, but they show a definite tendency for the shock-wave angle to be smaller than the theoretical value, for a given angle of the conical dead-air region. The explanation of this is probably that the apparent edge of the dead-air region, as shown in the photographs, is inclined to the axis at a greater angle than the displacement-thickness contour of the separated boundary layer.

### (c) *Pressure Distribution and Drag*

Measurements of pressure distribution were made on the hemispherical-nosed body for $K=1{\cdot}44$. This case was selected as a typical example of the nearly steady conical flow; a photograph for the same value of $K$ is shown in fig. 7 ($a$). The arrangement of the pressure holes and the definition of the angle $\theta$ are shown in fig. 2.

Fig. 9

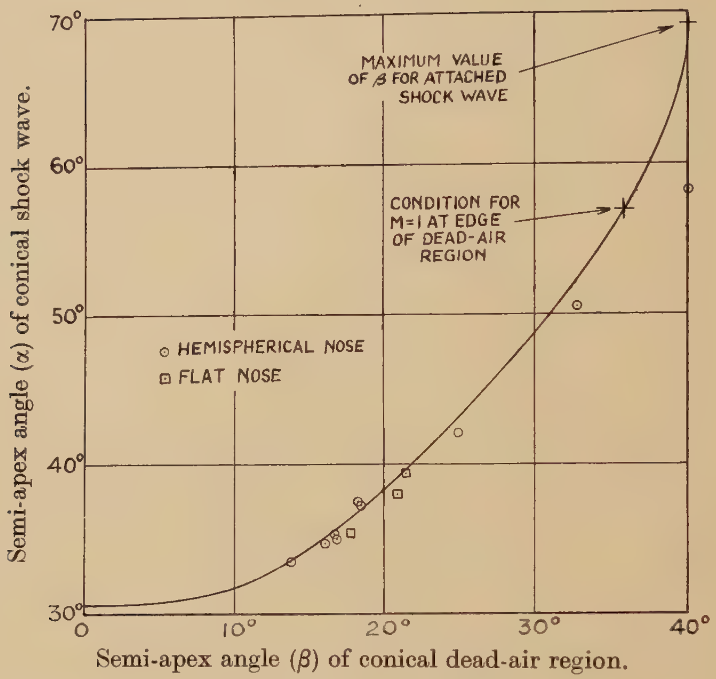

Conical shock-wave angles.

Fig. 10

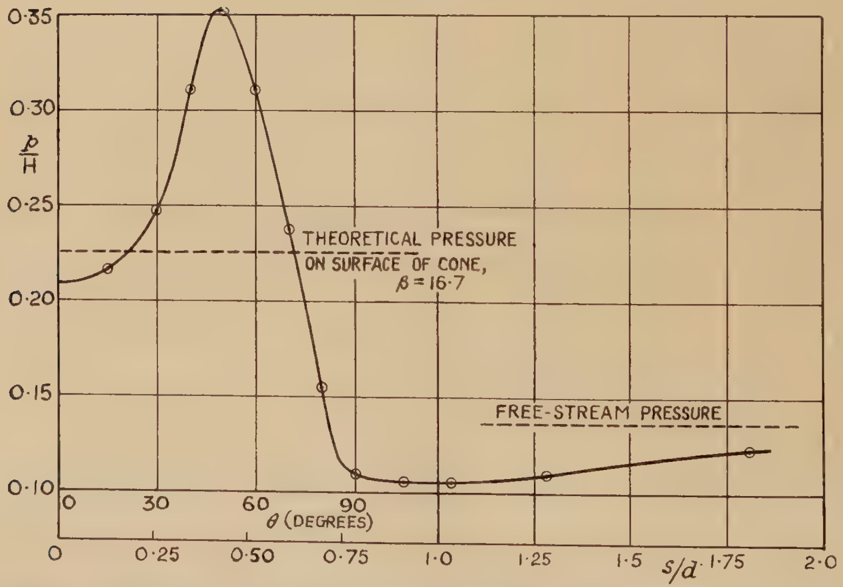

Pressure distribution on hemispherical-nosed body with probe ($K=1{\cdot}44$).

Figure 10 shows the pressure distribution on the body, expressed as the ratio of the measured static pressure $p$ to the stagnation pressure $H$ in the undisturbed stream. $s$ is the distance along the surface of the body, measured downstream from the centre of the probe. The semi-apex angle $\beta$ of the conical dead-air region was found from the photograph (fig. 7 ($a$)) to be 16·7°, and the theoretical pressure on the surface of a cone of this angle is shown in fig. 10. For small values of $\theta$ the measured pressures fall slightly below the theoretical value, but when $\theta$ exceeds about 30° the effect of the compression near the shoulder of the body becomes important, and the pressure rises rapidly. The maximum pressure ($p/H=0{\cdot}35$) occurs at $\theta\approx 50°$, and is followed by a rapid fall of pressure to a minimum just behind the shoulder. In the neighbourhood of the shoulder the maximum inclination of the shock wave to a streamline appears from the photograph to be about 40° (it is not possible to measure this angle accurately). This value is only a few degrees greater than the Mach angle on the surface of a cone with $\beta=16{\cdot}7°$, and the calculated value of $p/H$ on the downstream side of the shock wave is only about 0·25. This shows that a considerable rise of pressure must occur between the shock wave and the surface of the body. This rise of pressure, occurring immediately after the shock wave, may perhaps explain why the shock wave *appears* to be so strong in the photograph.

From the pressure distribution shown in fig. 10, the drag coefficient of the body was calculated, neglecting skin friction and assuming that the pressure on the downstream end of the body was equal to the static pressure of the undisturbed stream.

The value found was

$$C_D=\frac{D}{(\frac{1}{2}\rho U^2)(\pi d^2/4)}=0{\cdot}36,$$

where $D$ is the drag force calculated on the above assumptions.

The drag of the hemispherical-nosed body without the probe was not measured, but an approximate value was found by extrapolating to higher Mach numbers the values found for Mach numbers up to 1·8 by Holder and Chinneck (1952). The drag coefficient obtained in this way was 0·76. Thus the addition of the probe *halves* the drag of the hemispherical nose.

The drag coefficient was also calculated for a cylindrical body of revolution with a conical nose of semi-apex angle 16·7° (the value found for the dead-air region in fig. 7 ($a$)). The value of $C_D$ for this body was 0·25, i.e. only about two thirds of the value for the hemispherical-nosed body with probe. Figure 10 shows the reason for this difference of drag; on the body with probe the pressure for $\theta\approx 50°$ is considerably greater than the pressure on the corresponding conical-nosed body.

### (d) *Oscillating Flow*

As already mentioned, an oscillating flow occurred with the flat-nosed body for values of $K$ less than about 1·3. The oscillation was of such a high frequency (about 6000 cycles per second) that it could not be recorded satisfactorily with any ciné camera that was available. The flow was therefore investigated for several values of $K$, by taking a number of photographs in successive runs of the tunnel, using the short-duration flash-tube for each photograph. This was equivalent to taking photographs at random time intervals in a single run of the tunnel. It was found possible to arrange most of the photographs in the order in which they would have been taken if they had all referred to one cycle of the oscillation. Moreover, it was possible to estimate the order of magnitude of the time intervals between the phases represented by the various photographs. The photographs reproduced here have been selected to show the various stages of the oscillation as clearly as possible. They include some shadowgraphs, as well as schlieren photographs with horizontal and vertical knife edges. It was not possible to restrict the selection of photographs to any one arrangement of the knife edges.

Figure 11 shows the flow *as it appeared on the screen* for $K=1{\cdot}24$. This photograph was taken with an exposure of 3 seconds, using a mercury-vapour lamp and 'Process' film, with a yellow filter to reduce the effective speed of the film. The shock-wave pattern as observed on the screen (and as shown in fig. 11) appeared to be steady, but this was only because the oscillations were too rapid to be detected by the eye. The photographs taken with the short-duration flash show that the pattern seen in fig. 11 is formed from the extreme positions of different parts of the shock-wave system, but these extreme positions are reached at different times, so that the complete pattern as shown in fig. 11 does not exist at any one instant.

Figures 12 [figs. 12 *a–f*, Plate XXXIX] and 13 show a number of photographs of the oscillating flow, taken with the short-duration flash. Near the right-hand side of many of the photographs there is a curved line (sometimes double) where the bow shock wave meets the sides of the tunnel. This has already been discussed in connection with fig. 4. Most of the photographs also show a curved oblique shock wave, moving downstream from the shoulder of the body. This is caused by separation of the boundary layer at the shoulder, and is discussed later in more detail.

Figures 12 (*a*) to (*f*) show a series of photographs for $K=1{\cdot}00$. These are arranged so that the phases they represent are in chronological order ; the method used for finding the correct order is explained below.

In figs. 12 (*a*), (*c*), (*d*) and (*f*), a weak normal shock wave can be seen at a distance varying from about 1 to 3 body diameters behind the nose of the body. This shock wave can also be seen in figs. 13 (*a*), (*b*) and (*d*), (for different values of $K$) but it is not easily seen in the shadowgraph (fig. 12 (*b*)), or in the schlieren photographs taken with horizontal knife edges (figs. 12 (*e*) and 13 (*c*)). In fig. 12 (*d*) there is another normal shock wave just behind the nose of the body, in addition to the one about 3 diameters behind the nose.

The appearance of these normal shock waves in the photographs, as compared with the other shock waves, shows that they are weak, and they must therefore be moving downstream. It is shown later that a new normal shock wave starts moving downstream from the nose of the body once in each cycle of the oscillation (see fig. 12 (*d*)).

Since the normal shock waves are known to be moving downstream, consideration of the positions of the shock waves enables the photographs to be arranged so that the phases they represent are in chronological order. Moreover, by making a rough estimate of the velocity of the waves it is possible to estimate the frequency of the oscillation and the time intervals between the phases shown in different photographs.

In several of the photographs the normal shock waves corresponding to two successive cycles could be seen. The distance between successive waves, as found from the photographs, varied between 3·3 and 4·3 cm, the average value being about 3·8 cm. (The variation in this distance between different photographs, with different positions of the waves, is not surprising, because the strengths of the waves may vary as they move downstream.) Since the waves appear on the schlieren photographs as weak ones, it is reasonable to assume that the relative Mach number upstream of the wave is only a little greater than unity, say about 1·05. (This value makes the strength of the wave about five times that of the weakest shock wave that can be detected with the schlieren apparatus, with the sensitivity used in these experiments.) The time interval between successive waves is then found to be about 170 $\mu$sec, giving a frequency of oscillation of about 6 000 cycles per sec.

Using similar reasoning it is possible to estimate roughly the time interval between the phases represented in any two photographs. With the assumptions given above it is found that the waves move through a distance equal to the diameter of the body in a time of about 55 $\mu$sec. The time intervals given in the discussion below were all calculated in this way.

In fig. 12 (*a*), there are two bow waves in front of the blunt body ; the upstream wave is moving downstream and will soon merge into the downstream bow wave. This is shown by considering figs. 12 (*e*) and (*f*), representing phases immediately before fig. 12 (*a*). The downstream bow wave is nearly stationary, and fairly strong. In steady flow, this downstream wave would cause separation of the boundary layer on the probe, upstream of the bow wave. In the original photograph a weak conical shock wave from such a separation can just be seen, starting about half-way between the point of the probe and the upstream bow wave, but this may not be visible in the reproduction. The faint light line at the point of the probe, nearly normal to the stream, is caused by ‘ afterglow ’ from the flash tube (see below) and should be ignored.

At the instant when fig. 12 (*a*) was taken, the separation point was probably moving rapidly upstream, and after a time interval of about 50 $\mu$sec the flow would be like that shown in fig. 12 (*b*). In this photograph separation occurs at the nose of the probe and there is a fairly large dead-air region. At the nose of the probe there is a *strong*, nearly normal shock wave which extends only to a distance of about two probe diameters from the point. The fainter line in fig. 12 (*b*), appearing as a weak extension of the nearly normal shock wave from the point of the probe, is caused by the ' afterglow ' from the flash tube and shows the position of the shock wave at a later time (see fig. 12 (*c*), showing the flow about 30 or 40 $\mu$sec later than fig. 12 (*b*)). The faint, nearly normal shock wave at the point of the probe in fig. 12 (*a*), and the ' upstream branch ' of the bow wave on the probe in figs. 12 (*c*) and (*d*) and 13 (*a*), (*b*) and (*c*), can all be explained in the same way. In all these cases the velocity of any portion of the wave normal to itself is small, so that although the bow shock wave on the probe is spreading outwards, the afterglow can produce a visible effect on the photograph.

The strong shock wave at the point of the probe in fig. 12 (*b*) corresponds to the stronger of the two alternative conical shock waves that can theoretically be formed on a cone in supersonic flow. (At this Mach number the calculated semi-apex angle of the stronger conical shock wave is between 85° and 90° for all cones having semi-apex angles up to 20°.) It is to be expected that the stronger of the two alternative waves might be formed in a case such as this, where the downstream geometry requires a large rise of pressure over an extended region.

Disregarding the upstream branch of the bow shock wave, caused by afterglow from the flash tube, fig. 12 (*b*) shows that the strong shock wave extends only a short distance from the point of the probe, and at greater distances there is a weak shock wave, inclined to the stream at an angle only slightly greater than the Mach angle. This weak shock wave continues back to its intersection with the bow shock wave of the body.

Figure 13 (*a*) is a schlieren photograph for $K=1{\cdot}24$, showing the same phase of the oscillation as fig. 12 (*b*). Both these photographs show a well developed dead-air region in which the velocity must be small and the pressure nearly constant. There cannot be any shock wave in front of the body in such a dead-air region. In fig. 13 (*a*), the light region in front of the body must be caused by the part of the shock wave just outside the dead-air region, and does not represent a shock wave in front of the body. Since the flow is axially symmetrical, light rays passing in front of the body must also pass through this part of the shock wave, and this explains the effect shown in the photograph. Figure 12 (*b*) shows more clearly that the bow wave of the body does not pass through the dead-air region.

In fig. 12 (*b*) the bow wave of the body appears to split into several branches at a distance of about two body diameters from the axis. This region coincides with the outer limit of the downstream bow wave shown in fig. 12 (*a*), which by the time of fig. 12 (*b*) is at a greater distance from the body because the shock wave is growing. The apparent ' splitting ' of the shock wave is probably caused in some way by interaction with the upstream wave of fig. 12 (*a*), which by this time has moved further downstream. The ' splitting ' is also shown in many of the other photographs.

The weak normal shock wave moving downstream appears in fig. 12 (*a*) about one diameter behind the nose of the body. This shock wave is not visible in the shadowgraph (fig. 12 (*b*)), but it can be seen in fig. 13 (*a*) about one diameter further downstream than in fig. 12 (*a*), and also in many of the other photographs. The normal shock wave always occurs a short distance downstream of the region in which the bow wave on the body appears to 'split'. This would be expected from consideration of fig. 12 (*a*), where the normal shock wave is just behind the extremity of the downstream bow wave.

In fig. 12 (*b*) the boundary layer *on the blunt body* separates at the shoulder, as in fig. 4 (*b*), and an oblique shock wave is formed at the point of re-attachment. The schlieren photograph (fig. 13 (*a*)) shows the oblique shock wave more clearly, but it does not show the separated boundary layer because the knife edges of the schlieren system were vertical. The oblique shock wave can also be seen in fig. 12 (*a*), but there it is of limited extent because the boundary-layer separation has only just started. In fig. 12 (*f*) there is no indication of separation.

Between figs. 12 (*b*) and (*c*) there is a time interval of about 30 or 40 $\mu$sec, during which the dead-air region expands and the strong part of the bow shock wave on the probe spreads outwards. (As already explained, the 'upstream branch' of the bow wave is caused by afterglow from the flash tube and should be ignored.) The outer part of the bow wave on the probe is comparatively weak, and near its intersection with the main shock wave from the blunt body it is inclined to the axis at an angle slightly less than the Mach angle. This is only possible because this part of the bow wave is moving outwards.

The development of the bow wave on the probe may be understood by considering a succession of spherical shock waves, spreading outwards from a source that is moving to the left relative to the undisturbed air. The strong part of the bow wave is formed by superposition of these spherical waves, while the outer weak part is the remainder of the first one.

With the expansion of the dead-air region in front of the blunt body, the separation at the shoulder disappears and the oblique 're-attachment shock wave' moves away downstream. Successive positions of this shock wave can be seen in figs. 12 (*b*), (*c*), (*d*) and (*e*).

In fig. 12 (*c*) the normal shock wave that appears to extend right across the front of the body must in fact be annular in shape, since there cannot be any shock wave in the dead-air region in front of the body. The white band shown in front of the body must be produced in the same way as in fig. 13 (*a*), but the effect is more pronounced in fig. 12 (*c*) because the part of the shock wave just outside the dead-air region is normal to the stream, and therefore has a greater effect on the light rays.

Figure 12 (*c*) also shows the weak normal shock wave moving downstream, about $2\frac{1}{2}$ diameters behind the nose of the blunt body.

The most striking feature of fig. 12 (*d*) is the dark expansion region immediately behind the bow shock wave on the probe. This was the only photograph showing the expansion region, out of a total of about 25 dealing with this type of oscillating flow. This shows that the expansion region probably only persisted for a very short time. The expansion probably occurs when the dead-air region downstream of the boundary-layer separation starts to contract. It is reasonable to suppose that the dead-air region cannot continue for more than a very short time to contract rapidly enough to produce the expansion. The time interval between figs. 12 (*c*) and (*d*) is about 15 or 20 $\mu$sec.

The annular normal shock wave which in fig. 12 (*c*) is just in front of the shoulder of the body, moves downstream, and in fig. 12 (*d*) it is just behind the shoulder. This shows the origin of the weak normal shock waves moving downstream that have already been discussed. Further downstream in fig. 12 (*d*) the weak normal shock wave from the previous cycle can be seen.

The downstream movement of the annular normal shock wave, shown in figs. 12 (*c*) and (*d*), probably explains why the dead-air region starts to contract at about this time. When the normal shock wave lies in front of the shoulder of the body, with its inner boundary at the edge of the dead-air region, it helps to maintain the boundary-layer separation on the probe. As the shock wave moves downstream, so that its inner boundary is on the body and not on the dead-air region, it has much less effect on the boundary layer ; the separation point tends to move downstream and the dead-air region contracts.

In fig. 12 (*d*) the outer part of the bow wave on the probe is still moving outwards. This is indicated by the position of the ‘ upstream branch ’, caused by afterglow from the flash tube, and by the inclination of the outer part of the bow wave to the axis at an angle less than the Mach angle. Near the tip of the probe the bow wave is not symmetrical; this is probably because the lower part of the wave (in the photograph) begins to move downstream slightly earlier than the upper part.

Figures 12 (*e*) and (*f*) show two further phases of the oscillation, about 40 and 60 $\mu$sec later than fig. 12 (*d*). Comparison of these photographs with fig. 12 (*d*) shows that the dead-air region is contracting and the bow shock wave is moving downstream along the probe. At the same time the outer part of the bow shock wave, just upstream of the intersection with the normal shock wave, is still moving outwards. (The normal shock wave is not visible in fig. 12 (*e*) because the knife edges were horizontal in that case, but its position is shown by the sudden change of slope of the bow shock wave.)

In figs. 12 (*e*), (*f*) and (*a*) a new, nearly normal shock wave is developing in front of the nose of the blunt body. The earlier wave moving downstream subsequently coalesces with this new wave, to form a single wave as shown in figs. 12 (*b*) and (*c*).

In the absence of any large dead-air region in front of the body, the boundary layer separates at the shoulder, as in fig. 4 (*b*). The separation has just started in fig. 12 (*a*), where the oblique shock wave formed at the point of re-attachment can be seen.

The above description shows the changes that occur during one cycle of the oscillation. There cannot be much doubt about the main features of this interpretation, provided the photographs of fig. 12 have been placed in the correct chronological order. The evidence for the order given is quite definite. The normal shock waves downstream of the shoulder of the body are weak ; hence they must be moving downstream. This information is sufficient to determine the correct chronological order of the photographs.

The causes of the oscillation are not fully understood, but a partial explanation can be given as follows.

In fig. 12 (*a*), there are two bow waves in front of the blunt body. The upstream one is moving downstream and is relatively weak ; it will soon join the downstream bow wave. The latter is moving only slowly and is strong ; hence it influences the boundary layer further upstream on the probe and causes separation. The separation is just starting in fig. 12 (*a*) and is well developed in fig. 12 (*b*), about 50 $\mu$sec later. As the separation develops, a roughly conical dead-air region appears, and a *strong*, nearly normal shock wave is formed at the tip of the probe fig. 12 (*b*). (A geometrical arrangement such that the conical dead-air region must produce this stronger shock wave is probably essential to the appearance of the oscillation. This may explain why the oscillation does not occur with the hemispherical nose.) During the next 50 $\mu$sec the bow wave on the probe spreads outwards as shown in figs. 12 (*c*) and (*d*), and its intersection with the bow wave of the body moves gradually downstream. Hence the normal annular shock wave, occurring at this intersection, moves downstream. When this normal shock wave has moved past the shoulder of the blunt body (fig. 12 (*d*)), it has much less effect on the boundary-layer separation on the probe, and the dead-air region starts to contract rapidly. This causes the expansion shown in fig. 12 (*d*), and the downstream movement of the central part of the bow wave on the probe, shown in figs. 12 (*e*) and (*f*). When this bow wave starts to move downstream, it becomes fairly weak. A new, strong shock wave then develops in front of the blunt body, just as it would in supersonic flow started from rest. This new shock wave then causes separation of the boundary layer further upstream and starts a new cycle (fig. 12 (*a*)).

In the photograph taken with a long exposure (fig. 11) the curved dark line passing through the front of the probe shows the extreme positions of the different parts of the bow wave on the probe. The different parts of this bow wave do not reach their extreme positions at the same time, however, because the front part of the wave is moving towards the nose of the body while the rear parts are moving away (figs. 12 (*d*) and (*e*)). Thus the dark line in fig. 11 does not represent the position of the bow wave at any one instant.

The prominent dark line in fig. 11, passing just in front of the nose of the body, shows the bow wave of the body as in fig. 12 (*b*). The part of this line immediately in front of the body is probably formed mainly from the strong shock wave shown in fig. 12 (*f*).

The photographs taken for other values of $K$ showed that the oscillating flow was essentially the same for $K=0{\cdot}78$, $1{\cdot}00$ and $1{\cdot}24$. Figure 13 shows some photographs for various values of $K$, included to illustrate some features of the flow that do not appear very clearly in fig. 12. In figs. 13 (*a*), (*c*) and (*d*), $K=1{\cdot}24$, while in fig. 13 (*e*), $K=0{\cdot}78$. Figure 13 (*b*) shows the flow with a blunt-nosed probe for $K=1{\cdot}00$. With the possible exception of fig. 13 (*e*), it is believed that the differences between the flows shown in these photographs and in fig. 12 are due mainly to differences of phase, and not to variations in the length or shape of the probe.

Figure 13 (*a*) has already been discussed; it shows a flow that is very nearly the same as that in fig. 12 (*b*). Figure 13 (*b*) represents a stage between figs. 12 (*b*) and (*c*). The latter two photographs appear at first sight to be quite different, but a careful comparison between figs. 12 (*b*), 12 (*c*) and 13 (*b*) shows that the differences between these three photographs are not large.

Figure 13 (*c*) shows a phase between figs. 12 (*d*) and (*e*). The dead-air region is still fairly large in fig. 13 (*c*), but since the bow shock wave on the probe has started to move downstream, the dead-air region must have started to contract.

Figure 13 (*d*) shows nearly the same flow as fig. 12 (*e*). It has been included to show the weak normal shock wave downstream of the shoulder of the body. This does not show in fig. 12 (*e*) because the knife edges of the schlieren system were horizontal in that case.

Figure 13 (*e*) shows the flow for $K=0{\cdot}78$, at a phase in the oscillation that is probably about the same as that shown in fig. 12 (*e*). This photograph has been included because it shows an interesting vortex sheet from the intersection of shock waves in front of the body. The conical shock wave having its apex at the point of the probe has a semi-apex angle of about 35°. The semi-apex angle of the conical body producing a shock wave of this angle is about 16°, indicating that boundary-layer separation still occurs near the point of the probe. The curling up of the vortex sheet from the shock intersection is similar to that found by White (1951) in experiments on a shock wave passing a wedge. The faint line in fig. 13 (*e*), apparently showing a nearly normal shock wave at the point of the probe, is probably caused by afterglow from the flash-tube, i.e. the nearly normal shock wave occurs about 20 $\mu$sec later than the other features shown in the photograph.

The oscillating flow discussed above was found for values of $K$ down to about $0{\cdot}7$, but when $K$ was $0{\cdot}6$ or less the flow was quite different and appeared to be steady. Figures 14 (*a*) and (*b*) (Plate XXXVI) show the flow for $K=0{\cdot}60$ and $0{\cdot}51$ respectively. In both these photographs the greater part of the bow wave is the same as that found for the body without any probe, but there is a local deformation of the bow wave near the point of the probe. In fig. 14 (*a*) an expansion and a second shock wave can be seen downstream of the main bow wave. This pattern appears to be similar to the successive compressions and expansions that are observed in some conditions on an aerofoil at high subsonic speeds. In fig. 14 (*b*) no expansion or shock wave can be seen behind the main bow wave.

For $K<0{\cdot}44$ the point of the probe was behind the bow shock wave of the body, and the flow appeared to be the same as for the body without the probe.

The oscillating flow was not found with the hemispherical-nosed body, for any value of $K$. With this body the steady conical flow as shown in fig. 8 persisted for values of $K$ down to about 0·3. For $K=0{\cdot}26$ the probe caused only a small local deformation of the main bow shock wave, the flow being similar to that shown in fig. 14 (*b*) (for the flat-nosed body with $K=0{\cdot}51$). For the hemispherical-nosed body with $K<0{\cdot}18$ the probe was entirely behind the main bow shock wave and produced no visible effect.

The above discussion of the oscillating flow shows that the maintenance of the oscillation depends to a large extent on the collapse of the dead-air region as the annular normal shock wave moves downstream past the shoulder of the body. This suggests that the range of $K$ for which the oscillating flow occurs may depend largely on the position of the shoulder in relation to the point where the probe enters the body. Thus a slight rounding of the shoulder on the flat-nosed body would probably have little or no effect on the flow. For bodies with ellipsoidal noses, blunter than a hemisphere, the oscillating flow would probably occur for a range of $K$ more restricted than that found with the flat-nosed body.

## § 5. Two-Dimensional Plates

Figure 3 shows the arrangement of the plates used for the two-dimensional experiments and the notation used in discussing the results. The plates were mounted at zero incidence and extended across the whole width of the tunnel, except for a clearance of about 1 mm at each side. Schlieren photographs were taken with horizontal and vertical knife-edges for values of $K(=l/t)$ up to 3·5. No experiments could be made at larger values of $K$, because the thin plate was not strong enough. As with the bodies of revolution, cases of unsteady flow were investigated by taking a number of flash photographs at random time intervals.

Figure 15 [figs. 15 *a–f*, Plate XLI] shows photographs of the flow for various values of $K$. In fig. 15 (*a*) the thin plate has been removed and the gap between the two thicker plates filled with brass packing pieces. The spaces between these packing pieces show in the photograph as white bands along the centre line, but they do not affect the flow. The bow shock wave, boundary-layer separation, and shock wave at the point of re-attachment are similar to those found in other experiments, e.g. those of Holder and Chinneck (1952). The curved line on the photograph, apparently indicating a second bow shock wave behind the main one, is caused by the interaction of the bow shock wave with the boundary layers on the glass sides of the tunnel. As would be expected, the effect appears more prominently in the photographs with vertical knife edges.

Figure 15 (*b*) shows the flow for $K=0{\cdot}55$. The bow shock wave is the same as for $K=0$ (fig. 15 (*a*)), and the flow over the thin plate is subsonic. On each side of the thin plate the separated boundary layer can be seen, with a standing eddy in the ‘ dead-air ’ region. The separated boundary layer is no longer visible on the downstream side of the eddy, probably because it has then become turbulent. This type of flow was found in all cases where the leading edge of the thin plate was downstream of the bow shock wave of the thick plate.

For $K=2{\cdot}5$, 3·0 and 3·5 the flow was similar to that shown in fig. 15 (*c*) (for $K=2{\cdot}5$). The boundary layer on the thin plate separates at the shoulder, near the leading edge of the thin plate, and a wedge-shaped dead-air region is formed. In all cases the measured shock wave angles agreed fairly well with the values calculated from the measured angles of the wedge-shaped dead-air regions. As in the case of the bodies of revolution, there was a tendency for the measured shock wave angles to be slightly smaller than the calculated values. The explanation of this is probably the same as that already given for the bodies of revolution, i.e. that the edge of the dead-air region, as shown in the photograph, is inclined to the plate at a greater angle than the displacement thickness contour of the separated boundary layer.

In fig. 15 (*c*) the shock wave shown on the upstream side of the expansion region at the shoulder of the thick plate is a weak one. By measuring the angles, the strength ($\Delta p/p$) of this shock wave was calculated for several cases and found to be of the order of 0·1. This means that there is only a small outward deflection of the streamlines at the shoulder of the thick plate. For the corresponding case with the flat-nosed body of revolution the strength of this shock wave could not be found, because the unsteadiness of the flow made the shock wave appear as a wavy line (see fig. 7 (*b*)). The strength of the shock wave at the shoulder of the hemispherical-nosed body of revolution has already been discussed. In that case a considerable rise of pressure took place downstream of the shock wave, but a pressure rise of this kind would not be expected with the flat-nosed plate or body of revolution.

The photograph shown in fig. 15 (*c*) was taken with vertical knife edges in the schlieren system. The sign of the density gradient at the boundary of the dead-air region is such that this boundary would be expected to show as a light line in the photograph. The dark line seen in the upstream half of the boundary is caused by ‘ overloading ’ of the schlieren system, as explained in an earlier paper by the author (1952). This thin dark line therefore shows the position of the maximum density gradient, and its disappearance about half-way along the boundary of the dead-air region indicates a sudden reduction of the maximum density gradient, probably because the separated boundary layer becomes turbulent at that point. This would also explain the weak shock wave starting at the same point ; transition to turbulence is accompanied by a thickening of the separated boundary layer, and there is a slight outward deflection of the stream lines.

For $K=1{\cdot}5$ and $2{\cdot}0$ the flow was found to be unsteady. Figure 15 (*d*) shows a typical photograph for $K=1{\cdot}5$ and figs. 15 (*e*) and (*f*) show two for $K=2{\cdot}0$. The flows are very complicated, and the series of photographs did not show any regular cycle of oscillations. Since the bow shock wave is attached to the thin plate in all cases, the flows above and below the plate are independent of one another. Hence the asymmetry shown in the photographs is not surprising. In considering the interpretation of the photographs, the interaction between the bow shock wave and the boundary layer on the glass sides of the tunnel should be remembered. This causes an apparent second bow wave, as mentioned above.

In fig. 15 (*e*) a wedge-shaped dead-air region can be seen fairly clearly, and there is also some indication of this in fig. 15 (*f*). The photographs suggest that there may be a fluctuation between the two alternative shock waves, one strong and the other weak, that can produce the stream deflection required by the dead-air region. The flow is probably not strictly two-dimensional, i.e. the phase of the oscillation shown in any one photograph may not be the same at all points along the span of the plate.

For values of $K$ greater than $3{\cdot}5$ no experiments were made, but the flow under these conditions has been investigated by Moeckel (1951) and by Beastall and Eggink (unpublished work at the Royal Aircraft Establishment). When $K$ is so large that the boundary-layer separation no longer occurs near the leading edge of the thin plate, the flow depends partly on whether the boundary layer is turbulent or laminar at the point of separation. Beastall and Eggink found that when the boundary layer was turbulent, the edge of the dead-air region was nearly straight and an oblique shock wave was formed at the point of separation. When the boundary layer was laminar, the separation occurred at a greater distance in front of the blunt body, the streamlines just after the separation point were concave to the flow, and there was a region of gradual compression. Some experiments by Johannesen (1952) on flow in a concave corner showed, however, that the boundary of the dead-air region is nearly straight, even when the boundary layer is laminar, and there is a single oblique shock wave from the separation point. It is possible that in the experiments made by Beastall and Eggink the position of the separation point varied across the span of the plate, so that the photographs showed an apparent gradual compression when in fact the flow was similar to that found by Johannesen.

## § 6. LIMITING CONDITIONS FOR THE FORMATION OF ATTACHED SHOCK WAVES

It is of interest to consider the limiting conditions for the formation of attached shock waves at the front of the probe or thin plate, in flows like those shown in figs. 8 and 15 (*c*).

Considering first the axially symmetrical case, the maximum semi-apex angle of a cone having an attached shock wave at this Mach number is 40° (see fig. 9). Assuming that the boundary of the dead-air region may be represented by a tangent to the body, passing through the point of the probe, the corresponding limiting values of $K$ are 0·28 for the hemispherical nose and 0·60 for the flat nose. For the hemispherical-nosed body the experimental results are therefore as would be expected ; the conical type of flow (with an attached shock wave) was found for values of $K$ down to 0·30, but not for $K=0{\cdot}26$ or less.

For the flat-nosed body of revolution the minimum length ($K=0{\cdot}60$) for the formation of an attached conical shock wave coincides roughly with the *lower* limit of $K$ for the occurrence of the oscillating flow. This means that the oscillating flow only occurs for values of $K$ for which a conical flow with an attached shock wave (either weak or strong) is possible.

In the two-dimensional case, the maximum semi-apex angle of a wedge having an attached shock wave is 22·3° at this Mach number. With an assumption similar to that used for the axially symmetrical case, the corresponding limiting value of $K$ is found to be 1·22. This happens to be the same as the value of $K$ for which the leading edge of the thin plate would just touch the bow wave of the thick plate. Unsteady flows were found for values of $K$ *greater* than this, up to about 2 or more. Thus the conclusion is similar to that found in the axially symmetrical case, i.e. the unsteady flow only occurs for values of $K$ for which a wedge type of flow, with an attached shock wave, is possible.

## REFERENCES

BARDSLEY, O., and MAIR, W. A., 1951, *Phil. Mag.*, **42,** 29–36.

CHESTERMAN, W. D., 1951, *The Photographic Study of Rapid Events* (Oxford University Press).

GOLDSTEIN, S., 1938, (Editor), *Modern Developments in Fluid Dynamics* (Oxford University Press), Plate 19*b*.

HOLDER, D. W., and CHINNECK, A., 1952, *Aero. Quart.* (in press).

JOHANNESEN, N. H., 1952, *Phil. Mag.*, **43,** 568.

KOPAL, Z., 1947, *Tables of Supersonic Flow around Cones* (Massachusetts Institute of Technology).

LIEPMANN, H. W., ROSHKO, A., and DHAWAN, S., 1951, *N.A.C.A. Tech.*, Note 2334.

LIGHTHILL, M. J., 1951, *A.R.C.*, 14,497.

MAIR, W. A., 1952, *Aero. Quart.* (in press).

MOECKEL, W. E., 1951, *N.A.C.A. Tech.*, Note 2418.

WHITE, D. R., 1951, *Princeton University Department of Physics Technical Report*, II--10.

# LXIX. *A Heavy Particle Selector*

By T. Duerden and B. D. Hyams
The Physical Laboratories, University of Manchester *

[Received May 22, 1952]

## Abstract

A system of Geiger counters and a Čerenkov light detector is described which responds selectively to the passage of slow cosmic ray particles heavier than about 550 electron masses.

It has been shown to count at a rate consistent with the known flux of sea level protons, and cloud chamber photographs show that at least 80% of the counts are caused by protons of range less than 170 g cm$^{-2}$ lead.

## §1. Introduction

In the course of measuring the intensity of the Čerenkov light (Čerenkov 1937, Mather 1951) emitted by single mesons (Jelley 1951) it was noted that this could be much more readily detected by bringing the photomultiplier into optical contact with the liquid. It was then found that by using multiple reflection of the light (as opposed to using the directional properties of the radiation), and the adoption of diffuse reflecting surfaces, a very high efficiency could be obtained for the detection of single relativistic particles. Because of the small self absorption of Čerenkov light by pure liquids it proved practicable to detect relativistic particles incident on a 400 cm$^2$ surface over a cone of half angle of 45°. This Čerenkov detector has been used to select cosmic ray particles with a mass greater than that of the $\mu$ meson. A similar principle has been used by Winckler (1952).

## §2. Theory of the Method

If a particle has a velocity $\beta c$ and a mass $M$ then its residual range will be given by

$$R_c=\frac{Mc^2}{A}(1-(1-\beta^2)^{1/2})^2\,(1-\beta^2)^{-1/2}\text{ g cm}^{-2},$$

where $A=1{\cdot}2$ when $Mc^2$ is expressed in MeV, and using the approximate range-energy relationship given by Janossy (1948, p. 127) :

$$R=\frac{W_K{}^2}{A(W_K+Mc^2)}\text{ g cm}^{-2}\,.$$

Then if $\beta c$ is less than or equal to the Čerenkov critical velocity for water $(\beta_c c)$ where $1/\beta_c$ is the refractive index of water it follows that

$$Mc^2\geqslant 6{\cdot}85\,R_c\text{ MeV}.$$

---

* Communicated by Professor P. M. S. Blackett, F.R.S.

Thus if a charged particle is observed to give no Čerenkov signal in water, and to have a range greater than 15 g/cm$^2$ it must have a rest energy greater than 100 MeV, and therefore be heavier than a $\mu$ meson (fig. 1).

In practice however it must be noted that a particle heavier than an electron travelling with $\beta \leqslant \beta_c$ does give some Čerenkov radiation, caused by high velocity knock-on electrons produced in the medium.

Fig. 1

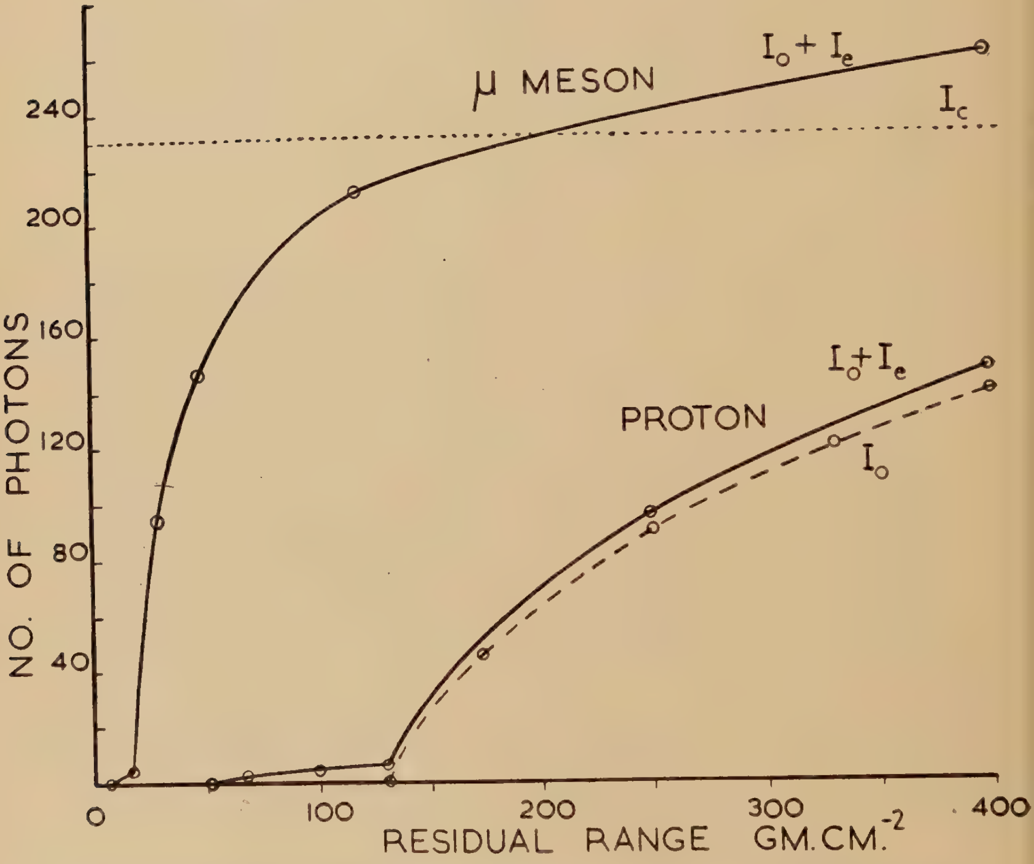

Theoretical Čerenkov photon intensity ($4000 < \lambda < 7500$ A.U.) per centimeter track length for heavy particles as a function of their residual ranges in water. Dashed line ($I_0$) shows signal from heavy particle only, full lines ($I_0 + I_e$) show total signal including contribution from knock-on electrons. Dotted line ($I_c$) shows maximum attainable signal (for a particle with velocity $c$) not including the knock-on electron contribution.

The intensity of this radiation $I_e$ has been calculated with approximations introducing errors less than 10%, and a graph of $I_e + I_0$ (fig. 1) shows the actual variation of total Čerenkov radiation per centimeter, in water, for protons and mesons as a function of their residual range, $I_0$ being the radiation from the heavy particle itself.

It is to be noted that for particles of very high energy the total Čerenkov signal will be subject to large statistical fluctuations of the same order as the fluctuations in ionization loss predicted by Landau (1944), on account of the radiation from high energy knock-on electrons.

## §3. Experimental Technique

A cubical metal box with sides 24 cm had its interior covered with waterproof $MgCO_3$ powder surfaces, and was filled with distilled water. An EMI type VX5045 photomultiplier was inserted 2 cm into the box and was held by a watertight rubber gland (fig. 2).

Fig. 2

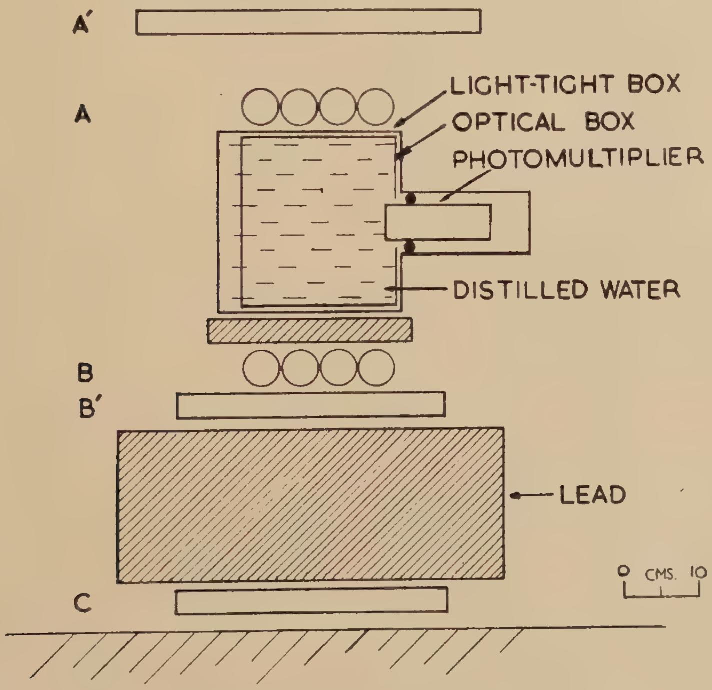

Selector above lead absorber.

Above the box there were two trays of Geiger counters A¹ and A and below it two trays B and B¹. Between the Čerenkov box and trays B, B¹ a layer of 3 cm of lead was interposed, to prevent the decay electrons from $\mu$ mesons stopping in the water from reaching the lower counters. Since the total absorbing material in the selector is 40 g $cm^{-2}$ (water equivalent) the condition $Mc^2 \geqslant 6{\cdot}8\ R_c$ places a lower limit of 540 electron masses on the mass of particles recorded.

Heavy particles were selected by registering only four fold coincidences $A^1+A+B+B^1$ with no anti-coincidence pulse from the photomultiplier, such events will be referred to as 'heavy particle' counts. The coincidence resolving time was 6 microseconds.

The particle trajectories were determined only by the trays **A** and **B** which ensured that the particles traversed the box, the other two trays were required to reduce the rate of spurious coincidences not due to a single particle traversing the system.

Fig. 3

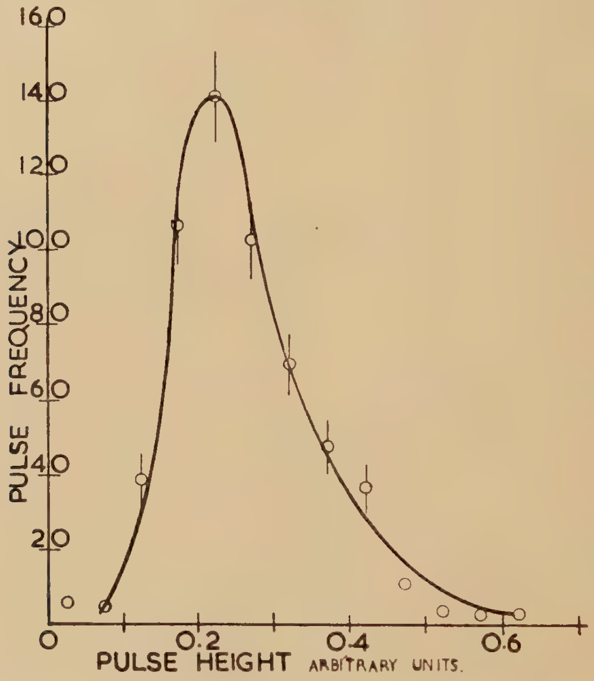

Experimental Čerenkov pulse height distribution from single mesons.

The pulse height distribution (fig. 3) of Čerenkov signals from single cosmic ray particles traversing the system was measured by recording the pulse associated with each Geiger coincidence $A^1+A+B+B^1$. This result showed that the mean signal consisted of a pulse of about 30 electrons, in agreement with an optical measurement which showed that about 15% of the light generated was collected at the photomultiplier.

The bias setting for the anti-coincidence pulse for eliminating relativistic particles was determined by finding the bias level that halved the four fold counting rate, and then setting to one tenth of this value. By fitting a Poisson distribution to the distribution of fig. 3 it was calculated that less than one relativistic particle in twenty thousand could escape detection.

From fig. 1 it is seen that the mean Čerenkov signal from protons with $R<150\ \mathrm{g/cm^2}$ was much less than one tenth the mean signal of a relativistic particle, so that less than 1% of all protons with $\beta<\beta_c$ incident on the apparatus are expected to give anti-coincidence signals.

The stability of the photomultiplier Čerenkov sensitivity was monitored daily by bringing up a 1 millicurie radium source to a fixed point 30 cm distance from the box, when a galvanometer, permanently in the collector electrode circuit, gave a signal of about 0·2 $\mu$amps (some 80 times the dark current). By control experiments the signal was shown to be due to Čerenkov light from Compton recoil electrons and was in agreement with an approximate calculation of the expected signal.

## §4. Results

All the experiments described here were carried out under a roof of about $100\ \mathrm{g\ cm^{-2}}$ concrete.

In a preliminary experiment the heavy particle selector was placed above a layer of lead 20 cm thick with a further tray of Geiger counters C beneath it (fig. 2). It was found that the ratio of the 'heavy particle' counting rate to the simple four fold counting rate, $A^1+A+B+B^1$ (mesons), was $(2{\cdot}15\pm0{\cdot}15)/1\,000$ and it remained constant throughout all subsequent experiments. It was then observed that the ratio of rates, 'heavy particle'$+$C, to simple five fold $A^1+A+B+B^1+C$, fell to $(0{\cdot}32\pm0{\cdot}1)/1\,000$. Had all the 'heavy particle' counts been due to unaccompanied slow protons the ratio should have fallen to zero, since protons with less than the Čerenkov critical velocity are unable to penetrate the selector material and a further 20 cm of lead, or to give rise to secondary charged particles capable of doing so.

In order to test directly whether the 'Selector' was in fact recording protons it was placed above, and used to control, a cloud chamber containing six 2 cm thick lead plates of area $25\times30\ \mathrm{cm^2}$. We are indebted to Mr. Wolfendale and Mr. Leontic for allowing us to use their cloud chamber for this purpose.

A series of pictures was taken with a well collimated beam of particles, by raising tray $A^1$ and reducing the area of trays A and B. Alternate pictures were taken with the control pulse a 'heavy particle', and a simple four fold coincidence (meson). In all, 134 'heavy particle' initiated pictures were taken. Analysis of these showed that 50% of the 'heavy particle' pictures showed particles stopping in the chamber. The actual percentage of 'heavy particle' counts caused by slow particles was certainly higher than this, since corrections have to be made for the number of particles stopping before entering the chamber, and those leaving obliquely before stopping. These corrections were made by assuming the geometry of meson and proton tracks in the alternate pictures to be identical, and it could be shown that at least 80% of the counts were caused by protons.

Plates XLII and XLIII show protons stopping in the third and fifth lead plates of the cloud chamber.

## §5. Discussion of Results

The width of the experimental pulse height distribution of Čerenkov signals from fast particles (fig. 3) is mainly governed by the Poisson-like fluctuations in the number of electrons emitted from the photomultiplier photocathode. The long ‘ tail ’ is much greater than would be caused by ‘ Landau ’ fluctuations.

The proton flux observed may be compared with the sea level flux observed by Mylroi and Wilson (1951), who found an intensity of $3{\cdot}3\times10^{-5}$ protons $\mathrm{cm}^{-2}\,\mathrm{sec}^{-1}\,\mathrm{sterad}^{-1}$ in the momentum range ($700<p<1\,100$ MeV/c) observed here. When we allow for the absorption of the 100 g/cm$^2$ roof above our apparatus, and the further absorption in the selector itself, assuming simple exponential absorption with attenuation range 145 g cm$^{-2}$, we would expect to find an intensity of $1{\cdot}40\times10^{-5}$ protons $\mathrm{cm}^{-2}\,\mathrm{sec}^{-1}\,\mathrm{sterad}^{-1}$. We actually find, using Rossi’s (1948) value for the meson flux at our depth, and our proton to meson ratio, a flux of $(1{\cdot}50\pm0{\cdot}1)\times10^{-5}$ protons $\mathrm{cm}^{-2}\,\mathrm{sec}^{-1}\,\mathrm{sterad}^{-1}$.

We believe that the greater part of the 20% of the pictures which could not be unambiguously attributed to protons stopping in the chamber to be caused by slow protons suffering nuclear scattering, and thus not entering the chamber along the same trajectories as unscattered mesons. The rates of air showers, casual coincidences, and events caused by a single meson traversing two trays, and a knock-on electron traversing the other two without any particle entering the Čerenkov box, have all been considered. They were too low to account for more than 10% of the ‘ heavy particle ’ counts.

It could be seen from the absence of tracks at minimum ionization on the ‘ heavy particle ’ pictures that less than 5% of the ‘ heavy particle ’ counts could have been caused by inefficiency in the Čerenkov detection of relativistic particles.

## §6. Conclusions

The selector has been shown to count cosmic ray protons in the momentum band $700<p<1\,100$ MeV/c at a rate far exceeding any previously reported method. Its counting rate below a 100 g cm$^{-2}$ roof at sea level is 3·5 protons per hour.

The selector has the advantage of identifying protons entering at only 1·3 times minimum ionization, but has the disadvantage of failing to record heavy particles at all if they are accompanied by particles with a velocity greater than $\beta_c c$.

Even with an incident flux of two slow heavy particles per thousand fast particles, less than 5% of the counts are due to anticoincidence inefficiency, and in all not more than 20% can be due to spurious effects.

## ACKNOWLEDGMENTS

The authors wish to thank Professor P. M. S. Blackett and Dr. J. G. Wilson for their support and encouragement throughout the work.

They wish to thank Mr. Wolfendale and Mr. Leontic for interrupting their research programme to operate their cloud chamber for this experiment.

One of us, (T.D.) is indebted to the Department of Scientific and Industrial Research for a maintenance grant.

## REFERENCES

ČERENKOV, P. A., 1937, *Phys. Rev.*, **52,** 378.
JANOSSY, L., 1948, *Cosmic Rays* (Oxford : Clarendon Press).
JELLEY, J. V., 1951, *Proc. Phys. Soc.* A, **64,** 82.
LANDAU, L., 1944, *J. of Physics, U.S.S.R.*, **8,** 201.
MATHER, R. L., 1951, *Phys. Rev.*, **84,** 181.
MYLROI, M. G., WILSON, J. G., 1951, *Proc. Phys. Soc.* A, **64,** 404.
ROSSI, B., 1948, *Rev. Mod. Phys.*, **20,** 537.
WINCKLER, J. R., 1952, *Phys. Rev.*, **85,** 1054.

# LXX. *On a Case of Instability Produced by Rotation*

By J. L. Synge, F.R.S.
Dublin Institute for Advanced Studies*

[Received April 29, 1952]

We are so accustomed to the idea of gyroscopic stability that any dynamical system for which spin produces instability appears at first sight anomalous. Such systems are of course known, but for the most part on paper only, and so a toy which has recently appeared on the market is of interest as a practical example.

The toy is a spinning top of light construction, its outward form consisting of a spherical surface S and a projecting cylindrical leg L, the central line of L lying on a diameter of S. When set on a table, it takes up a position of stable equilibrium, with S in contact with the table and L pointing vertically upward. When it is given a sufficiently rapid spin about L, it turns over and stands on L, and continues in this position until friction has sufficiently reduced the spin; then it falls over and ultimately goes back to the position of stable equilibrium with L upward. The degree of roughness of the table does not seem to affect this performance markedly.

According to the theory given below, it appears that we may expect behaviour of this sort if the following conditions are satisfied:

(1) the exterior form of the body is a surface of revolution;

(2) the mass-centre lies on the axis of figure, outside the segment of that axis joining the centres of curvature at its two ends, but close to one of them;

(3) at the mass-centre the axis of figure is a principal axis of inertia, but the momental ellipsoid is not a surface of revolution about the axis of figure;

(4) the differences between the principal moments of inertia at the mass-centre are small, and these differences are such that they, with the small distance of the mass-centre from the adjacent centre of curvature, satisfy certain inequalities $F>0$, $G<0$, the meaning of which will be explained later.

Figure 1 shows a diametral section of the exterior surface of the body; $P_1$ and $P_2$ are the ends of the axis of figure; $\Gamma_1$ and $\Gamma_2$ are the corresponding centres of curvature of the surface; $O$ is the mass-centre; $Oxyz$ are the principal axes at $O$, with $Oz$ lying along the axis of figure. We shall denote the mass of the body by $m$ and the principal moments of inertia at $O$ by $mA$, $mB$, $mC$. The actual distribution of matter inside the surface is of no importance at all, since the dynamical behaviour is determined by the position of the mass-centre and the three quantities $A$, $B$, $C$.

---

* Communicated by the Author.

When the body is set on a horizontal table, there are two possible positions of equilibrium, a stable position with $P_1$ as point of contact and an unstable position with $P_2$ as point of contact. We are interested in the question of stability when the body spins about its axis of figure, that axis being vertical, and there are two cases:

(i) when $P_1$ is the point of contact;

(ii) when $P_2$ is the point of contact.

Fig. 1

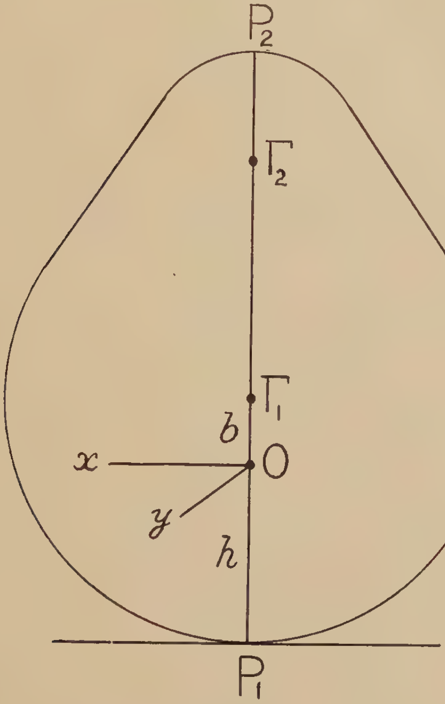

Case (ii) presents an ordinary problem, and we know that the motion will be stable if the spin is great enough. (This corresponds to the case when the top spins on the leg L.) Case (i) is the interesting case, and we shall confine our attention to it; fig. 1 shows the undisturbed position.

We shall write

$h$=height of the mass-centre $O$ above the point of contact $P_1$.

$b$=height of the centre of curvature $\Gamma_1$ above $O$.

Note that $b$ is positive. The table will be assumed rough enough to prevent slipping.

We do not have to work out the dynamics because this has already been done by E. J. Routh (*Advanced Rigid Dynamics*, London: Macmillan, 1905, p. 202) and the condition of stability has been given by him. To translate his formula into our notation we put $c=a=b+h$. Then the condition of stability is that all four roots of $\phi(\lambda)=0$ shall be real, where

$$\begin{aligned}\phi(\lambda)=&[(A+h^2)\lambda^2+\{B-C-hb\}n^2-gb]\\ &\times[(B+h^2)\lambda^2+\{A-C-hb\}n^2-gb]\\ &-\lambda^2n^2[A+B-C+h^2-hb]^2. \qquad (1)\end{aligned}$$

Here $n$ is the angular velocity of spin.

The problem of stability is thus reduced to a purely algebraic problem. To simplify the algebra, we define

$$A'=A+h^2,\ B'=B+h^2,\ F=B-C-hb,\ G=A-C-hb. \qquad (2)$$

Then

$$A+B-C+h^2-hb=A'+F=B'+G, \qquad (3)$$

and so we have

$$\begin{aligned}\phi(\lambda)&=[A'\lambda^2+Fn^2-gb][B'\lambda^2+Gn^2-gb]\\ &\quad-\lambda^2n^2(A'+F)(B'+G)\\ &=A'B'\lambda^4-\lambda^2[(A'B'+FG)n^2+(A'+B')gb]\\ &\quad+(Fn^2-gb)(Gn^2-gb). \qquad (4)\end{aligned}$$

Now if $P$ is positive, the conditions that the roots of

$$Px^2-Qx+R=0$$

shall be real and positive are

$$Q>0, \quad R>0, \quad Q^2-4PR\geqslant 0, \qquad (5)$$

and so the conditions of stability (viz., that $\lambda^2$ shall be positive) are as in (5) with

$$\begin{aligned}&P=A'B',\\ &Q=(A'B'+FG)n^2+(A'+B')gb,\\ &R=(Fn^2-gb)(Gn^2-gb). \qquad (6)\end{aligned}$$

Here $P$, $Q$, $R$ are continuous functions of the six quantities $A$, $B$, $C$, $b$, $h$, $n$, and we shall use this fact to explore stability when the first five of these quantities have values close to the values which they have in the degenerate case when the mass-centre is at the centre of curvature and $A=B=C$. In this degenerate case we have

$$B'=A', \quad F=0, \quad G=0, \quad b=0,$$

and so

$$P=A'^2,\ Q=A'^2n^2,\ R=0,\ Q^2-4PR=A'^4n^4. \qquad (7)$$

Thus the first and last of (5) are satisfied, but the second is violated by $R=0$; however, it is a border-line case.

Consider now a case near degeneracy, i.e. a body for which $A-C$, $B-C$ and $b$ are small. (Strictly, we should speak of the smallness of dimensionless quantities formed with the help of $h$.) Since the changes involved in the transition from this to the degenerate case are small, it is clear from (7) that the first and last of (5) are satisfied for any $n$, except possibly for $n$ small, but this is a triviality which we can dispose of otherwise. The important quantity is $R$, and the critical condition for stability is

$$(Fn^2-gb)(Gn^2-gb)>0. \qquad (8)$$

Division by the positive quantity $(n^2gb)^2$ gives the equivalent condition

$$\left(\frac{1}{n^2}-\frac{F}{gb}\right)\left(\frac{1}{n^2}-\frac{G}{gb}\right)>0. \qquad (9)$$

*Thus the condition for stability is that* $1/n^2$ *should lie outside the range* $[F/(gb), G/(gb)]$.

To interpret this condition, we note that we can, without loss of generality, take $F\geqslant G$, since we can interchange $F$ and $G$ merely by rotating the axes $Oxy$ in the body through a right angle. Let us omit the exceptional cases where $F=G$ or $F=0$ or $G=0$. Then there are three cases to discuss.

Case ($a$): $F>0$, $G>0$. Now (8) may be written

$$\left(n^2-\frac{gb}{F}\right)\left(n^2-\frac{gb}{G}\right)>0, \qquad (10)$$

and so we have stability for $n^2$ in either of the two ranges

$$n^2<\frac{gb}{F},\ n^2>\frac{gb}{G}. \qquad (11)$$

Case ($b$): $F>0$, $G<0$. Now (8) may be written

$$\left(n^2-\frac{gb}{F}\right)\left(n^2-\frac{gb}{G}\right)<0; \qquad (12)$$

the second factor is positive and so the condition for stability is

$$n^2<\frac{gb}{F}. \qquad (13)$$

Case ($c$): $F<0$, $G<0$. Now both factors in (8) have the same sign, and we have stability for all values of $n$.

Either of the cases ($a$) or ($b$) might be applicable to the top described earlier, but ($b$) is the more appropriate. In case ($a$) the range of instability is

$$\frac{gb}{F}<n^2<\frac{gb}{G}, \qquad (14)$$

and so too great a spin would cause stability, and the top would not behave as described. In case (*b*) the range of instability is

$$n^2 > \frac{gb}{F}, \qquad \ldots \qquad (15)$$

and so we shall get the prescribed behaviour provided the spin exceeds this lower bound.

Hence, in conclusion, we may say that the body will behave as required provided it is constructed to satisfy

$$F > 0,\ G < 0, \qquad \ldots \qquad (16)$$

or explicitly in terms of the original constants

$$B-C-hb > 0,\ A-C-hb < 0, \qquad \ldots \qquad (17)$$

it being understood that $A-C$, $B-C$ and $b$ are all small and $B > A$; to produce instability it suffices to spin the body with angular velocity $n$ satisfying (15), that is,

$$n^2 > \frac{gb}{B-C-hb}. \qquad \ldots \qquad (18)$$

Since (17) gives

$$A-C < hb < B-C, \qquad \ldots \qquad (19)$$

and $b$ is positive, it follows that $B$ exceeds both $C$ and $A$; the greatest moment of inertia is about a transverse axis, and not about the axis of figure.

# LXXI. *The Abundance of Lithium, Beryllium and Boron in the Primary Cosmic Radiation*

By A. D. Dainton, P. H. Fowler and D. W. Kent*
H. H. Wills Physical Laboratory, University of Bristol†

[Received March 20, 1952, revised May 1, 1952]

## Summary

In a previous paper, a method of determining the charge of heavy nuclei in the cosmic radiation was described which depended on measuring the δ-ray density along a track in a photographic emulsion and the multiple scattering of the particle. The results suggested the presence of a large proportion of the light elements lithium, beryllium and boron in the radiation, a result in contradiction with that of other workers.

The first part of the present paper describes a re-examination of the original method and evidence for its reliability. It is shown that an alternative method, based on observations of grain-density in the tracks of heavy particles recorded in less sensitive emulsions, gives results in agreement with those obtained by the δ-ray method. In the second part, the results of a more extended series of measurements by the δ-ray method are described. The results indicate that at geo-magnetic latitude 55° N., the flux of lithium, beryllium and boron nuclei in the cosmic radiation is equal to, or larger than that of carbon, nitrogen and oxygen. Finally, the bearing of the results on the origin of the cosmic radiation is briefly discussed.

## Introduction

The pioneer experiments of Freier *et al.* (1948) and of Bradt and Peters (1948) have shown that a large fraction of the primary cosmic radiation consists of atomic nuclei more massive than protons. Later measurements of the relative abundance of different elements have indicated that the 'charge spectrum' extends up to iron and nickel; heavier elements, if they are present, occur very rarely. The light elements carbon, nitrogen and oxygen, are more abundant than heavier ones, and the 'charge spectrum' from $Z=6$ to $Z=28$ is similar to that of the matter of the universe as deduced from astro-physical data.

Whilst the above conclusions are generally accepted, different observers, employing different methods, have obtained contradictory results in studying the problem of the abundance in the primary radiation of the light elements lithium, beryllium and boron. Thus, Bradt and

---

* Now at the Bartol Research Foundation, Swarthmore, U.S.A.

† Communicated by Professor C. F. Powell, F.R.S.

Peters (1950) concluded that these elements, as in stellar matter, occur infrequently. On the other hand, experiments in this laboratory suggested that they are important constituents, about as numerous as carbon, nitrogen and oxygen (Dainton *et al.* 1951).

A knowledge of the proportions of the light elements in the primary radiation has an important bearing on the problem of the origin of the radiation and its history before reaching the upper atmosphere. Thus, if lithium, beryllium and boron are absent, or present in only small amounts, it can be assumed that in their journey to the earth, the primary particles have only a small chance of colliding with the nuclei of interstellar hydrogen. If there were an appreciable probability of a primary particle making a collision, any detailed features in the original charge spectrum, such as the absence of the lithium, beryllium and boron, would be obliterated, for collisions commonly lead to fragmentation of the nuclei involved.

Because of the difference in the results obtained in the two experiments, we undertook a more extensive investigation in order to test the reliability of our experimental methods and the validity of the results obtained with them. The new measurements here described appear to us to confirm our previous results and, in particular, to indicate that among the particles of the primary cosmic radiation, at a geo-magnetic latitude of 53° N., lithium, beryllium and boron nuclei are as numerous as those of carbon, nitrogen and oxygen.

In presenting the new material, it will be convenient to begin by describing in § 1 the main features of the original experimental method. Possible sources of error will next be examined and shown not to be serious by experiments with relatively insensitive emulsions. In § 2 the results of a more extensive application of the original methods, undertaken in order to give observations of greater statistical weight, will be described.

## §1. THE EXPERIMENTAL METHOD

### 1.1. *Calibration of the δ-Ray Method*

In principle, our first method of determining the charge on a nucleus was as follows :

From the track of the particle in a photographic emulsion, we determined the average deviation, $\bar{\alpha}$, in its direction of motion per unit length, together with the number of δ-rays per unit length of track, $N_\delta$. If the ratio of the charge to the mass number of the nucleus, $Z/A$, is known, $\bar{\alpha}$ gives a measure of the velocity of the particle. This quantity, together with the observed value of $N_\delta$, which is a function of the velocity of the particle and its charge, gives the value of $Z$ for the nucleus.

In determining $N_\delta$, it is convenient to count all δ-rays which produce tracks containing four or more grains, i.e. with energy greater than ~15 kev. High energy δ-rays, which produce tracks with a grain-density near the minimum value, are commonly missed in the convention employed for counting. The quantity $N_\delta$ is therefore more nearly a measure of the number of δ-rays in the energy range from 15 to 75 kev, rather than of all those with energies greater than ~15 kev. For values of $Z<20$ no serious errors are introduced by assuming that $Z/A=\frac{1}{2}$.

The relations between $N_\delta$ and $\bar{\alpha}$, for different types of nuclei, can be determined in the following manner :

Suppose (*a*), that the grain-density, $g$, in the track of a particle with the elementary electronic charge has been determined as a function of the velocity of the particle, $\beta c$ ; and, (*b*) that there is a unique relation between the grain-density in a track, $g$, and the corresponding δ-ray density $N_\delta$ : the relation between $N_\delta$ and $\beta$ for particles of unit-charge ($Z=1$), $N_\delta=f_1(\beta)$, then follows. The corresponding relation for charge $Z$ is given by $N_\delta=Z^2 f_1(\beta)$.

For a given value of $Z$, the scattering parameter, $\bar{\alpha}$, is a known function of the velocity of the particle. We may therefore determine the relation between $N_\delta$ and $\bar{\alpha}$ for any particle.

In practice the relation between $g$ and velocity for singly charged particles has been determined by measurements of $g$ and $\bar{\alpha}$ on the tracks of mesons, protons, deuterons and tritons, emitted from nuclear disintegrations occurring in the emulsion (Fowler 1950).

The relation between $N_\delta$ and $g$ was determined by observations on the tracks of π-mesons, protons and deuterons and α-particles. It was thus shown that for the Ilford G5 emulsion, and for values of $g$ less than five times the minimum value ($g<5\,g_{\text{min}}$), there is a linear relation between $N_\delta$ and $g$ (Dainton *et al.* 1951). Further, the observations showed that the value of $N_\delta$ in the track of an α-particle moving at a velocity in the relativistic region was equal to that of a singly charged particle with a track of the same grain-density. A proton, for example, of velocity 0·38 c produces a track with a grain-density equal to that of a relativistic α-particle, and the values of $N_\delta$ for the two tracks are also equal.

The curves showing the relation between $N_\delta$ and $\bar{\alpha}$, obtained by this method for different values of $Z$, were given in fig. 3 of a previous communication (Dainton *et al.* 1951), and are identical with those given in fig. 4 of this paper. These curves correspond to a relation different from those obtained if the variation of $N_\delta$ with velocity is assumed to be given by the widely quoted theoretical formula due to Rutherford :

$$N_\delta=2\pi\mathcal{N}\left(\frac{e^2}{mc^2}\right)^2\cdot\frac{Z^2}{\beta^2}\cdot\left\{\frac{mc^2}{W_1}-\frac{mc^2}{W_2}\right\}, \quad . \quad . \quad . \quad . \quad (1)$$

where $e$ and $m$ are the charge and mass of the electron, respectively ; $\mathcal{N}$ is the number of electrons per unit volume ; $W_1$ is the minimum energy of the δ-rays considered, and $W_2$ is the smaller of the two quantities (*a*) the maximum energy considered in the convention, or (*b*) the maximum possible energy for ejected electrons.

Using the calibration curves obtained in the manner described above, a charge spectrum was deduced from the earlier results which indicated the presence of a large proportion of Li, Be and B nuclei in the primary cosmic radiation. An important feature of the results, which appeared to provide strong supporting evidence for the validity of the method, was that the charge spectrum showed a series of resolved peaks centred around the integral values of the charge. This result was obtained without any adjustment of arbitrary constants. The degree of resolution of the different peaks would have been lost if a different assumed variation of $N_\delta$ with $\beta$—such as that suggested by the Rutherford formula—had been adopted.

### 1.2. *Objections to the Method of Calibration*

In considering the discrepancy between our results and those of other workers, it occurred to us that the following objections might be made against our method of calibration. As described above, the calibration depends on measuring values of $N_\delta$ for singly and doubly charged particles, and the values of $N_\delta$ are small. In principle, it was therefore possible that the counts were vitiated by the general background of slow electrons in the plates, some of which might have been regarded, wrongly, as associated with the tracks of heavy particles. Such errors, if substantial, could lead to an underestimate of the charge of heavier nuclei, and could explain the discrepancy between the observed variation of $N_\delta$ with velocity for particles of charge $|e|$, and the relation predicted by the Rutherford formula. It could therefore be objected that the particles we had attributed to boron might have been due to carbon nuclei.

We found it difficult to accept the view that such effects resulted in a serious source of error because of the degree of resolution displayed by the observed charge spectrum. Further, such effects, if they exist, could not explain the observation that the values of $N_\delta$ were equal for the tracks of relativistic $\alpha$-particles and for singly charged particles of velocity 0·38 c. If an application of the Rutherford formula were valid, the value of $N_\delta$ for the track of a proton of velocity 0·38 c should be approximately 1·6 times as great as that of a relativistic $\alpha$-particle, and the measured values of $N_\delta$ on the two tracks would not be equal, whatever the contribution for background electrons. Nevertheless, because of the discrepancy between our results on the one hand, and those of Dr. Peters and his colleagues on the other, we made further checks of our method.

### 1.3. *Experiments with Sensitive and Insensitive Emulsions*

In addition to the possibility of confusion due to background electrons, the $\delta$-ray method suffers from the disadvantage that the values of $N_\delta$ in the tracks of particles of low $Z$ are small and the statistical errors correspondingly large. On the other hand, it is an important advantage of the $\delta$-ray method that the value of $N_\delta$, in contrast with the grain-density in a track, is very insensitive to the degree of development of the emulsion.

Because of the low statistical weight of the determinations of $N_\delta$ it would be an advantage to make grain-counts instead of δ-ray counts. The G5 emulsion is so sensitive, however, that only for the tracks of relativistic nuclei with $Z=1$, 2 or 3 can this be done. For higher values of the charge, the tracks are completely 'clogged' in conditions of normal development as is shown in Plate XLIV.

It has been shown by Bradt and Peters that in certain cases, these difficulties can be overcome by using less sensitive emulsions. In order to take advantage of this method, we made a series of exposures in which plates with G5 emulsions 400 $\mu$ thick, and C2 emulsions 200 $\mu$ thick, were exposed in pairs. The emulsions were face to face and separated only by a thin layer of tissue paper of weight 2 mg/cm$^2$.

With these plates it is possible to recognize the tracks due to a single particle in the two facing emulsions. Further, it is possible to identify a particle by measuring the values of $\bar{\alpha}$ and $N_\delta$ along its track in the G5 emulsions, and then to determine the grain-density in the track recorded in the C2 emulsion.

It is also possible to identify lithium nuclei moving at relativistic velocities by the measurement of scattering and *grain-density* along the track in the G5 *emulsion*, and then to determine the corresponding much smaller value of the grain-density in the C2 emulsion. If the relation between specific ionization and grain-density for the emulsion is known, it is then possible to compute the expected values of the grain-density in the tracks of relativistic beryllium, boron and carbon nuclei in the C2 emulsion, and to compare the resulting values with those actually observed.

An agreement between the values of the charge deduced for a number of nuclei by the two methods would provide strong evidence that the original measurements were not in error, either from a background of δ-rays or from other causes. In effect, it would establish an agreement between two alternative methods of measuring the charge of atomic nuclei moving at relativistic velocities, one based on grain-counts and the other on δ-ray counts.

### 1.4. *Identification of Lithium Nuclei*

In a systematic scan of the G5 emulsions, six tracks were found which were identified as due to relativistic lithium nuclei from the observed values of $g$ and $\bar{\alpha}$ in the G5 *emulsion*. The identification depended on the observations that the value of $\bar{\alpha}$ showed the velocity of the particle to be greater than 0·86 c, and that the grain-density corresponded to a specific ionization about nine times the corresponding value for a proton of the same velocity. The details of the observations are as follows :

| Particle | H | He | Li |
|---|---|---|---|
| Grain-density in G5 emulsion ; grains per 50 $\mu$ | $11\pm0{\cdot}5$ | $42\pm2$ | $74\pm3$ |
| Relative values of the specific ionization | 1 | 4 | 9 |

Observations on a number of long tracks due to $\mu$-mesons (fig. 1 (A)) show that the grain-density in the track of such a particle in the

G5 emulsion is equal to that of a relativistic lithium nucleus when the residual range of the meson is $300\,\mu\pm60\,\mu$; and equal to that of a relativistic α-particle when the residual range is $2\,000\pm300\,\mu$. The ratio of the corresponding values of the specific ionization is $2{\cdot}2\pm0{\cdot}2$ thus establishing the identity of the lithium nuclei.

The tracks of the six lithium nuclei were traced into *the C2 plates*, and the mean value of their grain-density in the insensitive emulsion was found to be $11{\cdot}8\pm0{\cdot}6$ grains per $50\,\mu$.

Plate XLIV shows photo-micrographs of an event in which appear characteristic tracks of all the three particles under consideration. A heavy primary particle collides with a nucleus in the G5 emulsion and the tracks of a proton, an α-particle and a lithium nucleus, can be distinguished among the relativistic particles emerging from the encounter.

Fig. 1

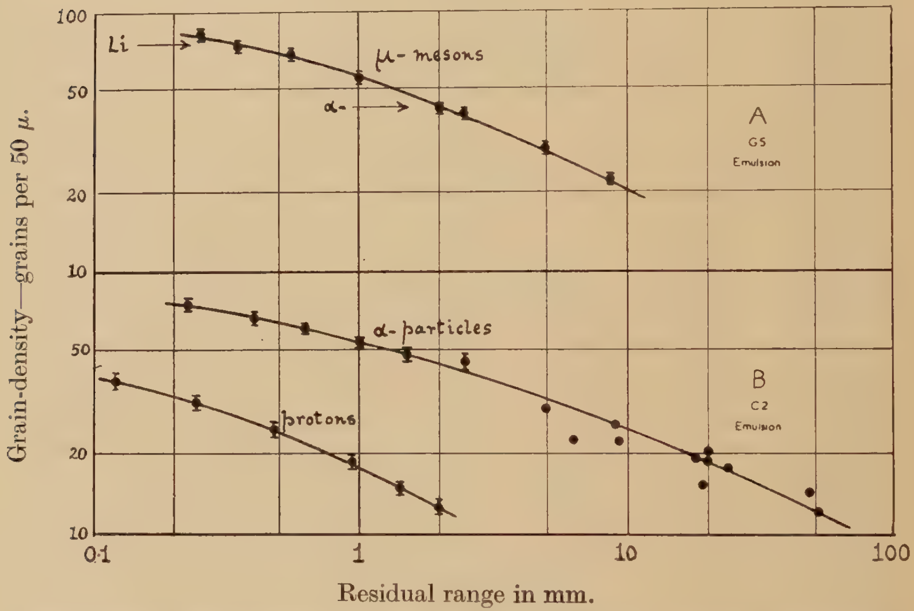

Grain-density as a function of residual range. Curve A is for μ-mesons in Ilford G5 emulsion; the grain-densities in tracks of relativistic nuclei of helium and lithium are indicated by arrows. Curves B are for α-particles and protons in Ilford C2 emulsion; the protons were distinguished from deuterons and tritons by multiple scattering measurements. The errors indicated are not statistical, but are calculated from the observed spread of the grain-densities of all the measured tracks. The points without indicated errors represent measurements on individual tracks.

### 1.5. *Predicted Grain-density in the Tracks of Heavy Nuclei*

In emulsions of low sensitivity the grain-densities in the tracks of particles with the same velocity but different charges, $Z$, will not be exactly proportional to $Z^2$ (Bradt and Peters 1950). The number of AgBr crystals traversed by any particle per unit length is about 150 per 50 $\mu$; the grain-density in the track of a particle cannot therefore exceed this figure, and thus $g$ does not vary linearly with the specific ionization.

Let the specific ionization of the charged particle be represented by $Z^2 f_2(\beta)$. We may assume, as an approximation, that all grains traversed by the particle have an equal probability of being developed. It then follows that the grain-density $g$ can be expressed by the relation

$$g=D\left[1-\exp\left\{-\frac{aZ^2f_2(\beta)}{D}\right\}\right], \quad . \quad . \quad . \quad . \quad . \quad . \quad . \quad (2)$$

where $D$ is the total number of silver bromide crystals traversed by the particle per unit length and $a$ is a constant to be determined.

We can test eqn. (2) by comparing the measured values of the grain-densities in the tracks of $\alpha$-particles and protons of the same velocity, that is, those with equal ranges (fig. 1 (B)). It may be shown that departures from the relation (2) are small and are insignificant for our immediate purposes.

Using the measured value of the grain-density in the track of relativistic lithium nuclei, and taking $D$ to be 150 grains per 50 $\mu$, we evaluate $a$ and so can compute the grain-density to be expected in the tracks of relativistic nuclei of beryllium, boron and carbon. The values are given in table 1.

Table 1

| Nucleus | Grain-density (predicted) | Grain-density (observed) |
|---|---|---|
| Lithium | — | 11·8±0·6 |
| Beryllium | 20·5±1·0 | 21·6±0·5 |
| Boron | 31 ±2 | 32·7±0·7 |
| Carbon | 42 ±3 | 42 ±1·0 |

### 1.6. *Observations on the Tracks of Heavy Primary Particles*

The G5 plates were scanned for all tracks longer than 4 mm, and with values of $N_\delta$ greater than, or equal to 1 per 100 $\mu$. Eighty-four examples were found, due either to slow $\alpha$-particles or heavier nuclei. The value $N_\delta$ for each track was determined and the track was then traced into the C2 emulsion where the corresponding grain-density was measured. Values of the scattering parameter, $\bar{\alpha}$, were obtained from measurements made in both plates.

In fig. 2, the value of $N_\delta$ for each track, has been plotted against the corresponding value of the grain-density in the C2 emulsion. In fig. 2 (*a*) each point represents measurements on a track for which the measured value of $\bar{\alpha}$ was less than 0·011° per 100 $\mu$ so that the velocity of the corresponding particles was greater than 0·86 c. Figure 2 (*b*) represents similar measurements on the remaining tracks.

A study of fig. 2 allows a number of important conclusions to be drawn :

(*a*) There are indeed groups of particles with velocities in the relativistic region ($\bar{\alpha} < 0{\cdot}011°$ per $100\,\mu$) which produce tracks in the C2 emulsions with values of the grain-density close to those predicted for the light elements (see table 1). The distribution in the observed values of $g$ shows resolved groups corresponding to all the light elements and indicates that 60% of the fast particles observed are due to lithium, beryllium and boron.

Fig. 2

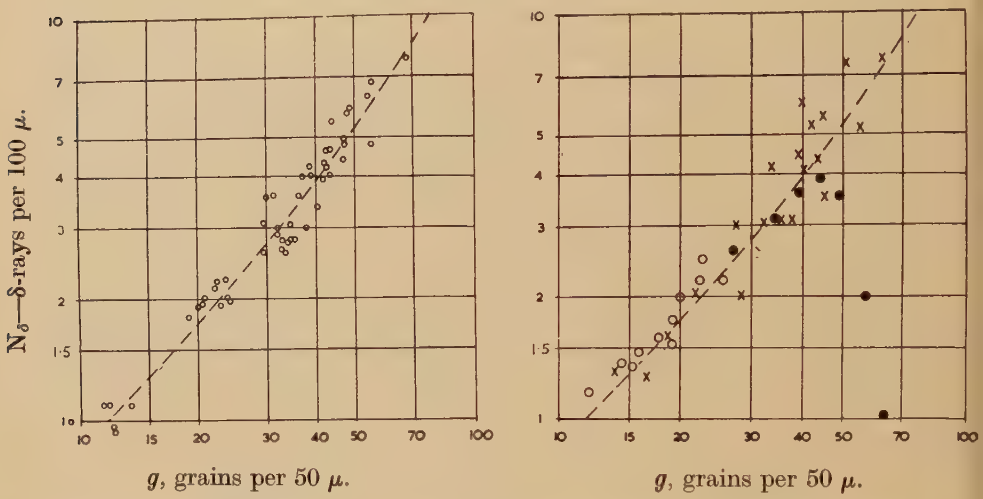

(*a*) (*b*)

Corresponding values of, $g$, in a C2 emulsion, and $N_\delta$ in a G5 emulsion, for 82 particles which traversed both emulsions. In fig. (*a*), the points represent measurements on individual tracks for which the value of $\bar{\alpha}$ was less than $0{\cdot}011°$ per $100\,\mu$. They therefore refer to particles with energies greater than 900 MEV per nucleon. In (*b*), the points represent measurements on all other tracks ; points marked thus ○ represent measurements on α-particles, and thus ×, heavier nuclei. The full circles ● represent measurements on α-particles coming to rest in the emulsion. The dashed curves in the two diagrams are identical.

The above result appears to establish the fact that after traversing about 70 g/cm$^2$ of air, a large proportion of the flux of relativistic nuclei, other than protons and α-particles, is composed of lithium, beryllium and boron. Briefly summarizing the argument, we can say that the lithium nuclei can be identified by grain-counting in the G5 emulsion, and then followed into the C2 emulsion. The grain-counts in the tracks of the heavier nuclei are then found to be in accord with expectations based on the $Z^2$ law, all the members in the sequence of elements up to carbon being clearly resolved. There therefore seems to be no possibility of errors in identification.

(*b*) Consider the values of $N_\delta$ for tracks in which $\bar{\alpha}$ is less than $0{\cdot}011°/100\,\mu$. Since the velocity of the parent particle was in the relativistic region, these values of $N_\delta$ will be close to the minimum values for the corresponding charges. For the tracks of lithium, beryllium, boron and carbon nuclei, which have been identified by grain counts, it will be seen that the values of $N_\delta$ in the G5 emulsion are proportional to $Z^2$. It follows that in the conditions of the experiment the contribution made by background electrons to the observed value of $N_\delta$ for relativistic lithium nuclei was small; in fact, it was less than 0·1 δ-rays/100 μ, a value which is negligible in the conditions of the experiment. Further, the result indicates that in the range of values involved, the method of determining $N_\delta$ gives results proportional to the true number of δ-rays, for there is no evidence of any loss in efficiency for the larger values of $N_\delta$ which would also be indicated by apparent departures from the $Z^2$ law.

(*c*) The distribution of the points in fig. 2 (*b*) representing the slower particles ($0{\cdot}23<\beta<0{\cdot}86$) is closely similar to that of the fast particles. Points marked thus: ○ represent measurements on 11 α-particles which traversed both emulsions and which had velocities within the limits stated above.

The points in fig. 2 (*b*), marked thus: ● correspond to the tracks of a number of α-particles which were brought to rest in the G5 emulsion. For these tracks $N_\delta$ was measured as a function of the residual range. The corresponding values of $g$ were obtained from fig. 1 (B) which gives the relation between grain-density and residual range in the C2 emulsion. The last measurements demonstrate the marked fall in the value of $N_\delta$ for particles with $\beta<0{\cdot}23$.

### 1.7. *Variation of δ-ray Density with Velocity*

The results of the preceding paragraphs show that the background of electrons does not disturb the observations significantly, and that the counting is reliable. We can therefore return to the determination of the variation of $N_\delta$ with the velocity for α-particles. This relation is required for computing the relation between $N_\delta$ and $\bar{\alpha}$ for any chosen value of $Z$ and so for determining the charge of the slower particles. It has been derived by the following method:

From fig. 2 and the curve drawn through the experimental points in fig. 1 (B), we can deduce $N_\delta$ as a function of range and thence as a function of velocity. Further, $N_\delta$ (min) for α-particles can be calculated from the observed values of $N_\delta{}^*$ in the tracks of fast particles of any known charge, assuming a $Z^2$ dependence. We have no experimental values of $N_\delta/N_\delta(\text{min})$ lying between 1 and 2·3. For this interval we have assumed that in G5 emulsions

$$N_\delta{}^* = N_\delta/N_{\delta(\text{min})} = g/g_{(\text{min})} = g^*. \qquad (3)$$

The above relation is known to be true, within the limits of error, for velocities 0·38 c and 0·54 c, velocities for which the values of $N_\delta{}^*$ are 4·0 and 2·25 respectively. Thus the value of $N_\delta$ in the track of an α-particle of velocity 0·38 c is equal to that for a relativistic beryllium nucleus ; and for $\beta=0{\cdot}54$, the value of $N_\delta$ for an $\alpha$-particle track is equal to that of a relativistic lithium nucleus. These equalities are confirmed by further measurements of greater statistical weight represented in fig. 4.

The relation between $N_\delta{}^*$ and $\beta$ thus obtained is shown in fig. 3 (curve 3). It is from this relation that the corresponding curves for particles of charge $Z$ and mass $A=2Z$ given in fig. 4 have been deduced, assuming that

Fig. 3

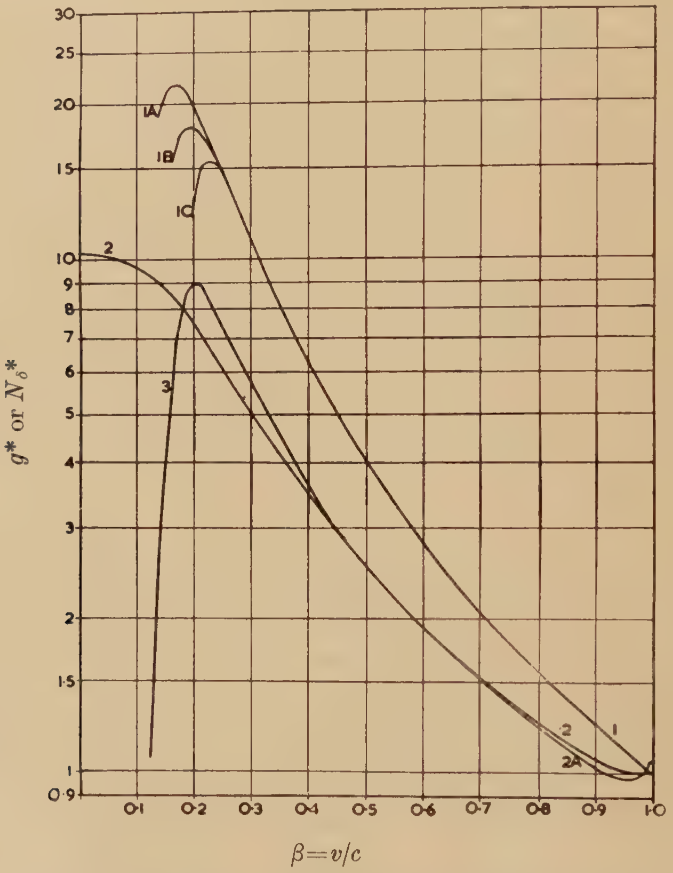

*Curve* 1.—$N_\delta{}^*$ as a function of $\beta$, as calculated from Rutherford's formula, for $\delta$-rays of energy less than 75 kev and greater than 15 kev, Curve A ; >20 kev, Curve B ; >30 kev, Curve C.

*Curve* 2.—$g^*$, i.e. $g/g_{\min}$, as a function of $\beta$, for an Ilford G5 emulsion.

*Curve* 2A.—Variation of grain-density with velocity as determined by Perkins *et al.* This curve is normalized to curve 2 at $\beta=0{\cdot}7$.

*Curve* 3.—Observed variation of $N_\delta{}^*$ with $\beta$ as determined by measurements on tracks of $\alpha$-particles. Between $\beta=0{\cdot}45$ and $\beta=0{\cdot}54$ the points lie on curve 2. No experimental points are available for $\beta>0{\cdot}54$.

$N_\delta = Z^2 f_1(\beta)$. This last assumption can now be made with confidence since background δ-rays have been shown to introduce no appreciable errors.

Included in fig. 3 for comparison are the relations between $N_\delta$ and $\beta$ deduced by an application of the Rutherford formula. Curves 1A, 1B and 1C show the results of using three alternative values for the minimum energy of δ-rays which are counted ($W_1$ in eqn. (1)). It will be seen that there are large differences between curves 1 and 3.

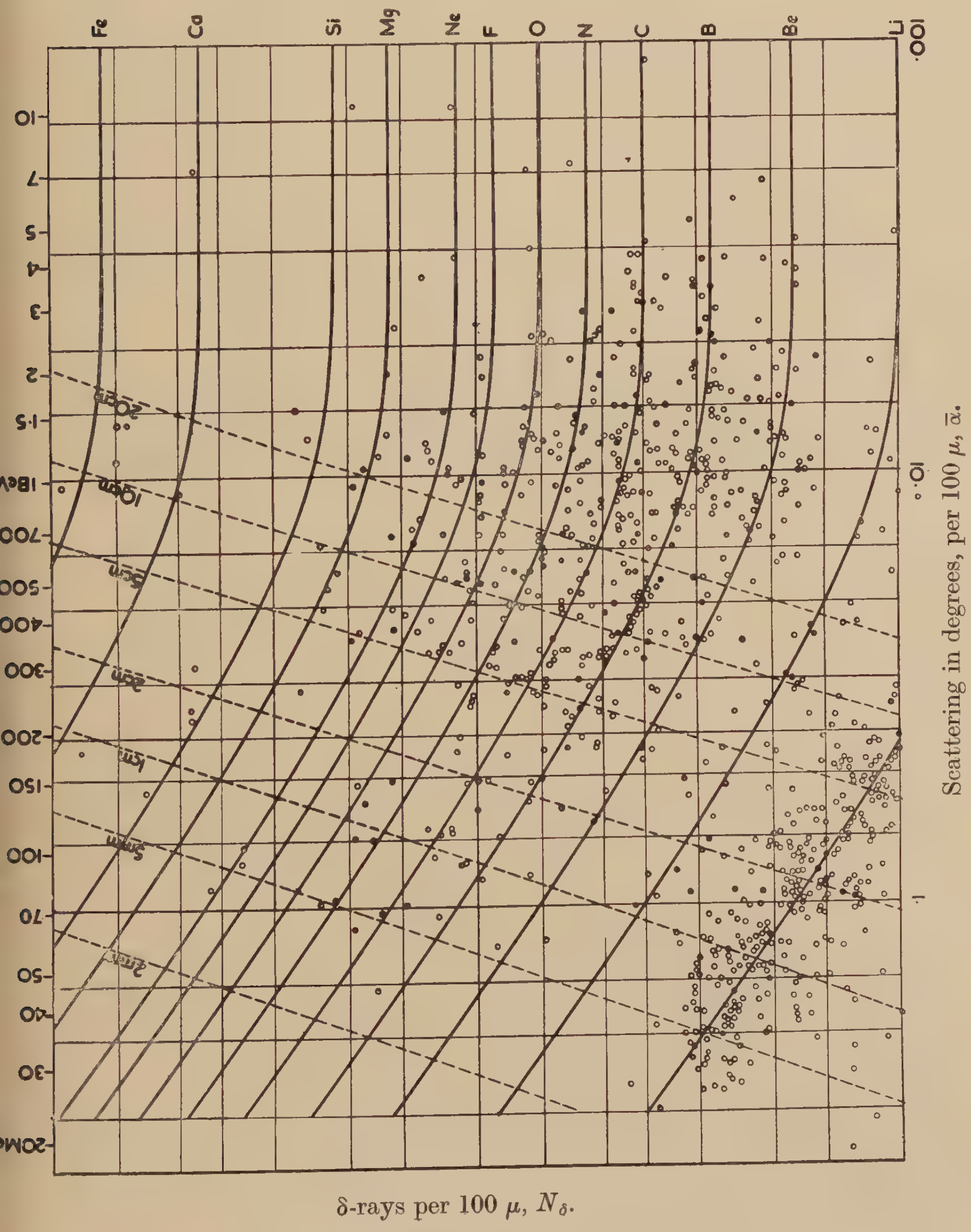

Relation between $N_\delta$ and $\bar{\alpha}$ (100 μ) for the tracks of 857 particles observed in a systematic scan of Ilford G5 emulsions exposed at geo-magnetic latitude 55° N. The family of full curves represents lines of constant charge, while the dashed lines are lines of constant residual range. A scale of energy per nucleon is included at the top of the figure.

Figure 3 also shows $g$ as a function of velocity,—curve (2)—as determined for G5 emulsions by Fowler (1950). It was upon this curve that the previous calibration was based, and it gives results closely similar to those based on curve (3).

Recent work in this laboratory by Voyvodic and by Perkins *et al.*, (in course of publication) proves that the grain-density in the tracks of particles of charge $e$ has a minimum value at $\beta=0{\cdot}94$, followed by a rise at higher velocities. The curve corresponding to the results of these authors is also plotted in fig. 3 (curve 2A), normalized to curve 2 at $\beta=0{\cdot}70$. Further work is required to determine the behaviour of $N_\delta$ for velocities greater than 0·54 c, but from the point of view of the present experiments, the magnitude of any departure from eqn. (3) will certainly be small and without any serious influence on the results.

### 1.8. *Variation of Grain-Density with Velocity*

Equation (2) may be applied, with appropriate values of the constants, to either C2 or G5 emulsions. The function $f_2(\beta)$ can be determined by observing the values of the residual range (and thence the velocity) at which $\alpha$-particles or protons produce tracks with grain-densities equal to the observed minimum values for particles of various charges. The results thus obtained are independent of the convention employed in grain-counting and suggest that the function is very similar for the two emulsions. Inserting in eqn. (2) a value of 11·8 grains/50$\mu$ for the grain-density in tracks of relativistic lithium nuclei and taking $D$ to be 150, we may deduce the relation between $g$ and $\bar{\alpha}$ for the C2 emulsion for particles of any charge for values of $g$ less than 50 grains per 50$\mu$.

## §2. EXPERIMENTAL RESULTS

### 2.1. *The Charge Spectrum under* 58 $g/cm^2$ *of Atmosphere*

The distribution in the values of $Z$ derived in the above manner from tracks in the C2 emulsion is plotted in fig. 6 ($a$). It represents the charge-spectrum of particles at geomagnetic latitude 53° observed under 58 g/cm$^2$ of residual atmosphere. The average amount of matter, traversed by the particles before detection, including small amounts of glass and packing material, corresponds to 70 g/cm$^2$ of air. Seven particles represented in the spectrum in fig. 6 ($a$) produced tracks in the C2 emulsion with $g>50$ grains per 50$\mu$. The charges of these particles were estimated from measurements of $N_\delta$ and $\bar{\alpha}$ in the G5 emulsion.

It will be seen that the majority of the tracks represented in fig. 6 ($a$) are of lithium, beryllium and boron nuclei. Some of these particles must be secondaries produced in interactions in and above the plate assembly, and the effect of such processes will be discussed in § 2.6.

### 2.2. *The Charge Spectrum at Geomagnetic Latitude* ~55°

The experiments to test the reliability of the method having been completed, it was important to increase the statistical weight of the observations on the charge spectrum at greater altitudes. Experiments

Fig. 5

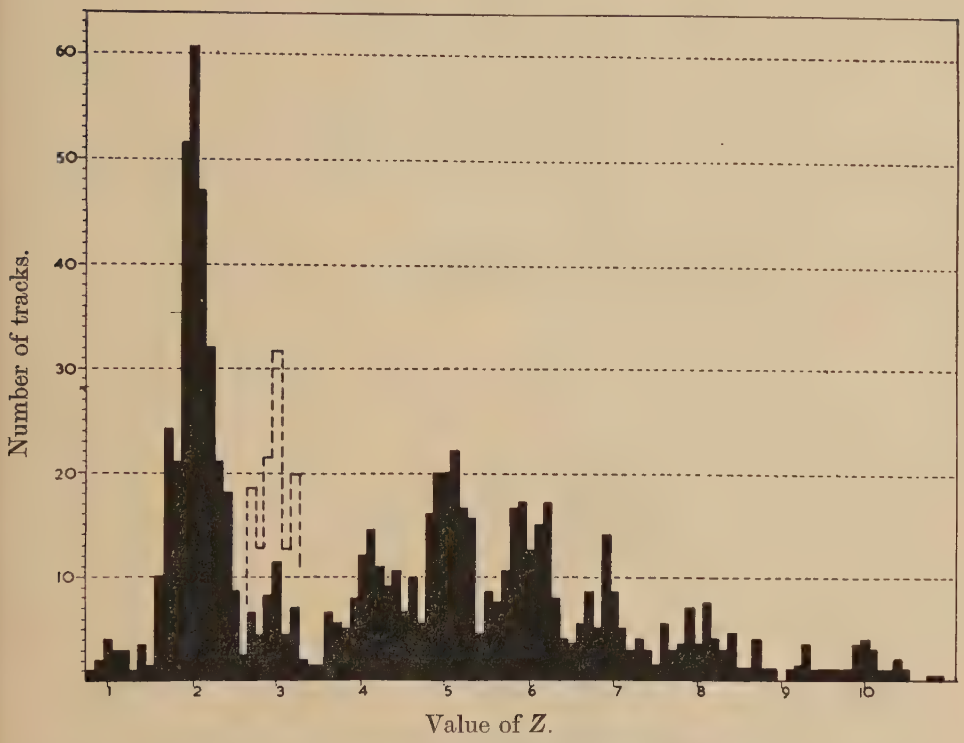

Charge distribution up to $Z=11$ deduced from the observations displayed in fig. 4. The estimated relative intensity of the Li nuclei after correction for loss is represented by the dotted line.

(*a*)

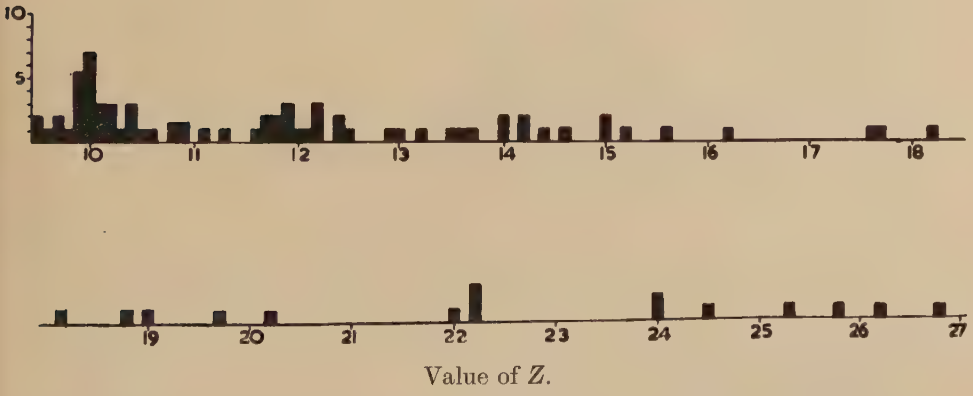

Charge distribution of all particles with track-length greater than 4 mm for $Z$ greater than 9·5.

(*b*)

Fig. 6

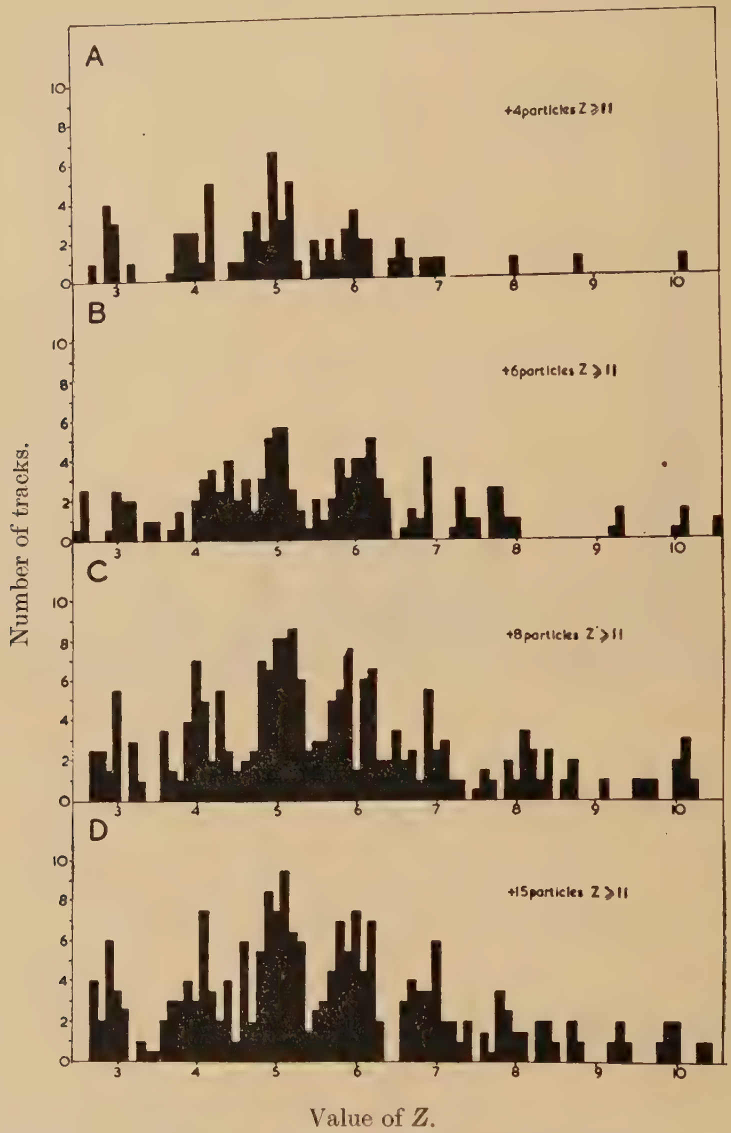

Observed charge distribution under different thicknesses of matter, $t$.

A $t=70$ g/cm$^2$ of air equivalent. Exposure under 58 g/cm$^2$ of air.

B $t>36$ g cm$^2$ of air and glass, average value 50 g cm$^2$.
C $23<t<36$ g/cm$^2$ of air and glass.
D $15<t<23$ g/cm$^2$ of air and glass.
} Exposure under 13 g/cm$^2$ of air.

In fig. 6 (A) the charge has been estimated from measurements of multiple-scattering and grain-density in C2 emulsions. The other spectra are based on measurements of $N_\delta$ in G5 emulsion.

at the highest possible altitude are desirable in order that the observed spectrum may correspond as closely as possible to that of the primary radiation ; in order, that is, to avoid as far as possible the distortion of the original spectrum as a result of nuclear collisions in the atmosphere above the recording apparatus. For this purpose, an extended series of measurements were made on tracks recorded in plates exposed at 95,000 ft. at Minneapolis, Minnesota. During the exposures, the 18 plates, coated with Ilford G5 emulsions 400$\mu$ thick, were arranged with the emulsions in a vertical plane. The plates were searched for tracks longer than 6 mm, in which $N_\delta > 1$ per 100$\mu$. For each track, $N_\delta$ and $\bar{\alpha}$ were determined, and the results for the 857 tracks are shown in fig. 4. These measurements include those for 230 tracks of which a preliminary account has already been given (Dainton *et al.* 1951).

The family of smooth curves in fig. 4 are lines of constant charge, drawn in accordance with the procedure discussed in § 1.7, and normalized on the observed $\delta$-ray density of slow $\alpha$-particles. A charge spectrum for $Z < 11$ derived from these results is displayed in fig. 5 (*a*). Figure 5 (*b*) shows the charge distribution for particles with $Z > 9{\cdot}5$. The results of measurements on all observed tracks longer than 4 mm have been included in fig. 5 (*b*) in order to increase the statistical weight of the observations. Because of the large values of $N_\delta$, the tracks of particles more massive than neon can be easily recognized even though they are short.

The results represented in fig. 5 (*a*) show that for particles with charge $Z < 11$ there is a satisfactory degree of resolution of different elements, the peaks being centred on the integral values of the charge. Helium nuclei occur most frequently, but only those with energies less than 200 MeV/nucleon are included in the analysis as the value of $N_\delta$ for the faster ones is less than 1 per 50$\mu$. Many of these slow $\alpha$-particles are either secondaries emitted from nuclear disintegrations produced by protons, or fragments of heavy primary particles which have made collisions at points above the plates.

Particles with charge $Z \geqslant 3$ are sometimes emitted from stars produced by protons, neutrons, or $\alpha$-particles (Sorensen 1949) but those with a residual range greater than 6 mm are extremely rare. Almost all observed particles with $Z \geqslant 3$ must therefore be regarded either as true primary nuclei, or as the fragmentation products of heavier ones.

### 2.3. *Correction for Loss of Lithium Nuclei*

Experience shows that in making a general search of the plates, the efficiency with which tracks are distinguished and recorded by an observer depends upon the value of $N_\delta$ ; and in the present experiment, for values of $N_\delta$ less than 1·5 per 100$\mu$, the efficiency of detection rapidly declined.

This effect was detected by an examination of the distribution in length of the tracks with $N_\delta < 1{\cdot}5$. From geometrical considerations we should expect

$$dN \propto dl/l^3$$

where $l$ is the length of the track. Tracks with $N_\delta > 1{\cdot}5$ do indeed have such a distribution in length, but among those with $N_\delta < 1{\cdot}5$ there is a much smaller proportion of short tracks, showing that many of the shorter, very light tracks, such as tracks of relativistic Li,—are missed.

The best method of estimating the magnitude of this effect on the observed number of tracks of lithium nuclei comes from the observed flux of the slow lithium nuclei with $N_\delta > 1{\cdot}5$ of which the tracks would not commonly be missed by the observer. Kaplon *et al.* (1952) have shown that the velocity distribution of heavy primary particles is independent of charge. Now the ratio of the number of beryllium and boron nuclei with $E < 300$ MEV/nucleon observed in our plates to that of lithium nuclei in the same range of velocities is 1·56 (39 : 25). The total observed number of beryllium and boron nuclei was 218. This suggests that the true number of lithium nuclei was $\sim 130$, approximately equal to the number of boron nuclei.

### 2.4. *Significant Features of the Charge Spectrum*

The geometry of the plate assembly, and differences in the directions of motion of the primary particles, result in a broad distribution in the amount of matter (air, glass and packing material) traversed by different nuclei before being recorded in the emulsion. It is therefore convenient to divide the results into 3 groups according to the amount of matter traversed by the corresponding particles. The resulting ‘ charge spectra ’ are shown in fig. 6 (B, C, D). The most significant feature is that the observed flux of lithium beryllium, and boron—even without correction for the failure to observe some lithium nuclei—is comparable with that of carbon, nitrogen and oxygen. This feature is as marked in the results for particles which have traversed less than 23 g/cm$^2$ as for the other two groups.

Apart from this feature, and an indication that the abundance of nitrogen is greater than that of oxygen, the results are similar in their general trend to those reported by Bradt and Peters, and no nuclei have been found with a charge significantly greater than that of iron.

For particles with $Z$ between 8 and 14 inclusive, nuclei of even charge are apparently three times as numerous as those with odd charge. It is tempting to assume that this feature is due to the following cause : that at some stage in the history of the radiation, nuclei of different mass number A are produced with a relative frequency that is a monotonic function of A. Such a mass distribution might be expected if the majority of the primary nuclei were in fact secondaries of nuclear interactions in interstellar space. In nuclear interactions it is the atomic weight rather than the stability of a given secondary nucleus that determines the frequency with which that nucleus is produced. Those nuclei which are radioactive then transform by $\beta$-decay into the stable isotopes of the different elements. For the range of values of A under consideration, the elements of even charge will then be three times more numerous than their immediate neighbours of odd charge, for they have three times as many stable isotopes.

The relative frequency of occurrence of lithium, beryllium, and boron appears to be in accordance with this view, for beryllium possesses only one stable isotope, whereas boron and lithium each have two. The measured abundance of beryllium is markedly less than that of boron, thus interrupting a general trend for values of $Z$ between 3 and 8 inclusive.

### 2.5. *The Energy Spectrum of the Heavy Primary Particles*

The scattering parameter, $\bar{\alpha}$, is related to the velocity of the particle by the familiar formula :

$$\bar{\alpha}=\frac{KZ\sqrt{(1-\beta^2)}}{A\beta^2}, \quad . \quad . \quad . \quad . \quad . \quad . \quad . \quad . \quad (4)$$

where $K$ is the so-called ‘ scattering constant ’. For particles of $Z\geqslant 2$, $K$ is practically independent of both $Z$ and $\beta$ ; it is only the slow dependence of $K$ upon the cell-size used in the determination of the scattering, for which allowance need be made. Detailed considerations of the variation of $K$ with velocity and cell-size for particles of unit charge, have been given by Gottstein *et al* (1951) ; from their results we have deduced the values of $K$ employed here for multiply charged particles.

The measurements of multiple scattering allow us, in principle, to derive the energy spectrum directly. We believe, however, that for values of $\bar{\alpha}$ less than about $0{\cdot}01°/100\,\mu$—corresponding to an energy of about 1 Bev/nucleon—measurements may be unreliable because of distortion of the emulsion. The values of $\bar{\alpha}$ shown in fig. 4, in the range $\bar{\alpha}<0{\cdot}01$ are therefore in many cases upper limits. Although this feature does not influence the observed ‘ charge spectrum ’, it makes it impossible to draw reliable conclusions about the distributions in energy for values greater than 1 Bev/nucleon.

In considering the distribution at lower energies, it is convenient to confine attention to tracks with zenith angles less than 60°. The energy of each individual particle at the top of the atmosphere was evaluated—making allowance for loss of energy through ionization in its path to the plates—on the assumption that it had suffered no loss of charge since its arrival at the top of the atmosphere. Further, from a knowledge of the distribution in the amount of matter traversed by particles before reaching the plates, it is possible to calculate, for any value of $Z$, the proportion of particles of a given energy which are not recorded through being brought to rest by ionization.

Rough estimates show that in our experimental conditions only approximately 15% of the observed particles will be fragments of heavier nuclei. The assumption that the charge of any particle has remained unaltered in its passage to the plates cannot therefore introduce serious errors in the energy distribution. The energy ‘ spectra ’ for $Z=4$ and 5, for $Z=6$, 7, 8 and 9, and for $Z\geqslant 10$, are shown in fig. 7. It may be seen that there is no significant variation in the distribution in the values of the energy per nucleon for the various elements although the observed proportion of high energy C, N, O and F nuclei appears to be lower than for other elements.

Figure 7 (*b*) shows the differential distribution in energy of particles with charge numbers between 4 and 9 inclusive. The limits of error shown are those due to statistical fluctuations in the measurements. The figure indicates that there is a definite and rather rapid rise of intensity at low energies, a feature which is a contradiction to the published spectra of Kaplon *et al.* (1952). It is difficult to see how any appreciable systematic error can have entered into our measurements on the low-energy particles for the corresponding values of $\bar{\alpha}$ are relatively large. The reliability of the measurements is confirmed by the distribution of the experimental points for α-particles shown in fig. 4, and by measurements on the very long tracks of particles which are sometimes arrested in the emulsion.

Fig. 7

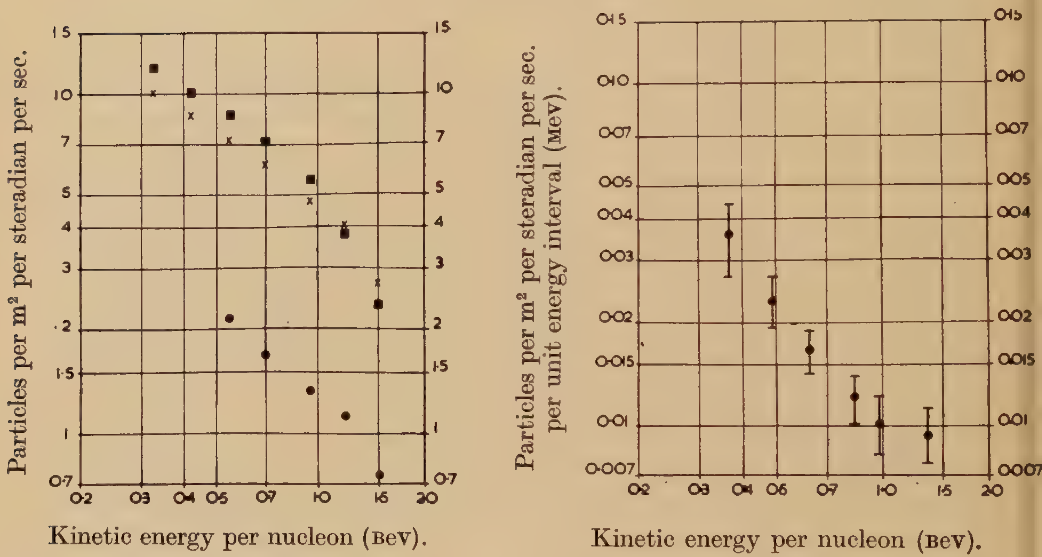

(*a*) (*b*)

(*a*) Integral energy spectra for 3 groups of particles. In order to avoid confusion, the errors for each point have been omitted. The number of CNOF nuclei with $E > 330$ MeV/nucleon was 160 :—points marked thus ■; Be and B nuclei with $E > 330$ MeV/nucleon, 150, marked thus × ; and the number of nuclei with $Z \geqslant 10$ and with $E > 540$ MeV/nucleon, 43 ; marked thus ●.

(*b*) The differential distribution in energy of particles of charge $4 \leqslant Z \leqslant 9$ ; the errors shown are those due to statistical fluctuations.

### 2.6. *The Flux of Heavy Nuclei at Geomagnetic Latitude* 55°

To obtain values for the flux of the different types of primary nuclei at the top of the atmosphere, corrections must be made for the effects of traversing matter before reaching the recording plates. For this purpose, it is convenient to exclude from the analysis those particles which traversed large amounts of material before detection. This procedure enables us to reduce the systematic errors due to an uncertainty in the magnitude both of the cross sections for the various possible nuclear collisions, and for loss by ionization in the absorbing material above the plates. The results for various groups of elements are shown in table 2 together with the values employed for the collision cross sections and the mean amount of matter traversed by particles with different values of $Z$. The magnitude of the correction for ionization loss in the case of beryllium and boron nuclei was 4% and for C, N, O and F nuclei about 14%.

Table 2

| Type of nucleus | Mean free path employed in calculation (g/cm$^2$) | Mean amount of matter traversed before detection (g/cm$^2$) | Flux (particles/m$^2$ ster. sec.) |
|---|---|---|---|
| Li | — | — | $\sim 5$ |
| Be, B | 33 | 22 | $10 \pm 1$ |
| C, N, O, F | 30 | 22 | $12 \pm 1$ |
| $10 \leqslant Z \leqslant 15$ | 25 | 20 | $3{\cdot}0 \pm 0{\cdot}5$ |
| $Z \geqslant 16$ | 20 | 20 | $1{\cdot}2 \pm 0{\cdot}4$ |

The values for the flux of C, N, O, F nuclei, and for those of $Z \geqslant 10$ are similar to those given by Peters (1952) and by Ney and Thon (1951). The present experiments show, however, a flux of lithium, beryllium and boron nuclei greater than 80% of that of all heavier elements. This result is consistent with that which we obtained previously, but it is in contradiction with the observations of Bradt and Peters (1950) who reported a flux of Li, Be, and B less than 10% of the C, N, O, F flux at geomagnetic latitude 30°.

Using the values of the flux shown in table 2, the expected form of the charge distribution of a parallel beam of such particles after traversing different thicknesses of matter, can be calculated.

We have made such a calculation neglecting the loss of particles which come to rest through loss of energy by ionization. At high latitudes this approximation leads to an overestimate of the number of particles of $Z > 10$ observed at any given depth; the ratio, $R$, of beryllium and boron nuclei to those of carbon, nitrogen, oxygen and fluorine—with velocity greater than 0·86 c ($\bar{\alpha} < 0{\cdot}11$)—is only slightly modified. We have used Peters data for the composition of the secondary fragments of nuclear collisions of different types. The results are presented in fig. 8 and suggest that at a depth of 70 g/cm$^2$ the ratio $R$ should be 1·1. This agrees with our observations displayed in fig. 2 (*a*).

### 2.7. *Summary of Evidence for the Presence of Lithium, Beryllium and Boron in the Primary Radiation*

The evidence for the presence of the light elements ($Z=3$, 4, 5) in the primary cosmic radiation provided by the observations described in the preceding sections of this paper, can be summarized under five headings :

(1) The values for the total flux of particles of $Z \geqslant 3$, $E > 330$ MEV/nucleon, is 31 particles/m$^2$/steradian/sec. This is considerably greater than the value obtained by Peters, viz. 19 particles of $Z \geqslant 6$ per m$^2$/ster./sec.

Fig. 8

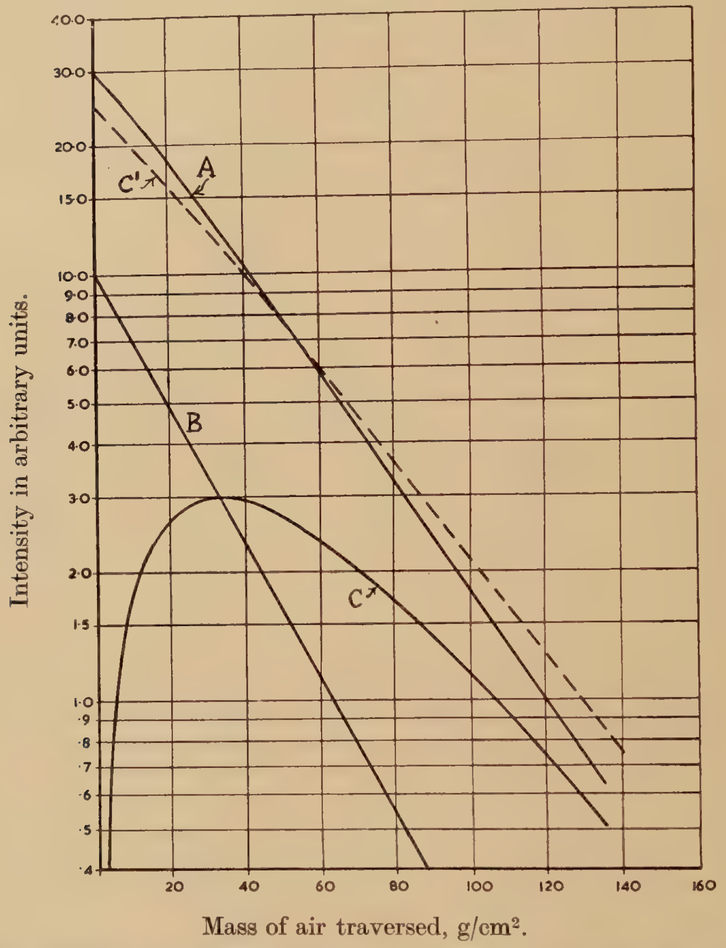

Estimated intensity of parallel beams of heavy nuclei, of various charge groups, as a function of the mass of air traversed.

*Curve* A.—The number of CNOF nuclei at various depths, including those produced in the atmosphere by collisions of heavier nuclei.

*Curve* B.—Similar results for nuclei of charge $Z \geqslant 10$. The indicated relative intensity of the two groups at the top of the atmosphere, 3 : 1, is the generally accepted value.

*Curve* C.—The variation with depth of the number of secondary Be and B nuclei arising from collisions of heavier particles. Assuming a primary flux of Be and B equal to 83% of the CNOF flux, curve C′ represents the variation in the total number of these nuclei.

(2) Errors due to distortion will tend to increase the observed value of $\bar{\alpha}$. It is therefore certain that the majority of tracks for which $\bar{\alpha} < 0{\cdot}01^\circ/100\,\mu$ were produced by particles with kinetic energy greater than 1 BeV/nucleon. Since all such particles have a specific ionization less than 1·13 times the minimum values, the determination of the charge is effectively independent of errors in $\bar{\alpha}$. The ratio of Be and B to C, N, O and F nuclei among such fast particles is found to be closely similar to the corresponding quantity for all particles taken irrespective of their velocity, see fig. 4. The number of lithium nuclei observed in the energy range above 1 BeV per nucleon, is relatively small because of inefficiency of detection (§ 2.3).

(3) It is possible to deduce a charge spectrum for the slower particles which is independent of the relation between ionization and velocity. The measurements on those tracks for which the value of $\bar{\alpha}$ is greater than $0{\cdot}04^\circ/100\,\mu$ are not appreciably affected by distortion. We may therefore determine a charge distribution by directly comparing the values of $N_\delta$ for heavy nuclei with the mean values for $\alpha$-particles with the same velocity, i.e. the same value of $\bar{\alpha}$. This procedure shows that the proportion of lithium, beryllium and boron nuclei is large. It must be noted, however, that in this case, ionization loss will have reduced appreciably the relative number of particles with charge $Z > 8$.

(4) The charge spectrum of particles with $\bar{\alpha} < 0{\cdot}011^\circ/100\,\mu$ under 58 g/cm$^2$ of atmosphere, measured by grain-counting, shows that lithium, beryllium and boron constitute $\sim 60\%$ of the observed particles.

(5) The beryllium-boron ratio is observed to be nearly independent of depth in the atmosphere (see fig. 6). In the event of an incorrect calibration this quantity might be taken to represent the boron/carbon ratio. In the absence of primary boron nuclei this ratio should be about 0·15 under 20 g/cm$^2$, and should increase to about 0·5 under 70 g/cm$^2$ of residual atmosphere.

## §3. COMMENT ON THE NATURE OF THE PRIMARY RADIATION

The evidence presented in the preceding paragraphs for the presence of considerable amounts of Li, Be and B nuclei in the cosmic radiation appears to us to be very strong. If generally accepted, it would make necessary a reconsideration of the origin and history of the radiation.

It is a matter of great interest to determine the amount of matter which the cosmic rays have traversed, before reaching the upper atmosphere, and limits can be set to this quantity. Thus, compare the number of nucleons entering the atmosphere in the form of nuclei of charge number between twenty and thirty, and with energy greater than 1 BeV/nucleon, with the total number of primary nucleons (including protons) with the same velocities. This observed ratio is 1 : 150. It follows that if all nuclei lighter than calcium are secondary in origin, then, on the average, the cosmic ray particles cannot have passed through more than about

10 g/cm$^2$ of hydrogen; for passage through a greater mass would have produced a more complete degree of fragmentation of the primary nuclei.

An independent value of this upper limit can be obtained from the observed velocity spectra of the different groups of nuclei, when taken in conjunction with certain assumptions about the origin of the radiation. Thus assume that all types of particles are initially produced with identical velocity distributions. Assume further, either that the primary particles are accelerated at sources distributed throughout the interstellar hydrogen; or, alternatively, that they originate in a distant source, all particles subsequently passing through equal amounts of hydrogen.

With the first assumption, the average amount of hydrogen traversed by a particular type of nucleus between acceleration and the top of the atmosphere is close to its mean free path for nuclear collision, and hence depends on its charge. In the second model, the amount of hydrogen traversed will be independent of charge. The effect of passage through the hydrogen will be to reduce the proportion of particles of low velocity. For a given amount of matter the effect becomes more pronounced the higher the charge on the primary.

With the first assumption, no reliable estimate of an upper limit to the average amount of hydrogen traversed can be deduced. With the second, however, even with our present approximate knowledge of the velocity distributions, we can conclude that the cosmic rays cannot have passed through more than 10 g/cm$^2$ of hydrogen. To make this estimate more precise a closer investigation of the velocity distribution of low-energy particles is desirable.

Bradt and Peters (1950) have considered a model for the origin of the cosmic rays in which they assume that no Li, Be and B nuclei are accelerated, but that heavier nuclei are retained by magnetic fields in some region surrounding the source until they are destroyed by collisions with interstellar hydrogen. On these assumptions the radiation will contain a certain fraction of Li, Be and B nuclei produced in collisions. Bradt and Peters calculate that, under these conditions, the number of Li, Be and B nuclei to be expected at the top of the atmosphere, relative to the number of C, N, O and F nuclei, is $\sim 1$, a figure consistent with the observed flux-values we have found. Such a collision equilibrium can only exist if the sources of the particles are distributed roughly uniformly throughout interstellar space.

Using the second assumption, localized production, a lower limit of 8 g/cm$^2$ for the amount of hydrogen traversed can be deduced on the assumption that no lithium, beryllium or boron nuclei are accelerated at the source, but the assumption is, of course, an arbitrary one. Lithium, beryllium, boron, are known to be extremely rare in stars and their absence is commonly attributed to their disintegration in thermo-nuclear reactions early in the main radiating life of the star. But it has been estimated that perhaps one half of the total matter in the galaxy exists as gas or dust clouds in interstellar space. It seems improbable that this matter has ever constituted part of the stars. It may therefore never have been subjected, for a sufficient length of time, to the conditions of temperature and pressure suitable for the destruction of the light elements. It follows that there is no justification for assuming the absence of lithium, beryllium and boron in interstellar matter,* because of the absence of those elements in stars. If among the other elements, lithium, beryllium and boron are accelerated in appreciable numbers, no conclusions about the length of path traversed by the cosmic radiation in interstellar space can be deduced from the observed charge spectrum.

## Acknowledgments

In conclusion we wish to thank Professor C. F. Powell, F.R.S. for his continued interest and encouragement. We also wish to thank Miss M. Stott, and Miss A. Stradling who assisted in the scattering measurements, and Miss P. Curry and Miss E. James who scanned the plates. This investigation was part of a programme of research supported by the Department of Scientific and Industrial Research to whom one of us (A.D.D.) is also indebted for a maintenance grant.

## References

Bradt, H. L., and Peters, B., 1948, *Phys. Rev.*, **74**, 1828 ; 1950, *Ibid.*, **80**, 943.
Dainton, A. D., Fowler, P. H., and Kent, D. W., 1951, *Phil. Mag.*, **42**, 317.
Fowler, P. H., 1950, *Phil. Mag.*, **41**, 169.
Freier, P., Lofgren, E. J., Ney, E. P., and Oppenheimer, F., 1948, *Phys. Rev.*, **74**, 1818.
Gottstein, K., Menon, M. G. K., Mulvey, J. H., O'Ceallaigh, C., and Rochat, O., 1951, *Phil. Mag.*, **42**, 708.
Kaplon, M. F., Peters, B., Reynolds, H. L., and Ritson, D. M., 1952, *Phys. Rev.*, **85**, 295.
Ney, E. P., and Thon, D. M., 1591, *Phys. Rev.*, **81**, 1068.
Peters, B., 1952, *Progress in Cosmic Ray Physics* (North Holland Publishing Company, Amsterdam) p. 191.
Sorensen, S. O., 1949, *Phil. Mag.*, **40**, 947.

* *Note added in proof :* See, however, a footnote in Brown, H., 1949, *Rev. Mod. Phys.*, **21**, 634.

---

## EXPLANATION OF THE PLATES

### Plate XLIV.

A nucleus of carbon, with an energy of 2·5 bev per nucleon, interacts with a nucleus of the emulsion ; among the secondary products are relativistic particles of charge $Z=1$, 2, and 3. The two photographs should be joined at *a*.

(exposure at 68,000 ft.)

### PLATES XLV and XLVI.

Characteristic tracks of particles of the primary cosmic radiation. All the tracks were produced by particles with kinetic energy greater than 1·4 BeV/nucleon and the $\delta$-ray densities are therefore close to the minimum values. It will be seen that grain-counting on the ' core ' of the tracks is impossible for particles of $Z \geqslant 4$.

(exposure at 95,000 ft.)

### PLATE XLVII.

We interpret this event as the collision of a nucleus of carbon, of energy of 700 MeV per nucleon, with a hydrogen nucleus in the emulsion. The recoiling proton produces the lightly ionizing track at ~30° to the direction of the primary particle, and the carbon nucleus splits into three $\alpha$-particles. The two photographs should be joined at $a$.

(exposure at 95,000 ft.)

# LXXII. *Nuclear Interactions of Great Energy.—Part I. Evidence for the Creation of Heavy Mesons*

By R. R. Daniel,* J. H. Davies, J. H. Mulvey and D. H. Perkins
H. H. Wills Physical Laboratory, University of Bristol†

[Received May 2, 1952]

## Summary

The masses of charged mesons, produced among the 'shower' particles in the nuclear interactions of protons of great energy have been determined by scattering and grain-density measurements. For energies greater than 50 Bev heavy mesons of mean mass $\sim 1\,300\,m_e$, provisionally identified as $\kappa$-mesons, are produced with a frequency comparable with that of the $\pi$-mesons. Evidence for the creation of such heavy mesons is also provided by an observed decrease in the ratio of neutral $\pi$-mesons to shower particles at very high energies.

A method is described for measuring the lifetime of the neutral $\pi$-meson, which takes advantage of the existence of an alternative mode of decay : $\pi^0 \rightarrow \gamma + \beta^+ + \beta^-$. It is shown that the proportion of $\pi$-mesons which decay in this second mode is not greater than 4%. The preliminary observations suggest that the mean lifetime is about $10^{-14}$ sec.

## § 1. Introduction

In recent papers from this laboratory (Parts III, IV, VI and VII of the series 'Nuclear Transmutations produced by Cosmic-Ray Particles of Great Energy') an account has been given of an analysis of several hundred high-energy disintegrations which were accompanied by the creation of showers of mesons. The events were selected at random from photographic plates exposed to the cosmic radiation at high altitudes, and at geo-magnetic latitude ~55 N°, by means of free balloons. It was concluded that in the nuclear collisions of primary particles of energy less than 10 Bev—the highest value which it was possible to measure directly—nearly all the mesons created are $\pi$-particles.

In the present paper, we describe an analysis of 'showers' produced by primary protons, with energies in the interval from 50 to 3 000 Bev. These showers have been recorded in several flights at geo-magnetic latitude ~55 N°, using both rubber balloons and inextensible plastic balloons. In each case an approximately level flight was maintained for several hours, the altitudes ranging from 65 000 to 96 000 ft.

It has been suggested (Fowler *et al.* 1951) that it is possible to account for the observed numbers of $\tau$- and $\kappa$-particles brought to rest in photographic emulsions by assuming them to be produced in the nuclear interaction of primary protons of energy greater than about 10 BEV. The present results establish that heavy mesons are indeed emitted in showers produced by protons in this energy range. The more detailed analysis presented later in the paper and in Part II, which is to follow—in which an attempt is made to determine the proportions of the energy available in the disintegrations which appear in the form of different types of mesons—is based on observations of small statistical weight, but it has been included because the results are suggestive and illustrate various modes of attack on the problems met in studying very energetic nuclear collisions.

---

* On leave from the Tata Institute of Fundamental Research, Bombay.
† Communicated by Professor C. F. Powell, F.R.S.

In the course of the work evidence was obtained which appears to establish a mode of decay of the $\pi^0$-meson according to the equation $\pi^0 \rightarrow \gamma + \beta^+ + \beta^-$. The results have a bearing on the present experiments, and the evidence is given in detail at the end of the paper.

It will be convenient to adopt the nomenclature for stars of different types employed by Camerini *et al.* (1951). Thus $n_s$ represents the number of shower particles associated with a disintegration of which the grain-density in the tracks is less than 1·5 times the minimum value; $N_h$ is the number of heavily ionizing particles with $g^* > 1{\cdot}5\, g_0$; and $E_p$ is the energy of a primary particle producing a disintegration. Mean values are indicated by square brackets, thus $\langle n_s \rangle$.

## § 2. MASS SPECTRUM

### (i) *Method of Measurement*

The mass and energy of the secondary particles emitted from nuclear disintegrations have been determined by measuring the small-angle scattering, $\bar{\alpha}$, and grain-density, $g$, along the tracks. The 'events' were recorded in Ilford G5 emulsion, 400 $\mu$ thick. Great care was taken to remove systematic errors in the measurements, and particular attention was given to establishing a satisfactory convention for grain-counting. For this purpose, subjective errors were reduced by counting all unresolved clusters, or 'blobs', as single units, a procedure which also facilitates rapid counting. The statistical error in a particular determination of the grain-density in a track was assumed to be $0{\cdot}67/\sqrt{n}$, where $n$ is the total number of 'blobs' counted. There is some indication (Hodgson 1951, Voyvodic 1952) that the distribution in the numbers of blobs/cell is more peaked than in a normal statistical sample. If this is so, the error in grain-density is well represented by the above formula. In practice, $n$ was not less than a 1000 for each of the tracks chosen for measurement.

Recent experiments (Voyvodic 1952) have shown that there is an increase in the grain-density in the track of a particle as its velocity approaches that of light. The grain-density is at a minimum for values of the quantity $p\beta/\mu c^2 = 3{\cdot}5$, where $p$ is the momentum of the particle and $\mu c^2$ its rest mass, and it increases by $\sim 8\%$ as $p\beta/\mu c^2 \rightarrow 10$.

Other experiments have shown that for greater values of $p\beta/\mu c^2$ the grain-density remains constant within the limits of experimental error (Occhialini 1949, McDiarmid 1951, Morrish 1952). In what follows, the values of the grain-density for the tracks of the particles in the extreme relativistic region will be termed 'minimum' and represented by $g^0$. Whenever possible, events were selected with primary particles for which $p\beta/\mu c^2 > 10$, and of which the track length in the emulsion was greater than 4 mm. The measurements then gave a value of $g^0$ with a probable error less than $2\frac{1}{2}\%$. The values of the grain-density for the tracks of the secondary particles of the same event were then compared with the value $g^0$ of the primary. In several events the tracks of two or more shower secondaries for which $g/g^0 < 2$ were sufficiently long to be accepted for measurement, and the degree of consistency of the results thus obtained provided an additional check on the reliability of the observations.

The values of the grain-density in the tracks of about 25% of the secondaries were normalized by comparison with that of the primary particle. In the others, the normalization was based on the tracks of primaries of neighbouring events in the same plate. The variation of the grain-density with depth was investigated, and corrections were made in the few cases where it was necessary. No event was accepted which was within a few mm of the edge of the plate where distortion of the emulsion and anomalous grain-densities are commonly found.

The scattering parameter, $\bar{\alpha}$, was determined by a method similar to that described by Fowler (1950). Each of the microscopes employed (Cooke, Troughton and Simms M.4000) had a 'stage noise' less than $0{\cdot}1\,\mu$ for cell sizes of length $\sim 200\,\mu$. The statistical error in the value of $\bar{\alpha}$ was assumed to be given by $0{\cdot}6/\sqrt{m}$, where $m$ is the number of independent cells. The cell-size was so chosen that the mean deviation, $\bar{d}$, was five times the noise level. All tracks which were too short to give a significant value of $\bar{d}$ were rejected. The other possible sources of error in the determination of $\bar{\alpha}$ were as follows:

(*a*) Distortion of the emulsion. This was detected by the rapid increase in $\bar{d}$ with cell-size, and tracks showing this effect were rejected.

(*b*) The effect of single large-angle scattering was eliminated by means of a 'cut-off' at four times the value of $\bar{d}$.

(*c*) 'Smoothing' or 'narrow-chamber' effects. This effect was particularly noticeable in the case of long tracks of mesons with energy less than 100 MeV. It was reduced to a minimum by using the shortest possible cell-size for determining the scattering.

(*d*) Change of scattering constant. In order to facilitate mass determinations, the parameter $p\beta$ was evaluated for each track using curves giving the variation of the scattering constant $k_{co}$ (for the truncated distribution) with cell-size and $\beta$. The curves have been computed by Voyvodic and Pickup (1952) and Voyvodic (1952).

Figure 1 illustrates the form of the relation between the normalized grain-density $g^*=g/g_0$ and $p\beta$. The points represent the results of measurements carried out by three groups of experimenters, viz.: (i) Danysz, Lock and Yekutieli; (ii) Voyvodic, and (iii) the present authors.

Figure 1 shows that there is satisfactory agreement between results in spite of the use of three different conventions in making grain-counts. The broken curve represents approximate, theoretical values of the ionization losses in silver bromide—normalized to correspond to the observed 'plateau' in the extreme relativistic region—as calculated by Voyvodic (1952). The solid curve drawn to fit the experimental points shows that the increase in the specific ionization with velocity is more rapid than is suggested by the theoretical treatment.

Fig. 1

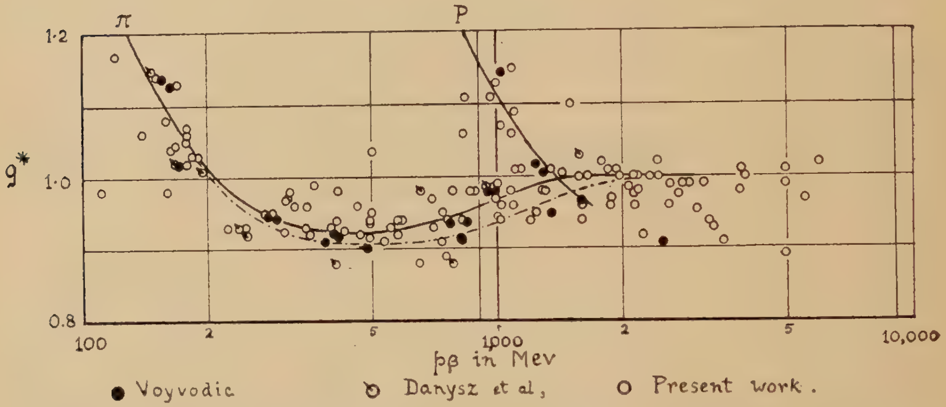

Relation between grain-density, $g^*$, and momentum × velocity, $p\beta$, for the tracks of particles from 'stars' as determined by different observers. The full lines for π-particles and protons represent the best fit to the observation. The broken line represents a theoretical relation calculated by Voyvodic.

(ii) *Mass of Secondary Particles produced by Protons of Energy*~15 Bev

Figure 2 shows the values of $p\beta$ and $g^*$ for the secondaries of showers having $N_h \geqslant 5$, and $n_s \leqslant 12$. In such events the primary energy $E_p$ is usually greater than 5 Bev and less than 50 Bev, and the average value, $\langle E_p \rangle$, was ~15 Bev. It has been assumed that, for $1{\cdot}1 < g^* < 2{\cdot}0$, the points for particles of a given mass lie on a straight line. This assumption appears to be in particularly good agreement with the results when the method of 'blob' counting is employed.

The best-fitting straight lines have been separately computed (*a*) for the π-mesons, and (*b*) for the particles with masses near that of the proton. This second line is nearly identical with that ancitipated for protons, basing the estimate on the observed line for π-mesons and assuming a mass ratio $m_p/m_\pi = 6{\cdot}66$. This result suggests that almost all the particles composing group (*b*) are protons, and that heavy mesons, if they occur at all in these events are rare compared with $\pi$-particles.

Figure 2 also includes four points obtained by determining $\bar{\alpha}$ and $g^*$ along the tracks of four $\pi$-particles which were brought to rest in the emulsion and showed the characteristic decay into a $\mu$-meson.

Fig. 2

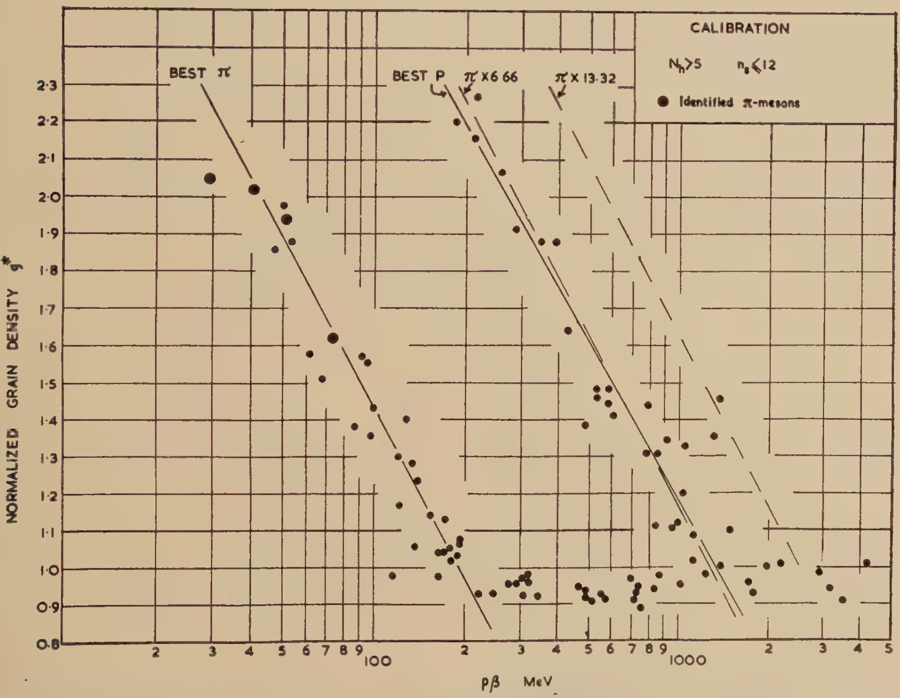

Results of measurements on tracks of particles associated with ‘ stars ’ of type $N_h \geqslant 5$, $n_s \leqslant 12$, $\langle E_p \rangle \sim 15$ BeV.

From the results shown in fig. 2 the mass corresponding to any point in the diagram can be deduced from its relationship to the line for $\pi$-particles. Figure 7 (*a*) shows the mass spectrum thus obtained for all points with values of $g^*$ between 1·1 and 2·0, assuming the mass of the $\pi$-meson to be 276 $m_e$. The bars in this figure indicate the half-width in the expected distributions corresponding to particles of a given mass, as deduced from the estimated errors in the values of $\bar{\alpha}$ and $g^*$. The median values of the two distributions give a mass ratio $m_p/m_\pi = 6{\cdot}6 \pm 0{\cdot}25$.

In obtaining the results shown in fig. 7 (*a*) the results for some stars of the type 1*p* have been included in order to increase the number of protons. The relative numbers of $\pi$-mesons and protons have therefore no clear significance.

### (iii) *Mass Spectrum of Secondary Particles produced by Protons of Great Energy. Jets*

By measuring the energy of secondary particles from a large number of 'showers' it has been found possible to determine average values of the total energy of the charged particles emitted in a nuclear disintegration as a function of the multiplicity $n_s$ for different values of $N_h$. The results are shown in fig. 3. Reference to Part VI, fig. 3 (Camerini *et al.* 1951), shows, further, that the observed width of the angular distribution for a given value of $n_s$ increases with $N_h$. These results indicate that secondary interactions play an important part in the production of stars with large values of $N_h$ and $n_s$.

Fig. 3

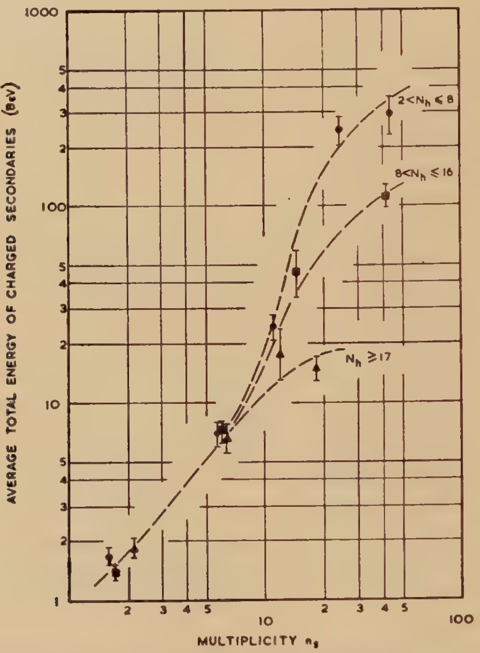

Relation between the average value of the total energy of the 'shower' particles as a function of the multiplicity $n_s$ plotted for three ranges in the value of $N_h$.

In contrast with this type of event, well-collimated showers, or 'jets', (Plates XLVIII, XLIX and LI) have been observed associated with stars having very few, and in some cases none, of the heavily ionizing tracks which are commonly produced in the 'evaporation' of a highly-excited nucleus. It will be shown later that it is reasonable to attribute many of these events to single nucleon-nucleon collisions, occurring either through the collision of the incident proton with a hydrogen nucleus or with a nucleon in the periphery of a nucleus. It seemed likely that the absence of secondary interactions in such encounters would ensure that there were only few protons among the secondary particles. If so, it appeared that such events would provide very favourable conditions for observing the emission of any heavy mesons with a mass near that of the proton. They have the further advantage that an estimate of the energy of the primary particle may be obtained from the observed angular distribution of the secondary particles. Thus, if $\eta$ is the median angle of the shower, the energy, $\gamma_p$, of the primary particle in proton mass-units is given approximately by the relation $\gamma_p=2/\eta^2$.

Table 1 shows the characteristics of a number of events of this type on which measurements have been made. When the primary energy $E_p \geqslant 50$ Bev, measurements were made on all those tracks of the secondary particles which allowed $g^*$ to be determined with a probable error less than 3%, and $\bar{\alpha}$ with an error less than 20%. The mean value of the probable error in $\bar{\alpha}$, for all tracks, was 13%. With this limitation 16% of all the shower particles associated with the events were accepted for measurement. It should be emphasized that the average value of $E_p$ for these showers is about 500 Bev.

Table 1

| $N_h$ | $n_s$ | $\gamma_p$ |
|---|---|---|
| 0 | 4 | 2000 |
| 0 | 7 | 300 |
| 0 | 7 | 2200 |
| 0 | 11 | 120 |
| 0 | 28 | 2000 |
| 1 | 9 | 1300 |
| 1 | 18 | 200 |
| 2 | 6 | 50 |
| 2 | 8 | 60 |
| 2 | 8 | 75 |
| 2 | 11 | 50 |
| 2 | 24 | 400 |
| 2 | 36 | 200 |
| 3 | 6 | 50 |
| 3 | 7 | 60 |
| 3 | 7 | 130 |
| 3 | 7 | 2300 |
| 3 | 16 | 110 |
| 3 | 26 | 150 |
| 3 | 36 ($\alpha$) | 500/nucleon |
| 4 | 20 | 50 |
| 4 | 20 | 800 |
| 4 | 22 | 100 |
| 4 | 27 | 70 |
| 4 | 50 ($\alpha$) | 800/nucleon |
| 5 | 16 | 50 |
| 5 | 26 | 650 |
| 5 | 33 | 60 |
| 7 | 43 | 300 |
| 9 | 41 | 200 |
| 14 | 47 | 400 |
| 22 | 35 | 180 |
| 25 | 54 | 60 |

The results of the measurements are shown in fig. 4, the curves being in each case identical with those drawn in fig. 2. Figure 4 includes the results for all events with primary energy estimated to be greater than 50 Bev. The mass distribution deduced from the results is given in fig. 7 (*b*), and is based upon all points for which $g^*$ lies between 1·05 and 2. The outstanding feature of the results is that almost all the secondary particles thus chosen are heavy mesons, with an average mass of about

1 300 $m_e$. We shall refer to these particles as $\kappa$-mesons since the observed mass is closely similar to that of $\kappa$-mesons arrested in the emulsion (O'Ceallaigh 1951).

Fig. 4

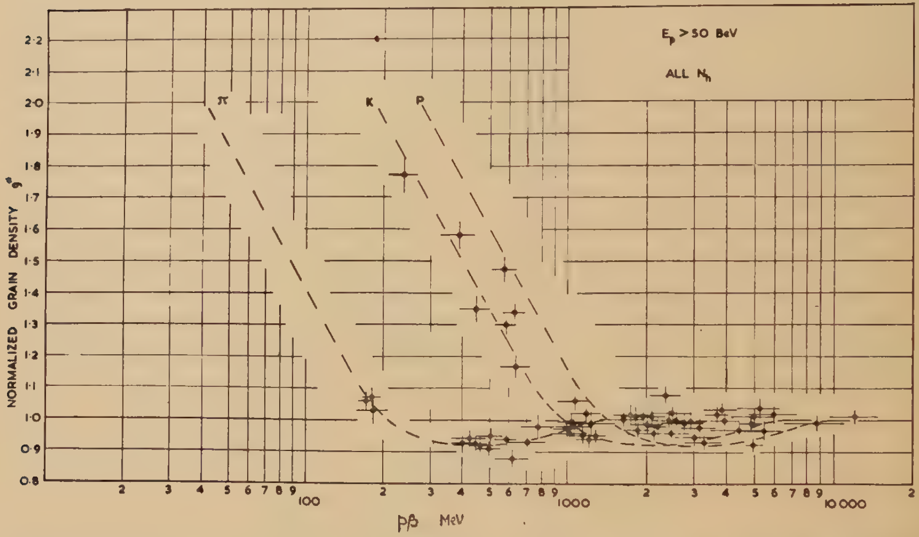

Measurements on 'stars' with $E_p > 50$ Bev., $\langle E_p \rangle \sim 300$ Bev., for all values of $N_h$.

Fig. 5

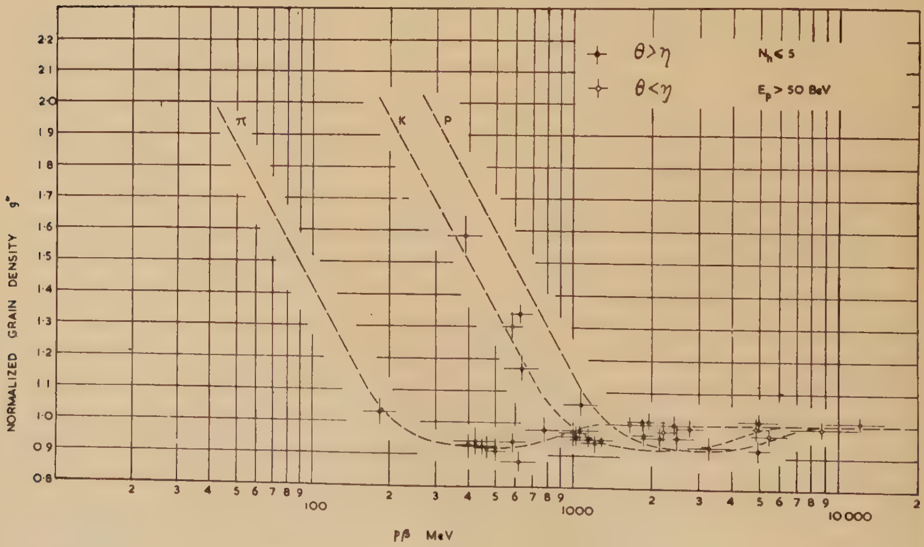

Measurements on 'stars' with $E_p > 50$ Bev., $\langle E_p \rangle \sim 500$ Bev., for values of $N_h \leqslant 5$.

It is to be emphasized that the results shown in figs. 2, 4, 5 and 6 are based on measurements made by exactly similar methods and on the same batch of plates. The distinction between them is based only on the types of parent stars with which the tracks are associated. This feature appears to exclude the possibility of systematic errors in the measurements.

Although the mass measurements are not sufficiently precise to allow a definite identification, the assumption that the slower secondary particles in the jets are $\kappa$-mesons allows us to estimate the frequency with which such particles will be observed to come to rest in the emulsion, and the result is in agreement with that observed (Menon 1951).

It is possible that more than one type of particle is present among these heavy mesons, but the spread in the observed values of the mass is consistent with the assumption of a single type. The results suggest that if there are $\tau$-particles among the heavy mesons created in events of this type they are rare. The proportion of protons among the particles is estimated to be $\sim 10\%$.

Fig. 6

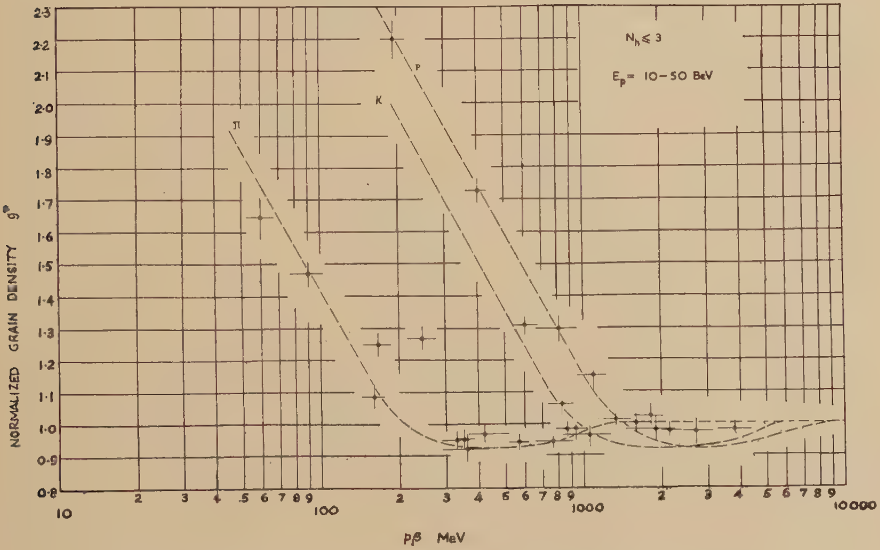

Measurements on ‘ stars ’ with $E_p = 10$–$50$ Bev., $\langle E_p \rangle \sim 30$ Bev.

Figure 5 shows similar results for jets with $N_h \leqslant 5$ and $E_p > 50$ Bev. The main features are similar to those shown in fig. 4, but it has been included because much of the more detailed analysis given later is based upon events of this type. The results for stars in which $N_h \leqslant 3$ and $10 < E_p < 50$ Bev given in fig. 6 show that the proportion of $\kappa$-particles in this energy range is small.

The measurements on one track in this series indicate that the mass of the corresponding particle was $520 \pm 70\ m_e$. Because of the possibility of occasional large statistical fluctuations in the measurements of $\bar{\alpha}$ and $g$, it cannot be stated with certainty that the particle was not a $\pi$-meson; but the probability that the particle was a $\pi$-meson is, however, less than 10%. Any systematic errors in these particular measurements can be shown to be absent because the identified secondary particles associated with the same star include a $\pi$-meson, a proton and a $\kappa$-meson. Figure 7 (*c*) shows the mass spectrum corresponding to the observations represented in fig. 6.

It is possible to make an estimate of the relative proportions of $\kappa$- and $\pi$-mesons among the secondary particles from the results given in figs. 4, 5 and 6. Some caution is necessary in interpreting them, however, because if there is a difference in the distributions in $p\beta$ for the two

Fig. 7

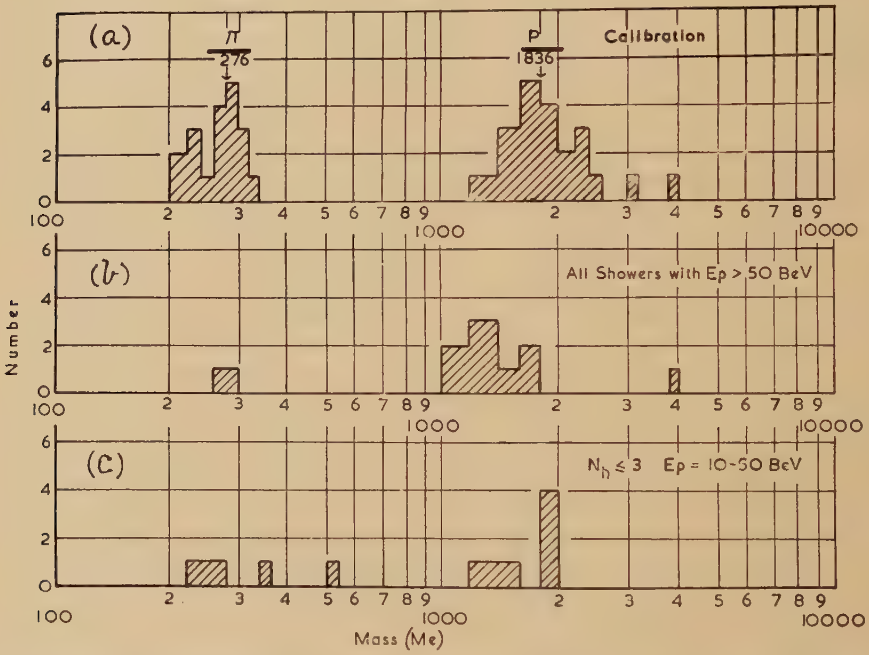

Mass spectra of secondary particles associated with ‘ stars ’ of different types.

types of particles, there may be a difference in the proportions of the two types which are accepted for measurement. In practice, any such discrimination can be reduced by considering only those tracks which make angles $\theta$ to the primary greater than $\eta$, the median angle. Such tracks correspond, we suggest, to particles emitted backwards in the C-system of the interacting nucleons, and they are represented by full circles in fig. 5. A simple analysis of the observations showed that the angular distribution of these *measured* tracks, with respect to the lines of motion of the primary particles, is indistinguishable from that of *all* tracks with $\theta > \eta$.

From the relative numbers of $\kappa$-mesons and protons on the one hand, and $\pi$-particles on the other, we find, from fig. 5,

$$\frac{N_\kappa+N_p}{N_\pi}=\frac{9}{18}=0{\cdot}5\pm0{\cdot}2.$$

For high values of $g^*$ the grain-counting convention here employed becomes impractical, and the analysis has been confined to tracks with $g^*<2{\cdot}0$. Among about 500 secondary particles in the jets with $N_h\leqslant 5$, however, only one measurable track was observed with $g^*>2{\cdot}0$.

Table 2

| Type of Event | $p\beta\leqslant 1$ Bev | | | | $p\beta\leqslant 7$ Bev | | | | $\theta>\eta$ | | | |
|---|---|---|---|---|---|---|---|---|---|---|---|---|
| | $N_k$ | $N_\pi$ | $N_p$ | $N_k/N_\pi$ | $N_k$ | $N_\pi$ | $N_p$ | $N_k/N_\pi$ | $N_k$ | $N_\pi$ | $N_p$ | $N_k/N_\pi$ |
| (*a*) $E_p\geqslant 50$ Bev All $N_h$ | 6 | 14 | 1 | 0·43 | 15 | 37 | 6 | 0·40 | — | — | — | — |
| (*b*) $E_p\geqslant 50$ Bev $N_h\leqslant 5$ | 6 | 11 | 1 | 0·36 | 8 | 22 | 4 | 0·36 | 9 | 18 | 3 | 0·50 |
| (*c*) $E_p=10$–$50$ Bev $N_h\leqslant 3$ | 2 | 11 | 3 | 0·18 | 3 | 19 | 3 | 0·16 | — | — | — | — |

## § 3. FREQUENCY OF PRODUCTION OF NEUTRAL $\pi$-MESONS

### (i) *Ratio of Neutral to Charged $\pi$-Mesons*

Additional information about the particles produced by very high energy protons can be obtained by observing electron-pairs associated with the interactions, most of which are due to the materialization of the $\gamma$-radiation produced by the decay of $\pi^0$-particles (Carlson *et al.* 1950). Knowing the average path-length of a $\gamma$-ray in the emulsion before it materializes into two electrons, a comparison of the observed number of electron pairs and the total track-length of the shower particles associated with the same ‘ stars ’ allows the relative numbers of charged and neutral $\pi$-particles $R=N_{\pi^0}/N_{\pi^\pm}$ to be determined.

In the case of high-energy distintegrations, however, in which the production of $\kappa$-particles becomes appreciable, the ratio of the number of electron pairs to the number of *shower particles* may be expected to decrease, for the latter now include some $\kappa$-particles. This argument presupposes, of course, that there are no $\gamma$-rays produced in an alternative mode in addition to those from the decay of $\pi^0$-particles. Such radiation might arise, for example, by the decay of short-lived heavy, neutral mesons or by the direct production of quanta in proton-proton collisions. If there is no such alternative source, an apparent change in the value of $R$ allows an estimate of the proportion of the $\kappa$-mesons among the $\pi$-particles to be made.

In order to employ such observations to estimate the proportion of $\kappa$-mesons amongst the shower particles it is necessary to know the value of $R$ for stars of lower energy—' stars ', that is, in which $\kappa$-mesons are never, or only rarely, produced. Carlson *et al.* (1950) found a value $R=0{\cdot}45\pm0{\cdot}15$, but later experimenters, employing other methods, have obtained different results. We therefore made new observations using a procedure similar to that previously described.

A selection was taken of stars with $n_s>6$, having secondary particles with tracks longer than about 1 mm. A sector of the plate was searched in the neighbourhood of each star, on the side opposite the track of the primary particle. A specially constructed microscope stage enabled the photographic plate to be rotated about the star as centre. The chosen area was scanned, radially from the star, for a length of 1 or 2 mm at each setting, the actual values depending upon the ' dip ' of the secondary tracks in the emulsion. The volume of emulsion thus searched contained the tracks of more than 80% of the shower particles. This procedure allowed an immediate discrimination between ' related ' and ' unrelated ' electron pairs ; for the bisector of the ' pair ' was immediately apparent, and ' pairs ' with tracks of sufficient length were already aligned for making scattering measurements. Pairs were assumed to be ' related ' and acceptable for the analysis if the bisector of the pair passed within a few microns of the star centre, and if the total energy of the pair, $E_T$, was greater than 100 MeV. The average value of the kinetic energy of the neutral mesons which produce $\gamma$-rays of 100 MeV is 70 MeV, and this is the minimum energy of a $\pi$-meson if it is to be classed as a ' shower ' particle.

Nineteen pairs satisfying the above conditions were found, associated with 140 stars, the total length of the tracks of shower particles in the area searched being 100 cm. From these observations the value of $R$ could be determined in the following manner :

(*a*) The contribution made by protons to the total track-length of the shower particles was estimated from the results given by Camerini *et al.* (1951) (fig. 5, Part VI). For the values of the multiplicity of the stars examined, $n_s=9$, the proportion of the protons in the shower particles is 16%. It follows that the total path length of the mesons in the emulsion was 84 cm.

(*b*) The angular distribution of the neutral $\pi$-mesons was assumed to be identical with that of the shower particles. It may be noted that, because the two photons arising in the decay of the neutral mesons diverge from one another, the total path-length of the photons in the emulsion is not exactly related to that of the charged mesons, but the appropriate correction was estimated to be only $\sim$2%, and can be easily applied.

(*c*) Allowance was made for the variation with energy of the average path-length of a photon before conversion into electrons, and the average value was computed to be 4·45 cm.

(*d*) Assuming that the true ratio $R_t$ of neutral to charged $\pi$-mesons is constant, it can be shown that, for a multiplicity of charged particles $n_s \neq 0$

$$R_t = R_0 \frac{n_s \cdot p(n_s)}{(n_s+1)p(n_s+1)},$$

where $p(n_s)$ is the number of stars with multiplicity $n_s$ and $R_0$ is the observed ratio. From the observed distribution in the values of $n_s$ of the stars scrutinized, the appropriate correction factor has been calculated to be 1·1.

In a single emulsion each photon commonly traverses a distance small in comparison with the average conversion length. The total length of path of the photons in the searched area of the emulsion must therefore have equalled $19 \times 4{\cdot}45 \times 1{\cdot}02 \times 1{\cdot}10 = 94$ cm. Assuming that the quanta all arise from the process $\pi^0 \rightarrow 2\gamma$, the equivalent length of path the neutral mesons would have traversed, but for their decay, is 47 cm. This is to be compared with the total length of track of the charged $\pi$-mesons, viz. 84 cm. It follows $R = 0{\cdot}56 \pm 0{\cdot}12$. This result is in good agreement with that given by the cloud-chamber experiments of Salvini (1952).

It should perhaps be emphasized that this result applies to stars of a particular classification, i.e. $n_s > 6$. This group corresponds to the interactions or primary protons of energy $E_p$ greater than about 10 Bev; the average multiplicity, $\langle n_s \rangle = 9$, corresponds to $\langle E_p \rangle \sim 25$ Bev.

In a previous paper (Camerini *et al.* 1951 b, Part VII) it was concluded that at multiplicities greater than $n_s = 10$ the multiple production of mesons predominates. A ratio $R = 0{\cdot}5$ is then to be expected. At small multiplicties, however, where mesons are produced singly, considerations of charge independence suggest that $R$ should equal 0·75. Further, if events of the type Op are included, the apparent value of $R$ will be increased. These considerations suggest that the apparent inconsistencies between the results of different experiments may be attributed, at least in part, to different distributions in the values of $n_s$ for the events on which the observations were made.

### (ii) *Alternative Mode of Decay of the Neutral π-Meson*

In addition to the nineteen electron-pairs referred to above, eleven narrow-angle pairs, identified as electrons by observations of $\bar{\alpha}$ and $g^*$, were found to originate at points less than 5 $\mu$ distant from the centre of a star. Figure 8 shows the corresponding distribution, $f(r)$, in the values of ' $r$ ', the distance of the origin of the pair from the star, for all electron pairs with values of $r$ less than 1 mm. Because of the escape of particles and quanta from the emulsion, there is a much larger chance of observing a pair for which the value of $r$ is small than one for which it is large. The effect on the observed distribution in the values of $r$ can be estimated from simple geometrical considerations, and appropriate corrections have been made to the results shown in fig. 8.

Suppose that the electron-pairs all arise by the decay of the short-lived $\pi^0$ mesons into photons. The corrected distribution $f(r)$ should then be independent of $r$ for the small values of $r$ here considered, $f(r)\,dr=k.dr$. The results shown in fig. 8 indicate, however, that a large proportion of the pairs originate at points very close to the centre of the parent disintegration. Most of these pairs cannot be attributed to the conversion of photons which have escaped from the parent nucleus.

It appears to be difficult to account for these pairs in terms of $\gamma$-radiation produced by *Bremsstrahlung* of the primary protons in the collision with the nucleus and subsequently converted into electron pairs in the field of the parent nucleus. They can, however, be readily explained in terms of an alternative mode of decay of the neutral $\pi$-meson, viz. $\pi^0\rightarrow\gamma+\beta^++\beta^-$, a process suggested by Dalitz (1951). If this assumption is correct, the results enable us to evaluate the ratio $\delta$ of the decay-constants corresponding to the two modes of decay. Thus we find that for 1 200 shower particles the numbers of $\pi^0$ mesons $=0{\cdot}56\times1\,200\times0{\cdot}84=565$, and the number of direct pairs $=11$. It follows that $\delta=11/565=0{\cdot}020\pm0{\cdot}006$.

Fig. 8

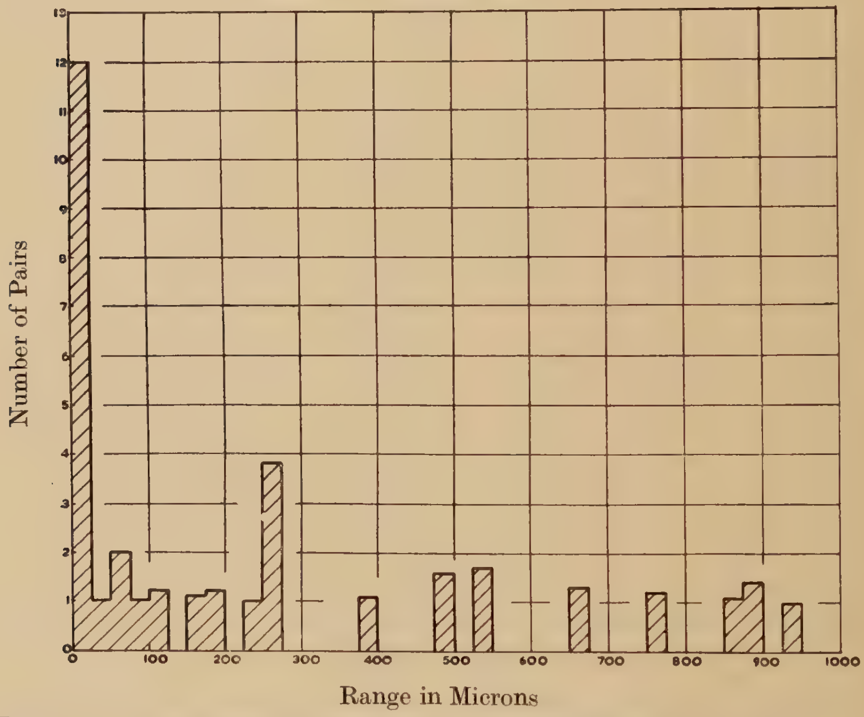

Frequency of occurrence of related electron pairs as a function of the distance of the point of origin of the pair from the parent star.

It may be pointed out that decisive evidence against the view that the close pairs are due to gamma radiation produced and converted in the parent nucleus would be provided if it could be shown that there exists a significant increase in the number of pairs originating at points near the parent nucleus, but distinct from it. At present the statistical weight of the evidence provided by the events of great energy is not sufficient for this purpose.

The calculations of Dalitz suggest that many of the pairs produced by the transmutation $\pi^0 \rightarrow \gamma + \beta^+ + \beta^-$ should show a wider angle of divergence than those of roughly the same energy arising from the conversion of $\gamma$-rays. A few single electrons have indeed been identified amongst the secondary particles which appear to emerge from nuclear explosions. In these cases a second electron may have been present, but emitted in such a direction that its track could not be identified. For this reason it is not yet possible to deduce the true distribution in the values of the angular separation of the two electrons arising in such an alternative mode of decay of the $\pi^0$-meson for comparison with the theoretical predictions.

Some pairs of electrons may also have escaped identification because their energy was too high. If, however, the energy spectrum of the electron pairs is independent of the mode of decay of the $\pi^0$-meson which leads to their production, 90% of the pairs with angular separation less than 3° have been included. If the angular distribution of the direct electron-pairs is correctly given by Dalitz's calculations, the median of the distribution of their angular divergence is, in our particular experimental conditions, $\sim 3°$. Our results therefore suggest that $\delta \ngtr 0 \cdot 04$.

The existence of an alternative mode of decay of the $\pi^0$-mesons has the consequence that there is a tendency to overestimate the average path-length of the photons by the procedure described in a preceding section. The effect is very small, however—of the order of 1%—and it has been neglected.

It should be noted that it has also been assumed that all the 19 pairs originating at points distant more than $18\mu$ from the parent 'star' are the results of photon conversion.

### (iii) *The Proportion of Mesons of Different Types*

The regions of the emulsion near high-energy 'jets' were next searched for electron-pairs in a manner similar to that described above. In general, because of the small inclination of the tracks to one another, it was possible to make a much longer scan than was profitable in the case of events of lower energy.

Twenty-three pairs were found, the corresponding total length of track of the associated shower particles being 101 cm, distributed in 33 'jets'. The energy of the primary particle was in every case greater than 50 BeV, and the total number of shower particles associated with the events was 740.

In these 'jets' any pairs arising from the direct decay process may not immediately be recognized because of the dilation of the time scale of the neutral $\pi$-mesons. (Average primary energy 500 BeV.) Assuming the probability of direct decay to be 2%, the apparent ratio of the neutral mesons to shower particles is found to be:

$$\frac{N_{\pi^0}}{N_{\pi\pm}+N_{k\pm}+N_p}=\frac{23}{(2\times101)/3\cdot75+(740\times0\cdot02)}=0\cdot33\pm0\cdot07.$$

In obtaining this result it was assumed that the mean conversion length for the photons of higher energy which are produced in jets is 3·75 cm, and that the effect of the angular divergence between each pair of photons can be neglected. Protons were estimated to contribute 10% of the total length of track of the shower particles. Corrections were also necessary because of the creation of photons in other processes. The contributions due to *Bremsstrahlung* of the primary protons, and *Abstrahlung* of the mesons in their mutual Coulomb field can be estimated from the theory of Oehme (1951). At very high energies ($E_p>1\,000$ BeV) a large proportion of the primary energy might appear in the form of photons if particles are produced in the nuclear collisions with spin greater than zero. For mesons with spin 0, however, the total contribution of *Bremsstrahlung* to the photon flux in jets appears to be only 5%.

Assuming that the mean lifetime of the neutral $\pi$-meson is $10^{-14}$ seconds or less (see below), the correction to be applied to the value of $N_{\pi^0}/n_s$ to allow for the finite path length of the $\pi^0$ is less than 2%. With these corrections we obtain

$$\frac{N_{\pi^0}}{N_{\pi\pm}+N_{k\pm}}=0\cdot35\pm0\cdot07.$$

Assuming that the value of $R$ is constant for disintegrations of all types and equal to 0·56±0·12, the value found for events of lower energy, it follows that

$$1+\frac{N_{k\pm}}{N_{\pi\pm}}=1\cdot6\pm0\cdot5\,;\quad \frac{N_{k\pm}}{N_{\pi\pm}}=0\cdot6\pm0\cdot5.$$

This value is in accord with that obtained by direct mass measurement. Although the errors are large, the results give additional support for the view that at primary energies above 50 BeV the production of heavy mesons becomes nearly as important as the production of $\pi$-mesons. It is an important feature of this second method that—in contrast with the direct determination of the mass of the shower particles, which can usually be applied only to tracks *outside* the median angle—the scan for electron-pairs includes the whole of the region of the central cone of the jets. A more extensive series of measurements to give results of greater statistical weight is therefore desirable. It may be noticed that if some photons are in fact due, not to decay of $\pi^0$-particles, but, for example, to *Bremsstrahlung* of the primary protons, the value $N(\pi^0)/N(\pi^\pm)$ will have been overestimated by the preceding method and the proportion of $\kappa$-particles underestimated.

The total energy of pairs of particles of small angular divergence associated with ' jets ' is often too great to allow the particles to be identified by measuring $\bar{\alpha}$ and $g$. In all cases, however, the observed values of the grain-density has been found nearly equal to $g_0$, and examples of *Bremsstrahlung* and trident formation have been observed along the tracks. All these features suggest that the particles are commonly electrons. Additional support for this view is provided by the observation that a slow electron, sometimes in the form of a short recoil or ' club ', is often observed at the origin of such a pair of tracks, see Plate L. Such recoil electrons are not formed by the transmutation of a neutral meson into charged particles but they are a common feature in the process of materialization of photons in the field of a nucleus through the ionization of the associated atom.

## § 4. THE SECONDARY INTERACTIONS OF THE SHOWER PARTICLES

If the heavy mesons emerging among the particles of the ' jets ' are nuclear force mesons and directly produced in high-energy nuclear collisions, they must have a cross-section for nuclear interaction of the same order of magnitude as the geometrical value. To test this view we have measured the total track-length of the shower particles associated with all the observed events produced by protons of energy $>50$ BEV, and have observed five nuclear interactions for a total length of track of 129·3 cm. Among the five interconnecting tracks, one was shown to be due to a $\pi$-meson. The measurements correspond to a mean free path for interaction of $26\pm12$ cm. If we assume that the nuclear cross-sections for interaction of all the secondary particles from the ' jets ' is equal to the geometrical value, we should expect a mean free path of 25 cm in the emulsion. Our results are therefore consistent with the assumption that the heavy mesons, as well as the $\pi$-particles, have a cross-section close to the geometrical value, and that they are directly produced in the nuclear interactions. But it will be necessary to increase the statistical weight of the observations before a final opinion is possible.

Among the shower particles from the ' jets ' we have observed two examples in which there are apparently large-angle deflections in the tracks—of 7° and 25° respectively. We have also observed a secondary particle emitted from one of the ' jets ' with an energy of $8{\cdot}8\pm1{\cdot}5$ BEV. After traversing a distance of about 1·5 cm, the scattering suddenly increases, the new value of $\bar{\alpha}$ corresponding to $2{\cdot}7\pm0{\cdot}5$ BEV. The effect can be attributed to the production of *Bremsstrahlung* by an electron. Electrons very rarely originate directly from showers, however, and then usually in pairs. It therefore appears more reasonable to interpret the event as the decay in flight of a heavy charged meson. It cannot be an example of $\pi$–$\mu$ decay because of the large decrease in energy.

It has been shown earlier that in events of the type $N_h\leqslant5$ and $E_p\geqslant50$ BEV the ratio of $N(k)/N(\pi)\sim0{\cdot}5$. This indicates a track length of 43 cm for the $\kappa$-mesons out of a total of 129 cm for all shower particles in events of this class. The $\kappa$-mesons have an average value of $\gamma \sim 7$ in the $L$ system. If we attribute the three events mentioned above to the process $\kappa - \mu$, we can make a rough estimate of the proper lifetime of the $\kappa$-mesons, and the result so obtained is $\sim 10^{-10}$ sec.

During the scan for the electron pairs we scrutinized the emulsion in the vicinity of the jets for evidence of the decay of $V^0$-particles, but without success. Assuming that the $V^0{}_2$-particles and the $\kappa$-mesons are produced in equal numbers, the path length of the $V^0{}_2$-particles in the scanned volume of the emulsion would be $\sim 43$ cm. Assuming, further, that the average value of $\gamma$ for these particles is equal to that of the $\kappa$-mesons, we obtain for the lifetime of the $V^0{}_2$-particles an upper limit of $2 \times 10^{-10}$ sec. This result is not inconsistent with the cloud-chamber evidence.

It is reasonable to suppose that in course of time the total observed length of the tracks of identified $\kappa$-particles will be sufficiently great to allow the interaction length for the particles to be determined accurately. The interaction of identified secondary particles would also be of interest in connection with the possible existence of negative protons. The annihilation of such a particle with a proton would produce a ‘ star ’ with a total release of energy greater than the kinetic energy of the parent particle by 2 BEV. In favourable conditions of observation it might be possible to recognize such an event.

## § 5. ANGULAR CORRELATION IN THE SECONDARY PARTICLES OF JETS

An investigation by Cosyns (1950) of the angular distributions of the particles emitted from high-energy disintegrations indicated a correlation in the direction of emission of pairs—and sometimes trios—of tracks. Recently the work of Danysz, Lock and Yekutieli (1952) has suggested that in stars produced by primary particles with energy less than $\sim 10$ BEV, $\sim 10\%$ of the shower particles appear as close pairs, a correlation which cannot be accounted for in terms of a random coincidence. In those cases where both particles have been identified as $\pi$-mesons, their energy is nearly equal. One interpretation of this type of event is that it is due to the decay of neutral mesons ($\zeta^0$) with a very short lifetime, the energy released in its decay being about 2 MEV.

In view of these results, a comparison of the expected and observed numbers of pairs among the shower particles in the ‘ jets ’ has been made. For this purpose it was convenient to derive an angular distribution from observations on the tracks of all events, measuring for each track the reduced angle, $\theta' = \theta/\eta$. From the distribution thus obtained the number of expected pairs due to random coincidences has been calculated for each star.

In table 3 the expected and observed numbers of pairs are shown for different values of $\delta\theta'$ and ranges of $\theta'$. The results suggest that any non-random associations are infrequent. For the smallest separation, $\delta\theta' \leqslant 0{\cdot}1$ we observed 15 pairs compared with an expected number of 8. The difference is only about twice the standard deviation but, if it is regarded as significant, it represents an association between about 3% of the shower particles. Allowing for the numbers of $\kappa$-mesons and protons present, this corresponds to about 4·5% of the $\pi$-mesons among the shower particles. The average separation for $\delta\theta' \leqslant 0{\cdot}1$ is 0·7°, which is of the right order of magnitude if the effect is attributed to the decay of $\zeta^0$-mesons, with an energy release $Q \sim 3$ MEV.

Table 3. Expected and Observed Numbers of Pairs for Different Values of the Separation $\delta\theta'$ and Angle to the Primary, $\theta'$

| Separations $\delta\theta' = \delta\theta/\eta$ | $\delta\theta' \leqslant 0{\cdot}10$ | | $\delta\theta' \leqslant 0{\cdot}15$ | | $\delta\theta' \leqslant 0{\cdot}20$ | | $\delta\theta' \leqslant 0{\cdot}25$ | |
|---|---|---|---|---|---|---|---|---|
| Intervals of $\theta' - \theta/\eta$ | Expected | Observed | Expected | Observed | Expected | Observed | Expected | Observed |
| 0·5–1·0 | 5·5 | 11 | 12·4 | 17 | 22·0 | 24 | 34·4 | 29 |
| 1·0–1·5 | 1·5 | 1 | 3·25 | 2 | 5·8 | 3 | 9·0 | 6 |
| 1·5–2·0 | 0·5 | 2 | 1·12 | 2 | 2·0 | 2 | 3·1 | 2 |
| 2·0–3·0 | 0·24 | 0 | 0·54 | 0 | 0·96 | 1 | 1·5 | 3 |
| 3·0–4·0 | 0·03 | 0 | 0·07 | 0 | 0·12 | 0 | 0·19 | 0 |
| 4·0–5·0 | 0·004 | 1 | 0·009 | 1 | 0·016 | 1 | 0·025 | 1 |
| TOTAL... | 7·7 | 15±4 | 17·4 | 22±4·5 | 31 | 31±5·5 | 48 | 41±6·5 |

At present the pairs with tracks long enough to allow determinations of $\overline{\alpha}$ and $g$ are too few to allow a search for a correlation in the energy of the particles forming a pair.

## § 6. THE LIFETIME OF THE NEUTRAL $\pi$-MESON

Dalitz (1951) has pointed out that a study of the pairs arising from direct decay of the neutral $\pi$-meson into electrons according to the equation

$$\pi^0 \rightarrow \gamma + \beta^+ + \beta^-$$

can, in principle, allow the mean lifetime of the neutral $\pi$-meson to be determined without the complications met in methods based on photon conversion.

In practice, whilst it is possible to discriminate between the pairs arising from the two modes of decay, it is not easy to determine precisely the point of origin of any pair produced by direct decay. The lifetime is so short that such pairs commonly originate very close to the centre of the parent disintegration, and no significant measurements are possible if the kinetic energy of the $\pi^0$-meson is less than 300 MEV.

At higher energies, however, the relativistic dilation of the time scale of the moving particle can increase greatly the length of path of the $\pi^0$-particles before its decay. It is then possible to measure the distribution in the value of $r/p$, where $p$ represents the quantity $\beta/\sqrt{(1-\beta^2)}$. A measure of $p$ for a given neutral meson has been obtained from the observation of its energy assuming that the photons and the pair of electrons share equally the total energy of the parent meson. The energies of a pair were determined in most cases by scattering measurements; but where this was not possible a lower limit to the energy was deduced from the angle of divergence of the electron tracks.

The probability of observing pairs at a distance $r$ from the star is

$$\left\{\frac{(2-\delta)(\exp[-r/L]-\exp[-r/pc\tau]}{L-pc\tau}+\frac{\delta}{pc\tau}\exp(-r/pc\tau)\right\}dr$$

where $L$ = mean conversion length. This expression can be normalized to correspond to the total number of $\pi^0$-particles, $N_0$. Changing the variable to $x=(r/p)$, we may write

$$N(x)\,dx$$

$$=N_0\left\{\frac{(2-\delta)\,(\exp[-xp/L]-\exp[-x/c\tau])}{L-pc\tau}+\frac{\delta}{pc\tau}\exp(-x/c\tau)\right\}p\,.\,dx.$$

Since $L$ is large and $\delta$ small, it follows that

$$N(x)\,dx \simeq N_0\left\{\frac{2\langle p\rangle}{L}(1-\exp[-x/c\tau])+\frac{\delta}{c\tau}\exp(-x/c\tau)\right\}dx,$$

Fig. 9

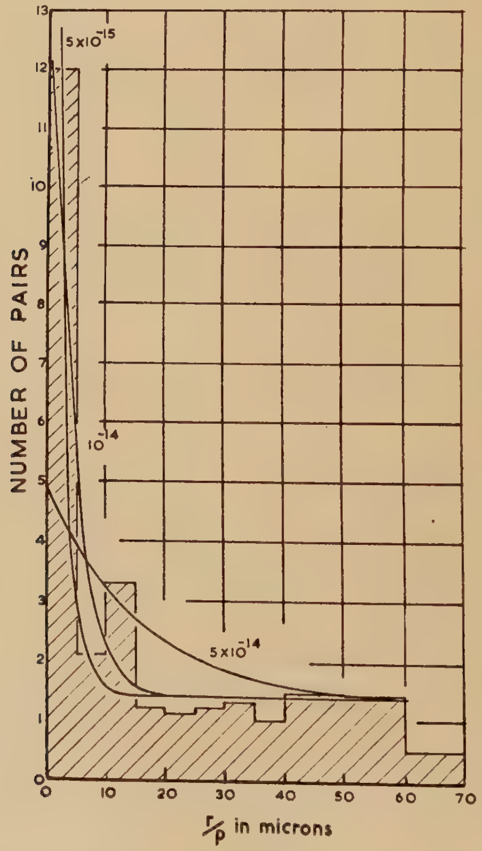

Frequency of occurrence of related electron pairs as a function of the quantity $r/p$, where $r$ is the distance of the point of origin of the pair from the parent star and $p$ is the quantity $\beta/(1-\beta^2)$. The curves were calculated for different values of the proper lifetime of the $\pi^0$-meson.

where $\langle p \rangle$ is the average value of $p$. Figure 9 shows this function plotted for $L=4$ cm using the observed value of $\delta=0{\cdot}02$ and values of $\tau$ equal to $5\times10^{-15}$, $10^{-14}$ and $5\times10^{-14}$ sec. The results may be compared with the experimental distribution after it has been corrected with the appropriate geometrical factors to allow for 'loss' from the emulsion. The corrections for loss become large as $r$ increases, and the distribution in $(r/p)$ is therefore plotted only up to $70\,\mu$.

The best fit between the experimental results and the theoretical curves appears to occur for $\tau=10^{\ 14}$ sec. While the results do not at present allow us to exclude a shorter lifetime, it appears reasonable to attach some significance to the slight increase in the observed number of pairs for small values of $(r/p)$, and the method appears to justify further attention. The value $10^{-14}$ sec agrees with that obtained by Kaplon, Peters and Ritson (1952).

## § 7. Conclusions

Our main conclusions may be summarized as follows:

1. In the nuclear collisions of primary protons of energy greater than 50 BEV production of heavy mesons, provisionally identified with $\kappa$-particles, competes strongly with $\pi$-meson production.

2. We have as yet no evidence that, even at the highest energies considered (1 000 BEV) production of charged mesons other than $\pi$- and $\kappa$-mesons is an important process. The energy available in the C-system in the events studied lies between 10 and 70 proton masses. It follows that the production of any strongly-interacting particles, of mass comparable with, or even considerably greater than, that of the nucleon, is energetically possible. No such particles have been observed.

3. There is rough agreement between the ratio of the numbers of $\kappa$- and $\pi$-particles produced in the disintegrations, as determined by direct measurement, and as deduced from the frequency of occurrence of related electron-pairs.

4. The mean lifetime of the $\pi^0$-meson is found to be $\sim10^{-14}$ sec, a result in agreement with those of Kaplon, Peters and Ritson (1952).

5. The probability of direct decay of the $\pi^0$-meson according to the scheme $\pi^0\rightarrow\gamma+\beta^++\beta^-$ is not greater than 4%.

6. The lifetime of the $\kappa$-mesons is $\sim10^{-10}$ sec.

## Acknowledgments

We have pleasure in thanking Professor C. F. Powell, F.R.S., for his continued interest and encouragement, Miss P. Dyer and Mr. A. R. Gattiker for the photographs, and the team of microscope observers of this laboratory for their careful scanning of the plates. J. H. M. wishes to thank the Department of Scientific and Industrial Research for a maintenance grant, and R. R. D. the Government of India for an Overseas Scholarship.

This work has been carried out as part of a programme of research supported by the Department of Scientific and Industrial Research.

## REFERENCES

CAMERINI, U., FOWLER, P. H., LOCK, W. O., and MUIRHEAD, H., 1950, *Phil. Mag.*, **41,** 413 (IV).

CAMERINI, U., DAVIES, J. H., FOWLER, P. H., FRANZINETTI, C., MUIRHEAD H., LOCK, W. O., PERKINS, D. H., and YEKUTIELI, G., 1951, *Phil. Mag.*, **42,** 1241 (VI).

CAMERINI, U,. DAVIES, J. H., FRANZINETTI, C., LOCK, W. O., PERKINS, D. H. and YEKUTIELI, G., 1951, *Phil. Mag.*, **42,** 1261 (VII).

CARLSON, A. G., HOOPER, J. E., and KING, D. T., 1950, *Phil. Mag.*, **41,** 701 (V).

COSYNS, M. G. E., 1949, *Nuovo Cim.* **6** (Supp. No. 3) 397 ; 1950, *Report of Harwell Conference*, **19,** 1950.

DALITZ, R. H., 1951, *Proc. Phys. Soc.* A, **64,** 667.

DANYSZ, M., LOCK, W. O., and YEKUTIELI, G., 1952, *Nature, Lond.*, **169,** 364.

FOWLER, P. H., 1950, *Phil. Mag.*, **41,** 169 (III).

FOWLER, P. H., MENON, M. G. K., POWELL, C. F., ROCHAT, O., 1951, *Phil. Mag.*, **42,** 1040, (II).

HEITLER, W., and JÁNOSSY, L., 1949, *Proc. Phys. Soc.* A, **62,** 364, 669 ; 1950, *Helv. Phys. Acta*, **23,** 417.

KAPLON, M. F., PETERS, B., and RITSON, D.M. (in course of publication).

MENON, M. G. K., 1951, *Bristol Conference on V-particles and Heavy Mesons.*

McDIARMID, I. B., 1951, *Phys. Rev.*, **84,** 851.

MORRISH, A., 1952. *Phil. Mag.*, **43,** 533.

OCCHIALINI, G. P. S., 1949, *Report of Como Conference.*

O'CEALLAIGH, C., 1951, *Phil. Mag.*, **42,** 1032 (I).

OEHME, R., 1951, *Z. Phys.*, **129,** 573.

SALVINI, G., 1952, Private communication.

VOYVODIC, L., and PICKUP, E., 1952, *Phys. Rev.*, **85,** 91.

VOYVODIC L., 1952 (in course of publication).

---

## EXPLANATION OF PLATES.

Photomicrographs of 'jets' produced by primary particles of various energies. The nomenclature $x+yp$ indicates an event containing $y$, shower particles, and $x$, heavily ionizing particles.

### Plate XLVIII

'Jets' produced by primaries of energy above 1000 BeV. One of the secondary particles in event (*c*) produces a second shower of type $(7+13p)$.

### Plate XLIX

Three 'jets' which provide evidence for the creation of heavy ($\kappa$) mesons. In stars (*a*) and (*b*) the mass of these particles has been determined from measurement of Coulomb scattering and grain density. In (*c*) the Coulomb scattering of one of the secondaries increases by a factor of three after it has traversed 12 mm of emulsion. This event is provisionally ascribed to the decay in flight of a heavy meson ($\kappa \rightarrow \mu$?).

### Plate L

A 'jet' of primary energy about 300 BeV, with an associated electron pair, total energy 5 BeV, created by conversion of a $\gamma$-ray originating from decay of a neutral $\pi$-meson. The initial grain density of the track of the electron pair is seen to be about twice that of one of the neighbouring shower particles. One of the electrons produces a second electron pair (trident formation).

### Plate LI

Two examples of 'jets' produced by energetic primary alpha particles.

# LXXIII. *The Unit Cell and Brillouin Zones of* $Ni_4Mn_{11}Al_{60}$ *and Related Compounds*

By Keith Robinson
Senior 1851 Exhibitioner, Crystallographic Laboratory, Cavendish Laboratory, Cambridge, England*

[Received March 19, 1952]

## Summary

The compounds based on the ideal formulae $Ni_4Mn_{11}Al_{60}$ and $Cu_2Mn_3Al_{20}$ have similar structures and a prominent Brillouin Zone which would be expected to contain 1·74–2·04 electron states per atom. $ZnMn_5Al_{24}$ has a different structure and a slightly smaller prominent Brillouin Zone. The size of the prominent Brillouin Zones is consistent with the known composition ranges of the compounds, provided the transitional metal atoms are assumed to remove loosely bound electrons from the structure as a whole, to about the extent suggested by Raynor (1944 b). Although the present work gives no information concerning the mechanism by which these electrons are removed, the magnitude of the effect strongly suggests that it is by absorption of otherwise free electrons into the vacancies in the 3d atomic orbitals of the transitional metal atoms. More direct evidence for this suggestion in the case of Mn atoms has been obtained by the author (Robinson 1952) in the examination of the structure of the compound $Mn_3SiAl_9$.

## §1. Introduction

On the basis of metallographic examinations Raynor (1944 a, b) has shown that related ternary compounds exist in the systems Al–Mn–Ni and Al–Mn–Cu. These compounds have been given formulae $Ni_4Mn_{11}Al_{60}$ and $Cu_2Mn_3Al_{20}$, respectively, but whereas different samples of the former deviate little from the ideal formula, the samples of the latter show a considerable variation of composition ranging from 7·8 atomic per cent Cu and 12·1 atomic per cent Mn when the phase is in equilibrium with both solid aluminium and $CuAl_2$ up to 6·9 atomic per cent Cu and 15·0 atomic per cent Mn when in equilibrium with aluminium and $MnAl_6$.

Raynor suggested that the formation of these two compounds is controlled to a considerable extent by two factors :—

(i) A composition based on four aluminium atoms to every atom of the heavier elements ;

(ii) The attainment of an electron/atom ratio of approximately 1·85, calculated on the assumption that each aluminium atom contributes three loosely bound electrons and each copper atom one loosely bound electron, whilst *on the average each manganese atom removes* 3·66, *and each nickel atom* 0·61, *of these electrons.* This led to the suggestion that a compound governed by the same factors might be found in the Al–Mn–Zn system. Such a phase has been found by Raynor and Wakeman (1947) with the predicted chemical composition, which is very close to $ZnMn_5Al_{24}$.

---

* Communicated by W. H. Taylor.

If the electronic factor is important in determining the stability of these phases, the theory of Jones (1934) would suggest that their structures should be associated with very prominent Brillouin Zones, and if the zones are symmetrical the inscribed spheres would be expected to contain about 1·85 states per atom, or possibly slightly less. The faces of the prominent Brillouin Zones are those across which there is a large energy discontinuity. As the magnitude of the energy discontinuity is roughly proportional to the structure amplitude of the corresponding crystallographic plane, the forms of the prominent zones may be obtained readily from x-ray data. For this purpose it is sufficient to know only the unit cell dimensions, so that indices may be attached to the very intense reflexions. This paper gives details of the determination from x-ray data of the prominent Brillouin Zones of the compounds $Ni_4Mn_{11}Al_{60}$, $Cu_2Mn_3Al_{20}$ and $ZnMn_5Al_{24}$. It is an abridged and amended form of part of a degree dissertation, Robinson (1951).

## §2. EXPERIMENTAL

Samples of single crystals of all three compounds have been kindly supplied by Professor Raynor and have been examined by standard oscillating-crystal and Weissenberg techniques using MoK$\alpha$ radiation (wave-length, $\lambda=0{\cdot}7107$ Å). The unit cell dimensions have been determined approximately either from the separation of high layer-lines, or from Weissenberg photographs on which no reflexions occur at Bragg angles, $2\theta$, greater than 120°. The accuracy is therefore probably only about a half per cent, but is satisfactory for the present purpose.

## §3. THE UNIT CELL AND PROMINENT BRILLOUIN ZONES OF $Ni_4Mn_{11}Al_{60}$

This compound crystallizes in the form of thin rectangular plates. The unit cell is orthorhombic with $a_0=23{\cdot}8$ Å, $b_0=12{\cdot}5$ Å and $c_0=7{\cdot}55$ Å when the *a*-axis is taken to coincide with the normal to the rectangular plate and the *b*-axis coincides with the shorter of the plate edges. Systematically absent reflexions indicate that the space group is $D_{2h}^{17}$–Bbmm, $C_{2v}^{16}$–Bbm2 or $C_{2v}^{12}$–Bb2m. From the observed density of $3{\cdot}62\pm0{\cdot}05$ g cm$^3$ it follows that there are 1·99 formula units per unit cell; it may therefore be inferred that there are two 'molecules' of $Ni_4Mn_{11}Al_{60}$, i.e. 150 atoms, per unit cell, whence the mean atomic volume is 15·0 Å$^3$.

Intensities of reflexions with $\sin\theta/\lambda<0{\cdot}28$ Å$^{-1}$ have been measured and corrected for Lorentz and polarization factors. On a scale of 10 units only 18 out of a total of 133 non-systematically absent reflexions have intensities greater than 1 unit, and 10 of these do not exceed 2 units. The remaining 8 reflexions are listed on the left hand side of table 1, and it is to be noted that they all occur at values of $\sin\theta/\lambda$ very close to 0·24 Å$^{-1}$. The first important Brillouin Zone of the structure is therefore bounded by faces which lie parallel to these 8 sets of crystallographic planes.

Table 1. Strong x-ray Reflexions from $Ni_4Mn_{11}Al_{60}$

| *hkl* | $\sin\theta/\lambda$ (Å$^{-1}$) | Int. | *hkl* | $\sin\theta/\lambda$ (Å$^{-1}$) | Int. |
|---|---|---|---|---|---|
| 650 | 0·236 | 4 | 11·61 | 0·339 | s |
| | | | 064 | 0·358 | s |
| 060 | 0·240 | 10 | 13·53 | 0·393 | s |
| 333 | 0·240 | 10 | | | |
| 11·01 | 0·240 | 8 | 006 | 0·398 | vs |
| 10·30 | 0·242 | 6 | 010·0 | 0·400 | vs |
| 832 | 0·245 | 8 | 18·02 | 0·400 | vs |
| 703 | 0·247 | 9 | 555 | 0·401 | s |
| 004 | 0·265 | 6 | 11·05 | 0·403 | vs |
| | | | 656 | 0·463 | s |
| | | | 066 | 0·465 | vs |
| | | | 10·36 | 0·465 | vs |

Intensities of reflexions with $\sin\theta/\lambda$ greater than 0·28 Å$^{-1}$ have only been estimated qualitatively. The strong (s) and very strong (vs) reflexions are listed on the right-hand side of table 1, the latter being several times as intense as the former. It is clear that the second and third prominent zones are formed by groups of planes with $\sin\theta/\lambda$ close to 0·400 Å$^{-1}$ and 0·465 Å$^{-1}$ respectively.

For the purpose of calculations on the first zone, the {650} faces, across which there would be the smallest energy discontinuity, have been omitted, but their inclusion would not appreciably affect the results. Figure 1 is a drawing of the first prominent Brillouin Zone in wave number ($k$) space; each zone face ($hkl$) lies at a distance from the origin of

$$1/2d(hkl)=\sin\theta/\lambda\ \text{Å}^{-1},$$

$d(hkl)$ being the crystallographic interplanar spacing. Because of the large number of faces, almost equidistant from the origin, the zone approaches a sphere in shape, the volume of the inscribed sphere being 0·85 of the volume of the whole zone. The volume of the inscribed sphere is $(4\pi/3)(0{\cdot}240)^3$ Å$^{-3}$, and since each unit volume of $k$-space corresponds to 2 electron states per unit volume of real space, the electron/atom ratio corresponding to the inscribed Fermi distribution of the zone is

$$2\times\frac{4\pi}{3}(0{\cdot}240)^3\times 15{\cdot}0=1{\cdot}74\ \text{electrons/atom},$$

15·0 Å$^3$ being the mean atomic volume.

This only serves to fix an *approximate* value for the electron/atom ratio which might be associated with any compound having a structure of the type possessed by $Ni_4Mn_{11}Al_{60}$. It assumes a spherically symmetrical Fermi distribution of states and does not allow for any bulging out towards the corners of the zone, nor for the fact that some of the faces (notably {004}) correspond to slightly higher energies. If, for instance, the calculation were based on a spherical distribution of radius equal to the *mean* $\sin\theta/\lambda$ of the appropriate planes, (=0·244 Å$^{-1}$, allowing for multiplicity of faces) then a value of 1·83 electrons/atom would be obtained.

The second prominent zone lies completely outside the first, and similar calculations show that an inscribed spherical Fermi distribution would need approximately 8·3 free electrons/atom.

Fig. 1

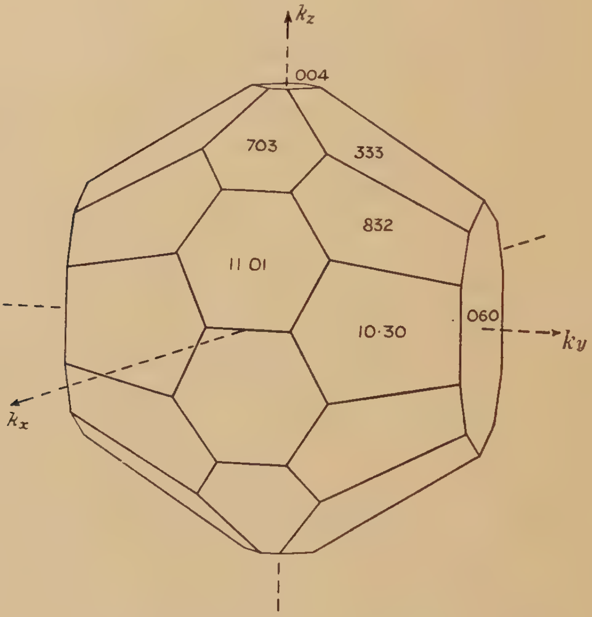

The first prominent Brillouin Zone of $Ni_4Mn_{11}Al_{60}$.

## §4. THE COMPOUNDS $Cu_2Mn_3Al_{20}$ AND $ZnMn_5Al_{24}$

In table 2 the unit cells of these compounds are compared with that of $Ni_4Mn_{11}Al_{60}$. Not only is the cell size of $Cu_2Mn_3Al_{20}$ very close to that of $Ni_4Mn_{11}Al_{60}$, but there is also very little difference in the intensities of those reflexions which it has been possible to compare, namely those of types $(h0l)$, $(h3l)$ and $(hkh)$. The basic structure may therefore be assumed to be essentially the same as that of $Ni_4Mn_{11}Al_{60}$. X-ray photographs from all crystals of $Cu_2Mn_3Al_{20}$, however, reveal twinning by reflexion across {101}. The crystals grow as rectangular plates, the longest edge being the *b*-axis ; the normal to the well-developed face is the direction [101] in one twin component and $[\bar{1}0\bar{1}]$ in the other.

The strongest scattering planes of $Cu_2Mn_3Al_{20}$ with $\sin\theta/\lambda$ less than 0·3 Å$^{-1}$ are the same as those listed in table 1 for $Ni_4Mn_{11}Al_{60}$, although there are very small changes in $\sin\theta/\lambda$ due to the slight change in cell dimensions. It is of interest to note, however, that the first zone for the different twin components remains approximately the same shape without any need for reorientation. This is shown in fig. 2, in which the poles of the zone faces are projected on the $k_xk_z$ plane; all the poles occur in pairs, one for each twin component.

Table 2. Unit Cell Dimensions (in Å) of the Three Ternary Compounds

| | $a_0$ | $b_0$ | $c_0$ |
|---|---|---|---|
| $Ni_4Mn_{11}Al_{60}$ | 23·8 | 12·5 | 7·55 |
| $Cu_2Mn_3Al_{20}$ | 24·2 | 12·5 | 7·72 |
| $ZnMn_5Al_{24}$ | 25·1 | 24·8 | 30·3 |

Fig. 2

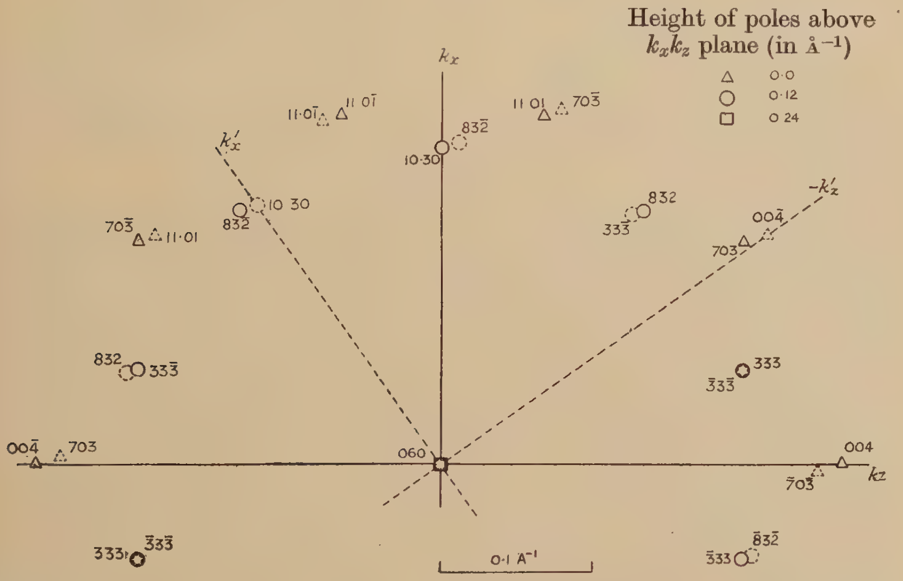

The poles of the faces of the first prominent Brillouin Zone of $Cu_2Mn_3Al_{20}$. The full and dotted lines refer to different twin components.

Single crystals of $ZnMn_5Al_{24}$ are approximately equi-axed; they too are orthorhombic (see table 2). Many exhibit an apparent 4-fold symmetry axis (*c*-axis) with well-developed {001} faces and smaller {101}, {011}, {110}, {031} and {301} side faces. Systematic absences indicate that the structure is centred on its *C* face. All reflexions with *h* or *k* odd are very weak indeed, and if these were to be ignored the remaining reflexions would correspond to a body-centred cell of size $a_0/2 \times b_0/2 \times c_0$. The x-ray intensities differ considerably from those of the other two compounds suggesting that the structure is appreciably different.

The very intense reflexions with sin $\theta/\lambda$ less than 0·3 Å$^{-1}$ are listed in table 3 and again they all lie in a small range of sin $\theta/\lambda$ values, the mean value allowing for multiplicity of faces being 0·237 Å$^{-1}$. The density of crystals of composition very close to $ZnMn_5Al_{24}$ is $3{\cdot}70 \pm 0{\cdot}02$ g/cm³ giving a mean atomic volume of 14·8 Å³. Hence the number of states per atom in a Fermi sphere of radius 0·237 Å⁻¹ would be

$$\frac{8\pi}{3}(0{\cdot}237)^3 \times 14{\cdot}8 = 1{\cdot}65,$$

which is somewhat smaller than the corresponding number for $Ni_4Mn_{11}Al_{60}$.

Table 3. Strong x-ray Reflexions from $ZnMn_5Al_{24}$

| *h* | *k* | *l* | sin θ/λ (Å⁻¹) | *h* | *k* | *l* | sin θ/λ (Å⁻¹) |
|---|---|---|---|---|---|---|---|
| 0 | 0 | 14 | 0·231 | 6 | 0 | 13 | 0·245 |
| 0 | 4 | 14 | 0·243 | 6 | 6 | 10 | 0·237 |
| 0 | 10 | 9 | 0·250 | 6 | 10 | 4 | 0·243 |
| 0 | 12 | 0 | 0·242 | | | | |
| | | | | 10 | 0 | 7 | 0·230 |
| 4 | 6 | 11 | 0·232 | 10 | 4 | 7 | 0·244 |
| 4 | 10 | 3 | 0·222 | 10 | 6 | 2 | 0·235 |
| | | | | 12 | 0 | 0 | 0·240 |

## § 5. DISCUSSION

The x-ray data from these three compounds show that there is only one Brillouin Zone which could be effective in limiting the number of loosely bound electrons, for the second and third prominent zones are much too large, whilst the energy discontinuities across other possible zone faces are too small to be of any importance. If for the compounds $Ni_4Mn_{11}Al_{60}$ and $Cu_2Mn_3Al_{20}$, the electronic factor is of importance, the number of loosely bound electrons per atom would be expected to lie between 1·74 when the electronic energy would first begin to rise rapidly and 2·04 when the first prominent Brillouin Zone would be completely filled. By assuming normal ' valencies ' of +3 and +1 for aluminium and copper respectively it is therefore possible to estimate the contribution of the transition metal atoms to the total number of loosely bound electrons in these compounds.

The work of Ekman (1931) has led to the suggestion that in certain metallic structures transitional metal atoms behave as if they possessed zero valency. This accounts satisfactorily for the β brass type of structure of FeAl, CoAl and NiAl, for the γ brass type of structure of $Fe_5Zn_{21}$, $Co_5Zn_{21}$ and $Ni_5Zn_{21}$ and for the occurrence of other phases (see for example Hume-Rothery, 1947). In the present case, however, application of this rule would yield electron/atom ratios between 2·4 and 2·5 which bear no relation to the sizes of the prominent Brillouin Zones. Similarly, Pauling's suggestion (1949) that Mn and Ni should be sexi-valent, whilst Cu and Zn should have valencies of 5·5 and 4·5 respectively, would not be consistent with the form of the zones, for these values would lead to ratios lying between 3·5 and 3·6.

On the other hand, the effective *negative* valencies for the transitional metal atoms suggested by Raynor (1944 b) or by the band theory of

Mott and Jones (1936) would give electron/atom ratios close to those predicted from the forms of the first prominent Brillouin Zones. The magnitudes of these negative valencies have in the first case been taken to be the numbers of vacancies in the atomic orbitals of the 3d shell of the model of the transitional metal atoms proposed by Pauling (1938), viz. an average of 3·66 vacancies per Mn atom and 0·61 per Ni atom, whilst similar reasoning based on the band theory model leads to the integral values of 3·0 and 0·0 vacancies respectively. Electron/atom ratios calculated on (*A*), the Raynor model, and (*B*), the band theory model, have been given for the compounds under consideration by Pratt and Raynor (1951) and are shown below :—

| | $Ni_4Mn_{11}Al_{60}$ | $Cu_2Mn_3Al_{20}$ | $ZnMn_5Al_{24}$ |
|---|---|---|---|
| (*A*) | 1·83 | 1·76–2·03 | 1·85–1·88 electrons/atom |
| (*B*) | 1·96 | 1·87–2·12 | 1·96–2·00 electrons/atom |

In the case of $Ni_4Mn_{11}Al_{60}$ with its almost invariant composition either (*A*) or (*B*) is consistent with the range 1·74–2·04 electrons/atom suggested by the form of the first prominent Brillouin Zone, but it is striking that for the copper phase (*A*) gives better agreement than (*B*), especially in that the upper limit of 2·12 electrons/atom exceeds the possible content of the full zone. Similarly, the slightly smaller first prominent zone of the zinc compound gives somewhat better agreement with the upper limit of the range of electron/atom ratios calculated for (*A*).

The agreement is sufficiently good to confirm that these phases are electron compounds characterized by an electron/atom ratio of about 1·8 to 2·0 electrons/atom and by a ratio of four aluminium atoms to each heavy atom. The fact that this agreement is achieved on the supposition that transitional metal atoms have an effectively negative valency is further evidence in support of Raynor's assumptions about the nature of the rôle played by these atoms in aluminium-rich intermetallic compounds. This in no way contradicts the suggestions of Ekman and Hume-Rothery that in the $\beta$ and $\gamma$ brass types of structure the transitional metal atoms are effectively zero-valent. Rather it implies that these atoms may play different rôles in different types of intermetallic compound. The chief characteristic of the aluminium-rich compounds is that the transitional metal atoms are in an electron-rich environment, whilst in the $\beta$ and $\gamma$ structures the other atoms provide far fewer loosely bound electrons. It may well be that in some structures transitional metal atoms may lie in different environments, so that an atom lying in an electron-rich part of the structure might behave as if it had a negative valency, whilst a similar atom lying in an electron-poor environment might be effectively zero-valent.

A further point of interest concerns the possible relationship of the structure of the compounds described in this paper to those of other aluminium-rich compounds not necessarily having a ratio of four aluminium atoms to each heavy atom. For instance, the unit cell dimensions of the binary compounds $Cr_2Al_{11}$ and $CrAl_7$ determined by Little (1949) are the same as those of $ZnMn_5Al_{24}$ within the limits of experimental error, and both give diffraction effects consistent with the presence of smaller sub-units of structure as in the case of $ZnMn_5Al_{24}$. The electron/atom ratios of these compounds, assuming each Cr atom to remove 4·66 electrons from the structure as a whole as suggested by Raynor, would be 1·82 for $Cr_2Al_{11}$ and 2·04 for $CrAl_7$. It remains to see whether or not the strongly scattering planes bear any relationship to those of the ternary compound, and it is hoped to examine this point as soon as possible.

## ACKNOWLEDGMENTS

I am indebted to Professor Sir Lawrence Bragg, F.R.S., and Dr. W. H. Taylor for the provision of facilities and for their interest in the progress of this work. Professor G. V. Raynor of the University of Birmingham very kindly supplied the crystals described in this paper. For financial assistance I wish to thank the Ministry of Supply (Basic Properties of Metals Committee) and the Royal Commissioners for the Exhibition of 1851.

## REFERENCES

EKMAN, W., 1931, *Z. phys. Chem.* B, **12,** 57.

HUME-ROTHERY, W., 1947, *Structure of Metals and Alloys* (London : Institute of Metals), pp. 112–116.

JONES, H., 1934, *Proc. Roy. Soc.* A, **144,** 225.

LITTLE, K., 1949, *Dissertation,* University of Oxford.

MOTT, N. F., and JONES, H., 1936, *The Theory and Properties of Metals and Alloys* (Oxford : University Press).

PAULING, L., 1938, *Phys. Rev.*, **54,** 899 ; 1949, *Proc. Roy. Soc.* A, **196,** 343.

PRATT, J. N., and RAYNOR, G. V., 1951, *Proc. Roy. Soc.* A, **205,** 103.

RAYNOR, G. V., 1944 a, *J. Inst. Met.*, **70,** 507 ; 1944 b, *Ibid.*, **70,** 531.

RAYNOR, G. V., and WAKEMAN, D. W., 1947, *Proc. Roy. Soc.* A, **190,** 82.

ROBINSON, K., 1951, *Ph.D. Dissertation,* University of Cambridge ; 1952, *Acta Cryst.*, in press.

# LXXIV. *An Example of Multiple Meson Production*

By W. Bosley and H. Muirhead
Department of Natural Philosophy, University of Glasgow*

[Received April 1, 1952]

## Summary

A description is given of an event, found in a nuclear emulsion exposed to the cosmic radiation, in which two $\pi$-mesons and a proton or deuteron are the only particles observed. Reactions which could produce this event are discussed.

---

## §1. Introduction

The event shown in Plate LII was found during the examination of a nuclear emulsion which had been exposed to the cosmic radiation at high altitude. From the point X three tracks diverge; the heavily ionizing track C follows the characteristic $\pi$-$\mu$-$e$ sequence, and the lightly ionizing tracks A and B move in nearly opposite directions. The projected directions of the three tracks in the plane of the emulsion and the angles which they make with this plane in the unprocessed emulsion are given in fig. 1. Track A remained inside the emulsion for 1 300 $\mu$ and track B for 4 400 $\mu$.

Fig. 1

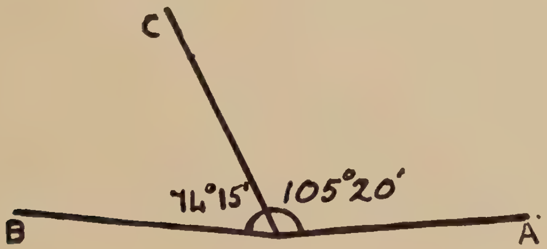

(*a*)

Angles which tracks A, B and C make with each other when projected onto the plane of the emulsion.

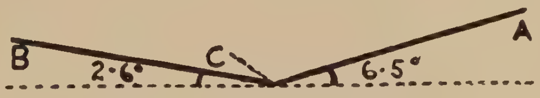

(*b*)

Angles of tracks A, B and C with respect to the plane of the emulsion. The track C lies flat in this plane within the limits of experimental observation.

---

* Communicated by Professor P. I. Dee, F.R.S.

## §2. IDENTIFICATION OF TRACKS

The identification of the tracks of fast ionizing particles in nuclear emulsions can normally be made by measurements on the grain density and multiple coulomb scattering (Fowler 1950). Curves relating these two quantities for normal emulsions have been published by the Bristol group (Camerini *et al.* 1950). The present event was found in a ×2 diluted Ilford G5 emulsion (Dodd and Waller 1951), and after measurements of the grain density and mean angle of scattering had been made for tracks A and B, the equivalent values for normal emulsions were obtained by using the data on the characteristics of normal and diluted emulsions, given in a previous communication (Bosley and Muirhead 1952).

The equivalent values of $\bar{\alpha}$, the mean angle of scattering, for tracks A and B were $0{\cdot}18 \pm 0{\cdot}08$ and $0{\cdot}018 \pm 0{\cdot}008°/100\,\mu$ respectively. (The effects of distortion were found to be negligible both by an examination of the experimental scattering measurements (Fowler 1950), and by tests for emulsion distortion (Cosyns and Vanderhaeghe 1950).)

The ratios of grain densities of tracks A and B to that at minimum ionization were $1{\cdot}13 \pm 0{\cdot}06$ and $1{\cdot}11 \pm 0{\cdot}04$ respectively. (The errors quoted here, and for the scattering measurements, are the standard deviations.) Thus the particle producing track A could be identified as a $\pi$-meson. The identification of track B is less certain but the values obtained agree with those to be expected if the track were produced by a proton. However, the large experimental error on the value of the mean scattering angle does not allow a deuteron to be excluded from our assumptions concerning the nature of the particle producing the track. A further factor which must be considered is the possibility that track B was produced by a $\pi$-meson. Recently, evidence has been presented by Pickup and Voyvodic (1950) that the grain density produced by particles of unit charge rises from the minimum value to a plateau at approximately 10% above it when their energies are roughly twenty times larger than their rest mass energy. Thus if track B were produced by a relativistic $\pi$-meson its grain density would not necessarily be at the minimum value. It should be noted, however, that the 'minimum' value given on the Bristol paper is made up from nucleons and fast $\pi$-mesons. At kinetic energies greater than 3 000 MEV the grain density of the latter particles would correspond to the 'plateau' value. Thus the Bristol value would lie between the value of the grain density at the true minimum and at the plateau. The tracks selected by us for the measurement of minimum ionization were from the following classes: (*a*) particles producing large stars or meson showers, (*b*) fast straight tracks passing through the emulsion, (*c*) decay electrons from the end of $\mu$-mesons. The grain densities of the tracks in the first two categories could vary between the true minimum and the plateau value as in the Bristol data, whereas the measurements of Pickup and Voyvodic assigned a plateau value to the grain density of the decay electrons. All the above tracks were found to possess grain densities smaller than track B. Further, using the electron tracks alone for the determination of minimum ionization the ratio of the grain density of track B to the mean grain density of the electron tracks gave a value of 1·10±0·05. Although the probability is small that the grain density of track B permits its classification as a meson from the consideration of statistical errors alone, it must be borne in mind that systematic errors can occur in the grain densities of tracks. These were avoided as much as possible by

(1) performing all the measurements on tracks in the same plate as the event,

(2) selecting tracks of length greater than 1 000 $\mu$ and inclined at very small angles to the plane of the emulsion,

(3) using only tracks at depths in the emulsion comparable with those of tracks A and B.

We therefore believe that the probability that track B was produced by a $\pi$-meson is very small.

We are confident that track C was formed by a $\pi$-meson. The range of track D is consistent with that to be expected in a ×2 emulsion for a $\mu$-meson from a $\pi$–$\mu$ decay. Further, rough checks on the multiple scattering as a function of range indicated that the masses of the particles producing tracks C and D were of the order of 200–300 $m_e$.

Since the errors associated with the mean scattering angles are considerably larger than those associated with the grain densities, the momenta and total energies of tracks A and B were calculated by the following procedure. Using the Bristol curve of grain density versus scattering angle (*loc. cit.*) and our measured values of the grain density, corresponding scattering angles together with their appropriate errors could be assigned to the particles dependent upon the assumption made of their nature. The energies and momenta of the particles assumed to be responsible for tracks A and B could then be calculated using the scattering constant for normal emulsions (Bosley and Muirhead 1952, Gottstein *et al.* 1951). The kinetic energy of the $\pi$-meson (track C) was calculated from its range, using the kinetic energy of a $\mu$-meson from a $\pi$–$\mu$ decay and the measured range of track D as a calibration point. Appropriate corrections were made for straggling. A value of 140±1 Mev was used for the mass of the $\pi$-meson (Cartwright 1951).

The values of total energy and momentum of the three tracks are given in table 1.

Table 1

| Track | Assumed nature of particle | Total energy $W$ (Mev) | Momentum $P\left(\frac{\text{Mev}}{c}\right)$ |
|---|---|---|---|
| A | $\pi$-meson | $260^{+40}_{-25}$ | $220^{+50}_{-30}$ |
| B | Proton | $1\,800^{+200}_{-130}$ | $1\,550^{+200}_{-150}$ |
| B | Deuteron | $3\,600^{+400}_{-260}$ | $3\,100^{+400}_{-300}$ |
| C | $\pi$-meson | $144{\cdot}5 \pm 1{\cdot}1$ | $35{\cdot}7 \pm 1{\cdot}3$ |

## §3. DISCUSSION

### (i) *Nature of Target Nucleus*

Since the only heavily ionizing particle associated with the disintegration is a $\pi$-meson, it is reasonable to assume that the target nucleus was that of hydrogen.

A further argument may be cited in support of this opinion. The $\pi$–$\mu$ decay sequence shows that the particle producing track C was positively charged. Slow $\pi^+$-mesons are rarely observed to accompany the stars produced by the cosmic radiation, and when they do occur, they normally have a residual range of the order of 1 mm or more. This may be partly explained by the existence of the nuclear potential barrier (Occhialini and Powell 1948). The bromine and silver components of a nuclear emulsion have potential barriers of 8·0 and 9·5 MEV respectively when the nuclei are not excited (Fermi 1950). This value will be lowered, however, if the nucleus is excited. If a silver or bromine nucleus were struck at the point X then the absence of slow protons or $\alpha$-particles suggests that the excitation of the struck nucleus was small. A lower limit of roughly 5 MEV may be assigned to the value of the potential barrier, for singly charged particles, from measurements on the evaporation of $\alpha$-particles from silver and bromine nuclei excited to about 100 MEV by the absorption of slow $\pi^-$-mesons (Menon *et al.* 1950). The particle producing track C possessed a kinetic energy of $4{\cdot}5 \pm 0{\cdot}3$ MEV, that is slightly less than the lower limit for the potential barrier. It would further appear unlikely that the event was produced in one of the lighter nuclei (carbon, nitrogen or oxygen) comprising the gelatine of the emulsion since at least some form of recoil would be expected at the point X in this case. We are therefore confident that the target nucleus was a free proton.

### (ii) *Analysis*

The event may be interpreted in more than one way depending not only on the nature of the particle producing track B, but also on whether it was the primary or a secondary particle. The inclination of track B to the vertical was 122°. The plate was exposed at an altitude of 97 000 ft. and in view of the nearly isotropic distribution of the primary cosmic radiation at this height the hypothesis that the track was made by the incident particle cannot be excluded. The Bristol group (Camerini *et al.* 1951) have shown, however, that the probability that an energetic particle travels backwards at high altitudes is small. This factor, coupled with that which shows that the probability for the production of one charged meson by a nucleon rises only to a value of 0·5 when the total energy of the nucleon is 2·5 BEV, (*loc. cit.*) makes the assumption that track B represents the path of the incident particle an unlikely one. Retaining this as a possible process, however, we may assume the following schemes :—

(1) Track B a secondary particle, neutron as primary particle,

(*a*) $\mathrm{n}+\mathrm{p}\rightarrow\pi^{+}+\pi^{-}+\mathrm{p}+\mathrm{n}$

(*b*) $\mathrm{n}+\mathrm{p}\rightarrow\pi^{+}+\pi^{-}+\mathrm{D}.$

(2) Track B the primary particle. The most probable nature of B is that of a proton, but even if it were a primary deuteron and produced the disintegration, it is reasonable to assume that stripping would occur. Allowing for charge conservation, we may then write

$$p+p\rightarrow\pi^{+}+\pi^{+}+n+n$$

for either particle.

We have made use of the following general equations in the analysis of the event (Blaton 1950):

$$\epsilon=\sqrt{[(W+M)^2-P^2]}-(M+m) \quad . \ . \ . \ . \ (1)$$

$$\beta_G=P/(W+M) \quad . \ . \ . \ . \ . \ . \ . \ . \ . \ . \ (2)$$

$$W_L=\sqrt{(1-\beta_G^2)}\ W_{\text{c.m.}}+\beta_G P_L\cos\theta \quad . \ . \ . \ . \ . \ (3)$$

$$\frac{W_L}{W_{\text{c.m.}}}\sqrt{(1-\beta_G^2)}=1+\beta_G\beta_{\text{c.m.}}\cos\phi \quad . \ . \ . \ . \ . \ . \ . \ . \ . \ (4)$$

$$P_L\sin\theta=P_{\text{c.m.}}\sin\phi \quad . \ . \ . \ . \ . \ . \ . \ . \ . \ . \ (5)$$

Fig. 2

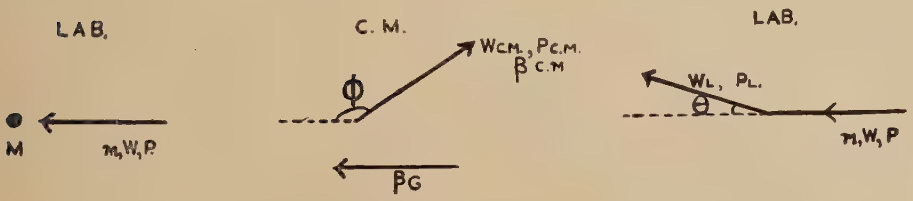

Angles, energies and momenta of particles in the laboratory and centre of momentum systems before and after the collision (eqns. 1–5 in text).

where $\epsilon$ is the energy available in the centre of momentum system for meson production, $W$ and $P$ the total energy and momentum of the primary particle of mass $m$, $M$ the mass of a target particle, $\beta_G$ the velocity of the centre of momentum system, $W_L$ and $P_L$ the total energy and momentum of a secondary particle ejected in the laboratory system at an angle $\theta$ to the primary particle and $W_{\text{c.m.}}$, $P_{\text{c.m.}}$ and $\phi$ the corresponding quantities for a secondary particle of velocity $\beta_{\text{c.m.}}$ in the centre of momentum system (fig. 2).

In the calculations we shall determine the inelasticity, $K$, of the collision in the centre of momentum system. This is defined as the fraction of the available energy carried away by the $\pi$-mesons in the centre of momentum system:—

$$K=\frac{\Sigma W_{\pi_{\text{c.m.}}}}{\epsilon}. \quad . \ . \ . \ . \ . \ . \ . \ . \ . \ (6)$$

For hypothesis 1 (*a*) we have also used the equations

$$W+M=W'+W_m \quad . \ . \ . \ . \ . \ . \ . \ . \ (7)$$

$$\vec{P}=\vec{P'}+\vec{P}_m \quad . \ . \ . \ . \ . \ . \ . \ . \ (8)$$

and for 1 (*b*)

$$W+M=W_m \quad \dots\dots\dots \quad (9)$$

$$\vec{P}=\vec{P}_m \quad \dots\dots\dots \quad (10)$$

where $W_m$ is the total measured energy of the charged secondary particles and $P_m$ the vectorial sum of their momenta. $W'$ and $P'$ are the energy and momentum of the secondary neutron.

$P_m$ lies almost along the direction of track B, the angular separation is approximately 2° for the secondary proton hypothesis and approximately 1° for the deuteron hypothesis.

Examining first the proposed scheme 1 (*a*), from the eqns. (7) and (8) we may set a rough threshold for the reaction at $W\sim 3\cdot 6$ Bev. At this energy the meson producing track C would be ejected at an angle of 168° in the centre of momentum system and track A at an angle of ~177°. The inelasticity of the collision, $K$, was found to be 0·85.

At primary energies above the threshold the direction of the primary neutron cannot be fixed, but by applying eqns. (7) and (8) it can be shown that $P_m$ never deviates from the direction of the primary particle by an angle of more than 19·5°. This represents the case when $W$ tends to infinity. Thus in applying eqn. (3) to determine the energy of the meson in the centre of momentum system errors due to uncertainty in angles do not seriously affect our calculations. At assumed energies of 4, 10, 20 and 100 Bev for $W$ the values of $K$ are 0·8, 0·6, 0·45 and 0·38 respectively, whilst the values for $\phi$ vary between 175° and 180° for track A and 170° to 178° for track C.

For hypothesis 1 (*b*) the measured value of $P_m$ was $2\cdot 85^{+0\cdot 4}_{-0\cdot 25}$ Bev/$c$, whilst the value of $P$ calculated from $W_m$ was $2\cdot 90^{+0\cdot 4}_{-0\cdot 3}$ Bev/$c$. The total energy of the primary neutron $W$ was calculated to be $3\cdot 05^{+0\cdot 35}_{-0\cdot 25}$ Bev.

Thus energy and momentum can be balanced in this case, but the errors are too large to give preference for this case over that of 1 (*a*). The value of $\epsilon$ in this case is 0·9 Bev whilst $K$ is 0·9. Thus the deuteron would possess a kinetic energy of roughly 0·1 Bev in the centre of momentum system. For such large energies the theoretical probability of deuteron formation is very low. The angles of emission of tracks A and C in this case would be 177° and 170° respectively in the centre of momentum system.

Reaction 2 is just energetically possible, $K$ is 0·9, whilst the values of $\phi$ for tracks A and C are 20° and 175° respectively.

Thus far no mention has been made of the possible production of neutral mesons. It is of interest to note that insufficient energy exists for the production of a third meson in schemes 1 (*b*) and 2. The production of one or more neutral mesons is possible for the proposed scheme 1 (*a*) at primary energies well above the threshold value of 3·6 Bev. If neutral mesons were produced in this case the value of $K$ would be raised but the angles of emission of the mesons associated with tracks A and C would be unchanged.

### (iii) *Conclusions*

Of the three possible processes discussed above that of 1 (*a*) ($n+p \rightarrow \pi^{+}+\pi^{-}+p+n$) would seem to be the most likely in view of the arguments cited. In conclusion we may say that regardless of assumptions concerning the nature of the reaction, the mesons ejected lie close to the path of the incident particle in the centre of momentum system. A similar result has been noted for two other showers involving single nucleons as targets, but in which the primary particles possessed energies which were probably at least two orders of magnitude higher than that in our example (Fermi 1951).

An event recently reported by the Manchester group (Goldsack and Page 1951) shows an interesting similarity to that described here, in that both have a free proton as the target nucleus and a slow $\pi$-meson is ejected in each case. Because of their low multiplicities both are presumably produced by nucleons with total energies of the order of 10 BEV or less (Camerini *et al.* 1951). Although the attention of the microscope observer is drawn to events of this type by the presence of the heavily ionizing track, slow $\pi$-particles accompanying meson showers produced in nuclei heavier than hydrogen are extremely rare. Thus it appears possible that not all the mesons produced by nucleons of high energy emerge from nuclei.

## ACKNOWLEDGMENTS

The authors wish to express their gratitude to Professor P. I. Dee, F.R.S., for his interest and encouragement during the course of this work, and to Professor J. C. Gunn for discussions concerning the theoretical probability of deuteron formation at high energies. We are especially grateful to Drs. T. Coor, M. M. Shapiro and B. Stiller of the O. N. R. organization for arranging the exposure of the plates at high altitude. One of us (W. B.) wishes to thank the Nuffield Foundation for the award of a grant which has enabled him to carry out this research.

## REFERENCES

BLATON, 1950, *K. Danske Vidensk. Selsk. Mat.-fys. Medd.*, **24,** No. 20.
BOSLEY and MUIRHEAD, 1952, *Phil. Mag.*, **43,** 63.
CAMERINI, FOWLER, LOCK and MUIRHEAD, 1950, *Phil. Mag.*, **41,** 413.
CAMERINI, DAVIES, FOWLER, FRANZINETTI, MUIRHEAD, LOCK, PERKINS and YEKUTIELI, 1951, *Phil. Mag.*, **42,** 1241.
CARTWRIGHT, 1951, *Phys. Rev.*, **82,** 460.
COSYNS and VANDERHAEGHE, 1950, *Bull. Nuc. Phys. Centre, Brussels Univ.*, No. 15.
DODD and WALLER, 1951, *Photographic Sensitivity, Bristol Conference Report*, 266.
FERMI, 1950, *Nuclear Physics*, 77 ; 1951, *Phys. Rev.*, **81,** 683.
FOWLER, 1950, *Phil. Mag.*, **41,** 169.
GOTTSTEIN, MENON, MULVEY, O'CEALLAIGH and ROCHAT, 1951, *Phil. Mag.*, **42,** 708.
MENON, MUIRHEAD and ROCHAT, 1950, *Phil. Mag.*, **41,** 583.
PICKUP and VOYVODIC, 1950, *Phys. Rev.*, **80,** 89.

# LXXV. *Multiple Scattering of* 0·59 MeV *Electrons*

By E. Hisdal
Fysisk Institutt A, University in Oslo, Blindern, Norway*

[Received April 28, 1952]

## Summary

The multiple scattering of electrons of 0·59 MeV kinetic energy in G5 plates has been investigated. The experimentally determined mean of the absolute multiple scattering angle is found to be significantly lower than the value predicted by theory.

## §1. Experimental Setup

A beam of electrons of 0·59 MeV kinetic energy† was obtained in a low resolution beta-ray spectrometer from a $P^{32}$ source. An Ilford G5 plate was inserted into the vacuum system of the spectrometer, the plane of the emulsion making an angle of 10° with the plane of the spectrometer. The electrons entered the plate through the surface of the emulsion. Prior to the exposure, the plate was left in vacuum for half an hour. This was done in order to be sure, that all water had evaporated from the emulsion. The composition of the emulsion was then obtained from the data supplied by Ilford for G5 plates at zero moisture content.

Only those tracks were selected for measurement which entered through the surface of the emulsion and which had such a direction, that they could have come from the spectrometer. A control plate was inserted into the spectrometer under exactly similar conditions, the only difference being, that the magnet current was not turned on. The two plates were developed together. No tracks were found on the control plate which would have satisfied the above criterions for selecting a track for measurement.

## §2. Measuring Method

The plate was examined under a Cooke M4005 microscope. Only one scattering angle was determined for each track. Fifty-seven tracks were measured.

It seemed, that neither the ‘ angular method ’ (Goldschmidt–Clermont 1950) nor the ‘ coordinate method ’ (Fowler 1950) would be satisfactory for the evaluation of such highly scattered tracks due to the difficulty

---

[*] Communicated by Professor J. Holtsmark.

[†] See § 5 for energy distribution of electrons.

of approximating a portion of the track by a straight line. The most suitable and exact method appeared to be the 'centre of gravity measuring method'.*

The portion of the track selected for measurement was divided into three cells of 17·6 microns each. The coordinate $y$ of each grain in a cell in a direction approximately perpendicular to the general direction of the track was then determined with a micrometer eyepiece especially supplied by Messrs. Cooke, Troughton & Simms for this purpose. The approximate distance $x$ of each grain from the beginning of the cell was also recorded. From these data the $y$ coordinate of the centre of gravity of each cell was calculated. The second differences between these coordinates gave a measure of the multiple scattering angle. As a short cell length could be used because of the large scattering angles, the method was not inhibitively laborious.

Since the stage of the microscope was not moved during the measurement of one angle, all 'noise' due to non-parallel displacement of the stage was eliminated. On the other hand it was found that slight vibrations of the building caused appreciable vibrations of the image under the microscope and were very disturbing to the accurate measurement of the coordinates of the grains. The microscope was therefore moved to the sub-basement of the building.

## § 3. COMPUTATIONS

The centre of gravity of each cell was calculated under the assumption that the track consisted of straight lines joining neighbouring grains, and that the direction of the track was nearly parallel to the $x$ direction. $y_0$ and $y_n$, the $y$ coordinates of the track at the beginning and end of the cell respectively, were found by interpolation of the $y$ coordinates of the nearest grain on each side of the cell division. If $(x_1, y_1)$, $(x_2, y_2), \ldots, (x_{n-1}, y_{n-1})$ are the coordinates of the grains in the cell, the $y$ coordinate of the centre of gravity of the cell is given by :

$$y_g = \frac{1}{2(x_n - x_0)}[(y_0+y_1)(x_1-x_0)+(y_1+y_2)(x_2-x_1)+\ldots \\ +(y_{n-1}+y_n)(x_n-x_{n-1})]$$

or

$$y_g = \frac{1}{2(x_n - x_0)}[y_0(x_1-x_0)+y_1(x_2-x_0)+y_2(x_3-x_1)+y_3(x_4-x_2)+\ldots \\ +y_{n-1}(x_n-x_{n-2})+y_n(x_n-x_{n-1})].$$

Let us denote by $\langle\phi_g\rangle$ the average of the absolute second differences of $y_g$ divided by the cell size. For the 57 tracks measured this turned out to be

$$\langle\phi_g\rangle_{\text{exp}} = 0{\cdot}114 \text{ radian.}$$

No cut-off procedure was used.

---

* I am indebted to Dr. O. Rochat for suggesting this method to me.

For a further discussion of the 'centre of gravity method' and a possible simplification of the calculations, see Appendix II.

The mean absolute value of the projected multiple scattering angle was computed according to the theories of Molière (1947, 1948, 1951) and Williams (1939, 1940). Since the parameter $\gamma = zZ/(137\beta)$ has, in the case of this experiment, a value of the order of magnitude of 1, neither the Born approximation nor classical approximation can be used in computing the minimum scattering angle due to screening, $\phi_{\text{min}}$. It was therefore necessary to use Molière's theory for single scattering (Molière I 1947) in computing $\phi_{\text{min}}$ in Williams' theory. (For the details of the calculation, see Appendix III and also Goldschmidt–Clermont 1950, Voyvodic and Pickup 1952.) When this was done both Molière's and Williams' theories gave the same answer for $\langle\phi\rangle$ to within less than 1%:

$$\langle\phi\rangle_{\text{theo}} = 0{\cdot}248 \text{ radian}$$

for a cell length of 17·6 micron in G5 emulsions at zero humidity content. The multiple scattering theory of Snyder and Scott (1949, 1950) also seems to give results in agreement with Molière's numerical values.

The above $\langle\phi\rangle$ refers to the angles between the tangents to the track. In the present case, where the second differences between the coordinates of the centres of gravity of three adjacent cells were divided by the cell size, it has been shown by Molière (III, 1951) that the above theoretical value for $\langle\phi\rangle$ has to be multiplied by the smoothing factor $(11/20)^{1/2} = 0{\cdot}7416$. Denoting this value of the multiple scattering angle by $\langle\phi_g\rangle$ we have:

$$\langle\phi_g\rangle_{\text{theo}} = 0{\cdot}184 \text{ radian} = 10{\cdot}54^\circ.$$

Figure 1 shows a histogram of the experimental scattering distribution. In fig. 2 the integral of the distribution is plotted on 'probability paper'. On the abcissa is marked off the percentage of angles which are smaller than the corresponding ordinate $\phi$. The distance of a point $x$ on the abcissa from the coordinate centre is proportional to $\phi/\sigma$ where $\phi$ is given by $x = 2/[(2\pi)^{1/2}\sigma]\int_0^{\phi} \exp[-\phi^2/(2\sigma^2)]\,d\phi$. A normal distribution will therefore appear as a straight line on such paper. The curve in fig. 1 and the straight line in fig. 2 represent the Gaussian part of a Molière distribution which has the same $\langle\phi\rangle$ as $\langle\phi_g\rangle$ of the experimental distribution.* The large angle scattering 'tail' can easily be observed in fig. 2 where all the points corresponding to large scattering angles lie to the left of the straight line. In other words the percentage of angles larger than a given angle $\phi$ is larger than in the normal distribution as a result of the 'tail'.

---

* Actually it is the Gaussian part of a Molière distribution for the angles $\phi$ between the tangents to the track. According to Molière III (1951) it appears that the width of this distribution should not differ by more than a few per cent from the width of the distribution of $\phi_g$.

The statistical standard error in $\langle\phi\rangle$ when $n$ angles are measured is $\langle\phi\rangle[(\pi-2)/(2n)]^{1/2}$ if we assume the angles to be normally distributed (Appendix I). Since the multiple scattering angles are nearly normally distributed (Williams 1939, Molière II 1948) no serious error should be introduced by using the above value for the standard error. This is also confirmed by the experimental sampling distributions of multiple scattering angles obtained by O'Ceallaigh and Rochat (1951, p. 1058). In the present case $n=57$. This gives a standard error of very nearly 10%.

Fig. 1

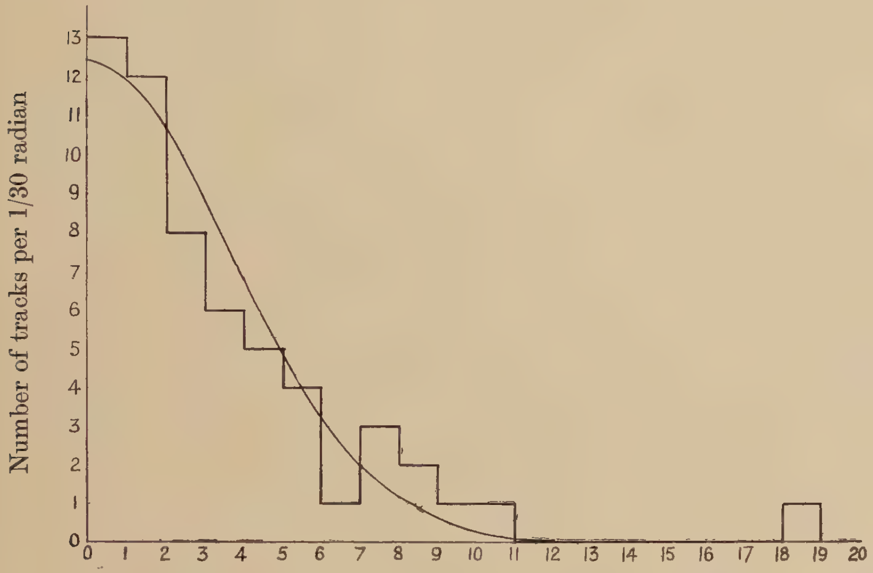

30 × scattering angle in radians

Histogram showing the distribution of the scattering angles. The curve represents the Gaussian part of a Molière distribution fitted to the experimental data.

## §4. RESULTS

As we saw above the theoretical and experimental values obtained for $\langle\phi_g\rangle$ are :

$$\langle\phi_g\rangle_{\text{theo}}=0{\cdot}184\text{ radian}=10{\cdot}54^\circ.$$

$\langle\phi_g\rangle_{\text{exp}}=0{\cdot}114\pm0{\cdot}011$ radian$=6{\cdot}515\pm0{\cdot}65^\circ$ where the standard error is that of a normal distribution with the same mean deviation. (For standard error of mean deviation, see Appendix I.)

The corresponding scattering constants $K$ (for the centre of gravity measuring method) as defined by Gottstein *et al.* (1951) are :

$$K_{\text{theo}}=21{\cdot}6\,\frac{\text{degrees}\times\text{MeV}}{(100\mu)^{1/2}}$$

$$K_{\text{exp}}=13{\cdot}4\pm1{\cdot}3\,\frac{\text{degrees}\times\text{MeV}}{(100\mu)^{1/2}}.$$

As can be seen the discrepancy between the theoretically predicted and the experimental values is larger than three times the standard error. It will be shown in § 5 that almost all sources of error must have increased the value of $\langle \phi_g \rangle_{\text{exp}}$ and that it does not seem possible to account for the difference between the theoretical and the experimental values of $\langle \phi_g \rangle$ by any experimental errors.

Fig. 2

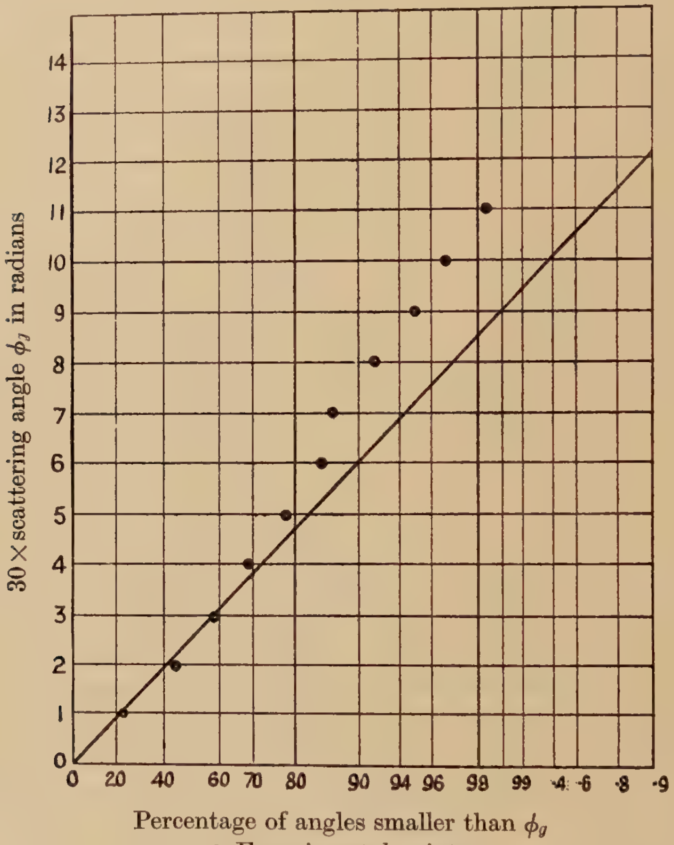

○ Experimental points

The straight line represents the Gaussian part of a Molière distribution fitted to the experimental points

A similar disagreement between multiple scattering experiments and theories in the case of electrons has been reported by several investigators. Molière (II, 1948) and Voyvodic and Pickup (1952) give a review of the experiments done in this field and comparisons with theory. Molière remarks that no exact agreement can be expected between the theory and the older experiments of Crother and Schonland and of Geiger and Bothe. When those are excluded from the data almost all experimental values lie lower than the theoretically predicted multiple scattering angles, in agreement with the present investigation.*

There does not seem to be any reason to doubt the correctness of the statistical part of the multiple scattering theories, also in consideration of the fact that the statistical treatments of the different theories give the same numerical answer. If it should turn out that no other sources of error can explain the discrepancy between theory and experiment, this might lead us to doubt the correctness of the single scattering law in the case of electrons.

An experiment of Biberman *et al.* (1949) seems to indicate that such a deviation from the theoretically predicted single scattering law exists. The authors measured the scattering of 30–80 kv electrons by very thin aluminium foils at small angles ($10^{-4}$–$10^{-2}$ radians) with the aid of an electron microscope. They compared the results for 60 kv with the theoretical angular distribution according to Mott's formula for elastic scattering computed for a Thomas–Fermi model. The agreement between the experimental and the theoretical curves is satisfactory for angles larger than $20\times10^{-3}$ radians. Between $3\times10^{-3}$ radians and $20\times10^{-3}$ radians the experimental curve lies up to 50% lower than the theoretical one. For angles smaller than $3\times10^{-3}$ radians the experimental curve rises very rapidly and lies far above the theoretical values. As the authors mention, this may be due to inelastic scattering of the electrons. But again it seems hard to explain what may have caused the experimental curve to lie lower than the theoretical one in the region of $3\times10^{-3}$–$20\times10^{-3}$ radians.

## §5. SOURCES OF ERROR

Each track was measured twice, one measurement beginning at the high energy end, the other at the low energy end of the three cells. $\phi_{g\,\mathrm{exp}}$ was calculated separately for each measurement, and the average of the two measurements was taken for the calculation of $\langle\phi_g\rangle_{\mathrm{exp}}$.

The difference in angle between two measurements of the same track should be a measure of the error due to what we might call ‘ microscope noise ’, i.e. trembling of the microscope, involuntary displacement of the track with respect to the objective, etc. The average error obtained in this way was 0·00375 radian.

The beginning of the first cell was always placed in the middle between the fourth and the fifth grain of the track, starting at the high energy end. The average distance between the point at which an electron entered the surface of the emulsion and the middle of the three cells measured was 44 micron. The energy used to calculate $\langle\phi_g\rangle_{\mathrm{theo}}$ was the energy of the electrons when they entered the emulsion. It is estimated that at the middle of the three cells the electrons had lost approximately 3·2% of their kinetic energy. This would increase $\langle\phi_g\rangle_{\mathrm{theo}}$ by about 1·6%.

---

* *Note added in proof:* The measurements of Corson (1950, 1951) form an exception. He found satisfactory agreement with Molière's theory when he combined multiple scattering measurements of positrons and electrons of 20 MeV.

The relative intensity of electrons having given radii of curvature was obtained from the geometry of the spectrometer and the width of the source. This is shown in table 1 :

Table 1

| Radius of curvature in cm | 5·4 | 5·5 | 5·6 | 5·7 | 5·8 | 5·9 | 6·0 |
|---|---|---|---|---|---|---|---|
| Relative intensity | 0 | 11 | 36·5 | 40·5 | 31 | 9·5 | 0 |

This gives an average radius of curvature of 5·69 cm. In the calculation of the theoretical value of the multiple scattering angle, the radius of curvature of the electrons was taken as 5·8 cm. Thus the theoretical value of the multiple scattering angle may be slightly underestimated.

The magnetic field in the spectrometer has been measured as a function of the magnet current by Holt (1949) with an accuracy of 3·2%. In the present case a current of 2·00 amp was used corresponding to a magnetic field of 559 gauss and $H\rho = 3\,243$ gauss cm.

In the multiple scattering theories it is assumed that the measured angles are projected on a plane containing the incident direction of the electrons. In the present case the incident electrons made an angle of about 10° with the surface of the emulsion. The angle between the direction of the track and the measuring plane is thus on the average somewhat greater than the angle between the direction of the track and the incident plane. The angles measured are therefore on the average slightly larger than they would have been if they had been projected on the incident plane as required by the theories. A correction due to this cause would decrease $\langle\phi_g\rangle_{\mathrm{exp}}$ somewhat.

It seems reasonable to suppose that the effects of distortion of the emulsion, radiation loss, and electrons scattered from the walls of the apparatus were negligible. The finite size of the grains will have given rise to some spurious scattering.

If the effect of inelastic electronic scattering had been included in the calculation it would have increased the value of $\langle\phi_g\rangle_{\mathrm{theo}}$ somewhat.

Corrections due to any of the above mentioned sources of error would increase the difference between the theoretical and the experimental value of $\langle\phi_g\rangle$. Spurious scattering or non-homogeneity in the energy of the electrons would have caused an increase in the dispersion of the experimentally measured angles and thereby too large a value of $\langle\phi_g\rangle_{\mathrm{exp}}$.

The ‘ flat chamber effect ’ seems to be the only important source of error that might lead to an underestimate of $\langle\phi_g\rangle_{\mathrm{exp}}$. It is due to the fact that an electron scattered through a large angle has a greater probability of being scattered out of the emulsion than an electron scattered through a small angle. One will therefore select too large a proportion of tracks with low scattering angles for measurement. Molière (II, 1948, eqn. (10.4′)) has calculated the mean scattering angle for the extreme case of an infinitely flat chamber. In the present case this would give a value for $\langle\phi_g\rangle_{\text{theo}}$ (flat chamber)=0·155 radian. Even this value cannot be reconciled with the experimental scattering angle of 0·114±0·011 radian. There is no doubt that in the present case the 'flat chamber effect' is not nearly as pronounced as in an infinitely flat chamber. The emulsion was 200 micron thick, and thus electrons scattered through large angles towards the bottom of the emulsion were included in the measurements. As the incident electrons made an angle of approximately 10° with the surface of the emulsion, electrons scattered towards the surface were also included in the measurements unless the scattering angle was quite large. It may be pointed out here, that much care was taken during the scanning of the plate not to miss any tracks with large scattering angles. The approximate similarity in shape between the experimental distribution and the fitted normal distribution as demonstrated in figs. 1 and 2, and the relatively big percentage of large scattering angles which can most clearly be observed in fig. 2 should also indicate that the 'flat chamber effect' and the effect of missing tracks with large scattering angles during the scanning were not serious.

Possibly a small correction should have been introduced because the shape of the track was approximated by straight lines joining neighbouring grains. The number of grains in the three cells measured was on the average of the order of 18.

Another possible correction may be due to the fact that the cell size used, 17·6 micron, was small and it is not certain, whether the composition of the emulsion may be considered as homogeneous as required by the theories.

Assuming a homogeneous composition Molière's theory should be exact in the present case where $\Omega_b$ as defined by Molière is 71.

The angle between the track and the $x$ direction was computed from the first differences between the coordinates of the centres of gravity divided by the cell length. This amounts to taking the tangent of the angle instead of the angle. A correction would increase the largest angle measured by 3·3%, the next largest by 0·7%, the correction being much smaller for most of the other angles.

## ACKNOWLEDGMENTS

I should like to thank Professor J. Holtsmark for his encouragement and for providing the facilities of his laboratory for this work, and Professor R. Tangen for help in many practical problems. I also take this opportunity of thanking the research workers of this institute, and in particular Dr. S. O. Sörensen, and also the group of research workers of the H. H. Wills Physical Laboratory, University of Bristol, for much help and many interesting discussions. I am very grateful to Dr. G. Molière for sending me the yet unpublished Part III of his paper. I am obliged to Norges Teknisk Naturvitenskapelig Forskningsråd for providing the funds for this work.

# APPENDIX I

## *Standard Error of Mean Deviation*

We assume that we have a normal population of the form

$$\exp\,[-x^2/(2\sigma^2)]/[(2\pi)^{1/2}\sigma].$$

Let us denote by $\langle x\rangle$ the mean of the absolute values of the deviations of $x$ from the mean. For a normal population $\langle x\rangle=(2/\pi)^{1/2}\sigma$.

Fisher (1920) found the standard error in a sample of $n$ of the mean deviation from the mean of the sample, i.e. the standard error of

$$\frac{1}{n}\sum_{i=1}^{n}\left|x_i-\frac{1}{n}\sum_{i=1}^{n}x_i\right|$$

where the $x_i$ are the sample values of $x$. His formula for the standard error is

$$\sqrt{\left(\frac{2}{\pi}\right)}\,\sigma\,\frac{\sqrt{(n-1)}}{n}\left[\frac{\pi}{2}+\sqrt{[n(n-2)]}-n+\text{arc sin}\,\frac{1}{n-1}\right]^{1/2}$$

(Kendall 1947).

For large $n$ this expression reduces to

$$\sqrt{\left(\frac{2}{\pi}\right)}\cdot\sigma\cdot\sqrt{\left(\frac{\pi-2}{2n}\right)}.$$

In the measurement of multiple scattering angles in nuclear emulsions the statistic used is :

$$\frac{1}{n}\sum_{i=1}^{n}|x_i|,$$

i.e. the mean deviation from the mean of the population. The latter is supposed to be known and equal to 0.

For the purpose of finding the standard error of this statistic we may regard $\langle x\rangle$ as the real mean of a population whose frequency distribution is 0 for $-\infty<x<0$ and $2\exp\,[-x^2/(2\sigma^2)]/(2\pi)^{1/2}\sigma$ for $0\leqslant x<\infty$.

The variance of this distribution, $\sigma_1^2$, equals the mean square deviation of $x$ about 0 minus $\langle x\rangle^2$ :

$$\begin{aligned}\sigma_1^2&=\frac{2}{\sqrt{(2\pi)}\sigma}\int_0^\infty x^2\exp\,(-x^2/2\sigma^2)\,dx-\langle x\rangle^2\\&=\sigma^2-\frac{2}{\pi}\sigma^2\end{aligned}$$

or substituting for $\sigma$ in terms of $\langle x\rangle$ :

$$\sigma_1^2=\frac{\pi-2}{2}\langle x\rangle^2.$$

The variance of the mean of a simple sample of $n$ is $\sigma_1^2/n$ irrespective of the form of the frequency distribution. (For overlapping cells this equation does not hold as the members of the sample are not independent.)

We therefore get for the standard error of the mean deviation from the mean of the population :

$$\left(\frac{\pi-2}{2n}\right)^{1/2}\langle x\rangle.$$

This formula is exact and is the same as the approximation for large $n$ in Fisher's statistic.

## APPENDIX II

### *Further Discussion of the Centre of Gravity Method*

As shown in § 5 an absolute error of the order of 0.00375 radian can be expected to be introduced by ' microscope noise ' in the measurement of an angle. The data seemed to indicate that this error was independent of the magnitude of the angle measured. This point has however not been more closely investigated. It therefore appears, that the method cannot be used for measuring electrons with energies of the order of 3 MeV or more.

In computing the centre of gravity of a cell it is possible to use a much simpler and quicker although not quite as accurate method than the one described in § 3. This consists of using the average $y$ coordinate of all the grains in a cell as a measure of $y_g$. For a single track this will not give the same answer as the above formula due to the fact that the grains are not evenly spaced. It can however be shown, that this should not lead to any systematic error unless there exists a correlation between grain density and scattering angle in tracks of a given energy.

Ten tracks were also computed according to the latter method with the only modification that if no grain was present at a distance of 0·25 cell sizes from the edge of a cell, the $y$ coordinate of the nearest grain in the neighbouring cell was included in the averaging in order to correct for such extremely uneven spacing. The averages of the second differences of the centres of gravity calculated by this method and by the exact method respectively differed by less than 0·5%.

## APPENDIX III

### *Numerical Values in Scattering Formulae*

In order to use Molière's single scattering law in William's theory the substitution

$$\phi_{\min}=1{\cdot}457\,\bar{\chi}_a \quad . \quad . \quad . \quad . \quad . \quad . \quad . \quad . \quad (1)$$

was made in the latter. $\bar{\chi}_a$ is defined by Molière (II, 1948, eqns. (6.3) and (6.10′)). With this substitution $\phi_{\min}$ agrees with the value given by Williams (1939, p. 564) in the limiting case of $\gamma \ll 1$. This method is equivalent to the one described by Goldschmidt–Clermont (1950) and Voyvodic and Pickup (1952).

Using eqn. (1) it can be shown that the numerical factor in eqn. (6 *a*) of Voyvodic and Pickup and eqn. (3 *a*) in Williams (1940) should be corrected to $0{\cdot}6535\pi$. According to Williams the factor is equal to $2\pi/(1{\cdot}75)^2=0{\cdot}653\pi$ in agreement with the above value. The factor in front of eqn. (6 *b*) in Voyvodic and Pickup and inside the log term in eqn. (2) of Goldschmidt–Clermont should be $1{\cdot}964\pi$. With these numerical values the two scattering formulae described by Voyvodic and Pickup and by Goldschmidt–Clermont are completely identical and either one of them can be used irrespective of whether $\gamma<1$ or $\gamma>1$.

It may be worth while to mention at this place some other slight inexactitudes of numerical values in different scattering papers for the benefit of workers in this field.

Equation (7) in Voyvodic and Pickup should read

$$M=M_B\left(1+\frac{\gamma^2}{0{\cdot}3005}\right)$$

and the equivalent expression when $M_a$ is used is :

$$M=M_a\left(1+\frac{0{\cdot}3005}{\gamma^2}\right).$$

The last term in eqn. (6) of Gottstein *et. al.* (1951) should be 0·1544 and not 0·115.

The Thomas Fermi radius of an atom as given by Molière (I, 1947, p. 141) should be $a=0{\cdot}4685\times10^{-8}Z^{-1/3}$ cm as is also mentioned in Molière III.

## REFERENCES

BIBERMAN *et al.*, 1949, *Doklady Akad. Nauk U.S.S.R.*, **69,** 519.
CORSON, 1950, *Phys. Rev.*, **80,** 303 ; 1951, *Ibid.*, **84,** 605 (also private communication).
FISHER, 1920, *Mon. Not. Roy. Ast. Soc.*, **80,** 758.
FOWLER, 1950, *Phil. Mag.*, **41,** 169.
GOLDSCHMIDT-CLERMONT, 1950, *Nuovo Cimento*, **7,** 331.
GOTTSTEIN, *et al.*, 1951, *Phil. Mag.*, **42,** 708.
HOLT, 1949, *Hovedoppgave i Fysikk, University in Oslo, Norway.*
KENDALL, 1947, *The Advanced Theory of Statistics* (Griffin, 3rd Ed.).
MOLIÈRE I, 1947, *Z. für Naturforschung*, **2a,** 133 ; II, 1948, *Ibid.*, **3a,** 78 ; III, 1951, unpublished.
O'CEALLAIGH and ROCHAT, 1951, *Phil. Mag.*, **42,** 1050.
SNYDER and SCOTT, 1949, *Phys. Rev.*, **76,** 220 ; 1950, *Ibid.*, **78,** 223.
VOYVODIC and PICKUP, 1952, *Phys. Rev.*, **85,** 91.
WILLIAMS, 1939, *Proc. Roy. Soc.* A, **169,** 531 ; 1940, *Phys. Rev.*, **58,** 292.

# LXXVI. CORRESPONDENCE

## *A 'Megamolecular' Structure Factor*†

By Dorothy Wrinch
Department of Physics, Smith College, Northampton, Mass., U.S.A.‡

[Received April 1, 1952]

An attempt is being made to discover how far the interpretation of the intensity maps obtained from x-ray diffraction studies of crystalline proteins may be facilitated by a ' synthetic ' approach. Studies have been undertaken (Wrinch 1946) to discover the manner in which various structural types in atomic space $S$ manifest themselves in reciprocal space $S^*$.

Chemical data require of structures proposed for protein molecules that their skeletons be polymers of the N—$C_\alpha$—C amino acid backbones. Biological data require that these polymers be, in some sense, regular and coherent. One way of meeting these requirements is to restrict the NCC motifs to positions at or suitably associated with nodes of a lattice or related lattices, a further restriction to positions at or suitably associated with points of a diamond network ensuring appropriate valency angles. A skeleton from which residues may be deleted which meets the requirements cited is the ' cage ' structure (Wrinch 1937) with symmetry $T$ in which the atoms of 72 N—$C_\alpha$—C motifs are at or near the sets of equivalent points

$$\begin{array}{llllll}
\mathrm{N}: 3\ \ 1\ \ 9, & 0\ \ \bar{2}\ \ \bar{8}, & 2\ \ 4\ \ 8, & \bar{3}\ \ \bar{1}\ \ \bar{7}, & 7\ \ 5\ \ 1, & \bar{4}\ \ \bar{6}\ \ 0, \\
\mathrm{C}: 2\ \ 2\ \ 10, & \bar{1}\ \ \bar{1}\ \ \bar{9}, & 3\ \ 3\ \ 7, & \bar{2}\ \ \bar{2}\ \ \bar{6}, & 6\ \ 6\ \ 2, & \bar{5}\ \ \bar{5}\ \ \bar{1}, \\
\mathrm{C}: 1\ \ 3\ \ 9, & \bar{2}\ \ 0\ \ \bar{8}, & 4\ \ 2\ \ 8, & \bar{1}\ \ \bar{3}\ \ \bar{7}, & 5\ \ 7\ \ 1, & \bar{6}\ \ \bar{4}\ \ 0,
\end{array}$$

expressed in the scale of $k$, with $k\sqrt{3}=a$, the metric of the diamond network, for which a value in the neighbourhood of $1\frac{1}{2}$ Å may be taken. (This skeleton is the natural starting point since it is, in effect, the basic skeleton from which residues may be deleted and sites made available for residues functioning as substituents, as for example in the case of the 48-residue skeleton (Wrinch 1948).) The Fourier transform of $g$, the corresponding set of point atoms with ' weights ' 6 and 7 at these points, has been computed throughout three-dimensional space§ to provide an opportunity of studying, in a specific case, the manner in which the fine structure and the gross structure of a regular and coherent distribution in $S$, comprising many point atoms, manifest themselves in $S^*$.

---

† This work is supported by the Office of Naval Research, U.S. Navy.

‡ Communicated by the Author.

§ The writer is greatly indebted to Dr. W. J. Eckert and the International Business Machine Corp. for making available the facilities of the Watson Scientific Computing Laboratory, to Dr. L. H. Thomas for planning and to Dr. John Sheldon for carrying out the calculation of the three-dimensional Fourier transform for $x^*$, $y^*$ and $z^*$ in sixtieths, from which the sections in the figures are drawn.

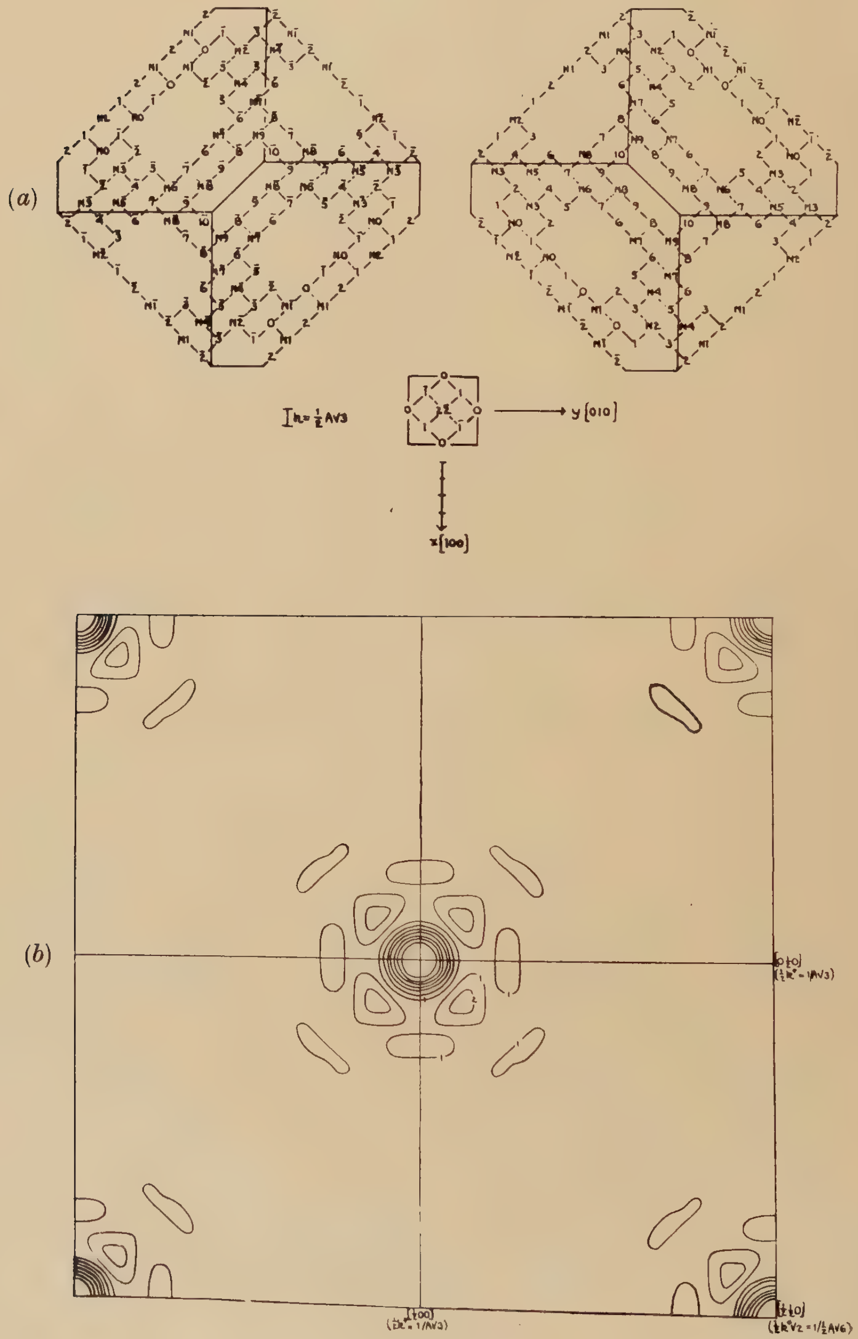

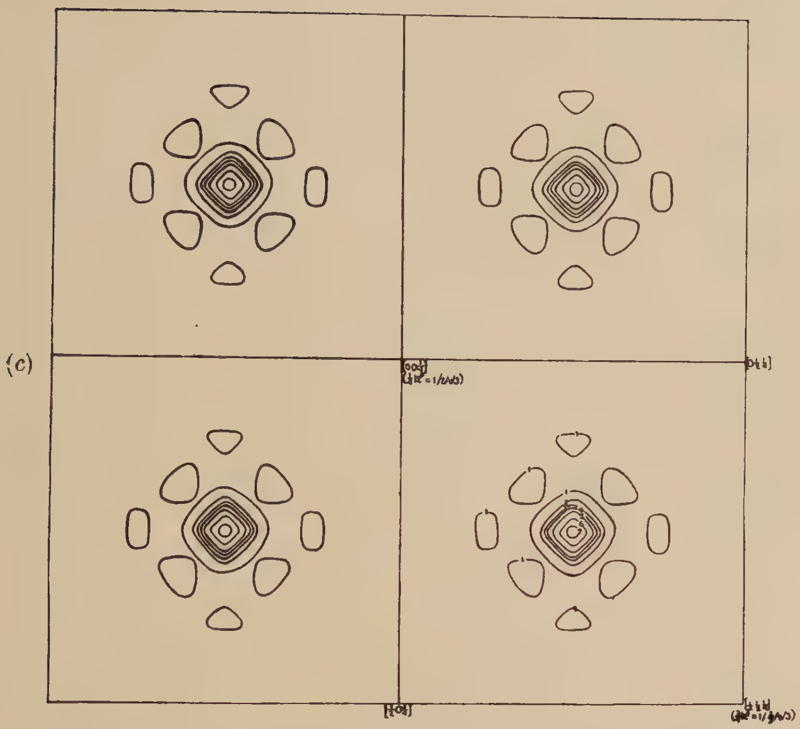

(*a*) The point set $g$, comprising 72 N, $C_\alpha$ and C point atoms, the nitrogens being marked N, on a diamond network $(000, \bar{1}\bar{1}\bar{1})$ in the scale of $k$ and its median polyhedron $[10\tfrac{1}{2}, 1\tfrac{1}{2}, 1\tfrac{1}{2}]$. Four unit cells of its body-centred cubic lattice are shown below, with a 'diamantane' fragment in position for comparison. The metric of the network is taken as $1\tfrac{1}{2}$ A, and $k$, in consequence, as $\tfrac{1}{2}\text{A}\sqrt{3}$. (*b*) The $z^*=0$ section and (*c*) the $z^*=1/4$ section of the periodic function $|G|$, where $G$ is the transform of the point set $g$ in which carbon and nitrogen atoms are given weights 6 and 7. The space group of $|G|$ is $T_h^3$: its cubic unit cell has an edge of length $k^*=1/k=1/\tfrac{1}{2}\text{A}\sqrt{3}$. Contours are drawn for $|G|G(000)=0{\cdot}1,\ 0{\cdot}2, \ldots 0{\cdot}7$. Major maxima at 1/4 1/4 1/4 etc., at which $|G|^2=\tfrac{1}{2}G^2(000)$, are seen in the $z^*=1/4$ section.

Of basic importance in all cases in which a set of point atoms is placed at nodes of a lattice is the fact that the resulting structure factor is periodic (Wrinch 1946), its lattice $L^*$ being reciprocal to the lattice $L$ in $S$. This fact is illustrated in the figures for this particular set of 216 point atoms, 144 of weight 6 and 72 of weight 7.

The coarsest lattice to nodes of which the $g$ points of symmetry $T$ and the $g_v$ points of symmetry $T_h$ (constituting the vector map of $g$) are confined is the body-centred cubic lattice $xyz=000$, 111, in the scale of $k$. It follows that $G=R+iJ$, the transform of $g$, and $|G|^2=R^2+J^2$, the transform of $g_v$, are periodic; their finest lattice is the face-centred cubic lattice $x^*y^*z^*=000$, $\tfrac{1}{2}\tfrac{1}{2}0$ in the scale of $k^*=1/k$. The figure depicts the $g$ set: it also depicts the sections $z^*=0$ and 1/4 of $|G|$, which is a periodic function with space group $T_h{}^3-Fm3$. We recognize, in the latter section, an indication of the fact that $g$ lies on a diamond network, with equal weights on both constituent *fcc* lattices (Wrinch 1950), namely, the existence of major maxima at 1/4 1/4 1/4 etc., points constituting a ($c$) set, the 8 point set of this space group, at which $|G|^2=\frac{1}{2}G^2(000)$.

There are many points of interest in the morphology of the Fourier transform of the $g$ set of weighted points over and above its lattice, its space group and its major maxima. A fuller study of the three-dimensional maps of $|G|$, and of $R$ and $J$, is in preparation.

## REFERENCES

WRINCH, D., 1937, *Nature, Lond.*, **139,** 972 and subsequent papers ; 1946, *Fourier Transforms and Structure Factors* (Monograph No. 2, of the American Soc. for X-ray and Electron Diffraction) ; 1948, *Science*, **107,** 445 ; 1950, *Acta Cryst.*, **3,** 76.

---

# *Quantum Hydrodynamics*

By R. EISENSCHITZ
Queen Mary College, University of London*

[Received April 25, 1952]

IRVING AND ZWANZIG (1951) applied quantal distribution functions in phase space for calculating hydrodynamical quantities. They suggest further development of the subject on the lines of Kirkwood's (1946) classical theory of transport processes. In the present note Kirkwood's theory is reconstructed in terms of quantum mechanics.

It is assumed that any function $g$ of the classical variables $\mathbf{p}$, $\mathbf{q}$ is represented by the function $G$ of the quantal operators $\mathbf{P}$, $\mathbf{Q}$ :

$$G(P, Q) = \int \gamma(\mathbf{r}, \mathbf{s}) \exp [i(\mathbf{r} \,.\, \mathbf{P} + \mathbf{s} \,.\, \mathbf{Q})] \, d\mathbf{r} \, d\mathbf{s}$$

where $\gamma(\mathbf{r}, \mathbf{s})$ is the Fourier inverse of $g(\mathbf{p}, \mathbf{q})$ (Weyl 1927). 'Probability distributions', $f(\mathbf{p}, \mathbf{q})$, are defined in such a way that the quantum-mechanical expectation for any $G$ is equal to the mean value of the corresponding $g$ as derived by means of the (not necessarily positive) $f(\mathbf{p}, \mathbf{q})$ (Wigner 1932, Moyal 1949). An important conclusion may be drawn. Let $G$ vary in time so that

$$G(t)=G_0+G_1t+G_2t^2+\ldots \qquad (1\,a)$$

This series is a term by term representation of the classical

$$g(t)=g_0+g_1t+g_2t^2+\ldots \qquad (1\,b)$$

If (1 $b$) complies with the classical equations of motion then (1 $a$) satisfies the corresponding quantal equations because the equations of motion are of equal form in both theories. In employing quantal distributions in phase space the variation in time of observables is accordingly derived from classical mechanics.

---

* Communicated by the Author.

The distribution function for a representative single molecule, $f^{(1)}(\mathbf{p}, \mathbf{q}, t)$, satisfies the equation

$$\begin{aligned} &\partial f^{(1)}/\partial t+\mathbf{p} \,.\, (\partial f^{(1)}/\partial \mathbf{q})/m \\ &\qquad =(4\pi/h) \int [\varTheta-(1/3!)\varTheta^3+(1/5!)\varTheta^5-+\dots]f^{(N)}\varPhi \, d\mathbf{p}^+ \, d\mathbf{q}^+ \qquad (2) \\ &\qquad \varTheta=(h/4\pi)(\partial/\partial \mathbf{p}) \,.\, (\delta/\delta \mathbf{q}) \end{aligned}$$

where $\mathbf{p}^+$, $\mathbf{q}^+$ are momenta and coordinates of all molecules except one, $f^{(N)}$ is the distribution function for all molecules, $\varPhi$ is the potential energy of molecular interaction; the symbols $\partial$, $\delta$, $\mathscr{D}$ mean differentiation of a distribution function, of a potential and of any function respectively.

Integrate eqn. (2) with respect to the time between the limits $-\tau$ and 0. Since $\delta\varPhi/\partial\mathbf{q}=-d\mathbf{p}/dt$ and time integration is carried out classically, the first term on the right-hand side gives $-f^{(1)}+\int f^{(N)}(p-\varDelta\mathbf{p})\, d\mathbf{p}^+ \, d\mathbf{q}^+$ where $\varDelta\mathbf{p}=-\int_{-\tau}^{0}(\delta\varPhi/\delta\mathbf{q})\, dt$. The higher terms can be integrated by means of the identity

$$(4\pi/h)\varTheta=(\mathscr{D}/\mathscr{D}\mathbf{q}) \,.\, (\partial/\partial\mathbf{p}) \quad - \quad (\partial/\partial\mathbf{q}) \,.\, (\partial/\partial\mathbf{p}).$$

The second term gives $(h/4\pi)^2\chi$ where

$$\begin{aligned} \chi=\int\{&[(\partial^2 f^{(N)}/\partial/\mathbf{p}^2) \,.\, (\partial^2 f^{(N)}/\partial\mathbf{p}^2)](d\varDelta\mathbf{p}/d\mathbf{q})^2 \\ &-(\partial^2 f^{(N)}/\partial\mathbf{p}^2) \,.\, [(\partial f^{(N)}/\partial\mathbf{p})(d^2\varDelta\mathbf{p}/d\mathbf{q}^2)]\}\, d\mathbf{p}^+ \, d\mathbf{q}^+. \quad . \quad . \quad (3) \end{aligned}$$

[Note that $(d\varDelta\mathbf{p}/d\mathbf{q})^2$ is a scalar and $(d^2\varDelta\mathbf{p}/d\mathbf{q}^2)$ is a vector.]

On assumptions similar to those made in the classical theory, in particular if the integrand in

$$\beta=(1/m\bar{k}T)\int_{-\tau}^{0} dt' \int_{-t'}^{0} \overline{[(\delta\varPhi(-t)/\delta\mathbf{q}) \,.\, (\delta\varPhi(O)/\delta\mathbf{q}]\, dt} \quad . \quad . \quad . \quad (4)$$

vanishes for $|t|\geqslant\tau$, a generalized Fokker–Planck equation is obtained

$$\begin{aligned} \partial f^{(1)}/\partial t+\mathbf{p} \,.\, (\partial f^{(1)}/\partial\mathbf{q})/m=\beta m\{&\mathscr{D}(\mathbf{p}f^{(1)})/\mathscr{D}\mathbf{p}+\mathscr{D}^2(kTf^{(1)})/\mathscr{D}\mathbf{p}^2\} \\ &+h^2\omega+(h/4\pi)^2\chi+\dots \quad . \quad . \quad . \quad . \quad . \quad . \quad . \quad (5) \end{aligned}$$

The last term is defined in (3); a term, denoted by $h^2\omega$, has been added in order to account for any contribution arising from the quantum correction in the equilibrium distribution.

The distribution function $f^{(2)}$ for a representative pair of molecules determines viscosity and thermal conductivity and should satisfy an equation similar to (5). The dissipative terms and condition (4) are modified as in the classical theory. On the left-hand side a series of terms is added

$$-(4\pi/h)[\varTheta-(1/3!)\varTheta^3+(1/5!)\varTheta^5-+\dots]f^{(2)}\phi_{12}$$

where $\varTheta$ is now defined in terms of the 6-component vectors $\mathbf{p}$ and $\mathbf{q}$ and $\phi_{12}$ is the potential energy of interaction of two molecules. The terms associated with higher odd derivatives of the distribution function are specific to quantum mechanics.

In deriving the distortion of the equilibrium distribution, part of the peculiar properties of quantum liquids may be obtained even if only the classical terms in (5) are taken into account. The non-classical terms are appreciable if the derivatives of the distribution function with respect to the momenta are sufficiently large ; those on the left-hand side may involve anomalous non-dissipative processes, those on the right-hand side do not lend themselves to any simple interpretation. Provided that the equilibrium distribution is known the quantum theory of transport processes does not seem to offer any difficulties other than the classical theory.

### REFERENCES

IRVING, J. H., and ZWANZIG, R. W., 1951, *J. Chem. Phys.*, **19,** 1173.
KIRKWOOD, J. G., 1946, *J. Chem. Phys.*, **14,** 180.
MOYAL, J. E., 1949, *Proc. Camb. Phil. Soc.*, **45,** 99.
WEYL, H., 1927, *Z. f. Physik*, **46,** 1.
WIGNER, E., 1932, *Phys. Rev.*, **40,** 794.

---

## *A Note on the Linearized Integral Equation of Green*

By H. I. SCOINS
King's College, Newcastle-upon-Tyne*

[Received May 14, 1952]

USING the super-position approximation together with an averaging process which introduces the parameter $\epsilon$, Green (1947) has established an approximation to the radial distribution function in a fluid of spherically symmetric molecules in the form

$$g(r)=\exp\left\{-\frac{\phi(r)}{kT}\right\}.[1+f(r)]$$

where

$$r[f(r)+\epsilon\alpha(r)]=\frac{1}{\sqrt{(2\pi)}}\int_{-\infty}^{+\infty}\frac{\epsilon u\beta(u)}{1-\sigma\beta(u)}\sin ru\,du \quad . \quad . \quad . \quad . \quad (1)$$

$$u\beta(u)=\frac{1}{\sqrt{(2\pi)}}\int_{-\infty}^{+\infty}r\alpha(r)\sin ru\,dr$$

and

$$\alpha(r)=\exp\left\{-\frac{\phi(r)}{kT}\right\}-1,\quad \sigma=\epsilon(2\pi)^{3/2}\rho.$$

The dependence of the distribution function on the density $\rho$ of the fluid only enters through the denominator of the integrand of (1), since $\epsilon$ is effectively independent of the density, as Rodriguez (1949) has shown.

The purpose of this note is to point out that Green's method of evaluating the integral (1) when the denominator has zeros on the real axis is incorrect, and that the correct solution to the linearized integral equation leads to an asymptotic form for the distribution function which may well be a characteristic of the liquid state.

---

* Communicated by Professor G. S. Rushbrooke.

Fig. 4

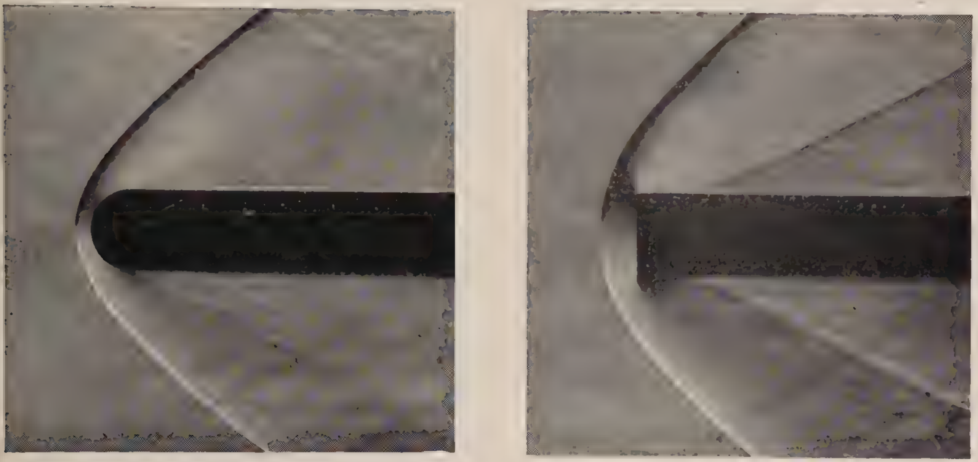

(a) (b)

Fig. 7

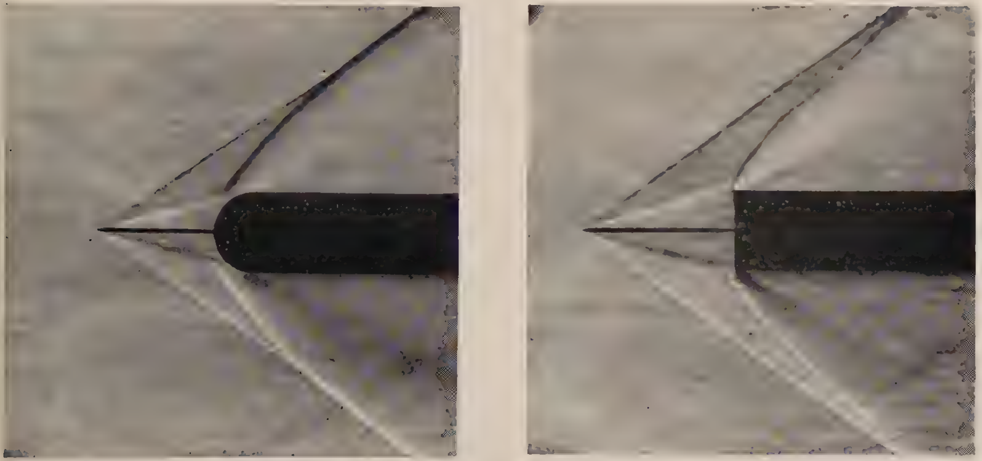

(a) (b)

Fig. 14

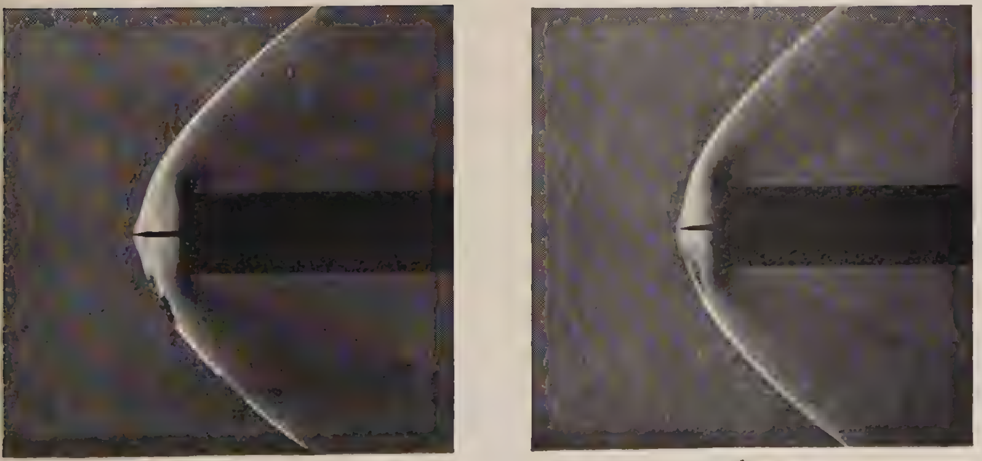

(a) (b)

Fig. 5

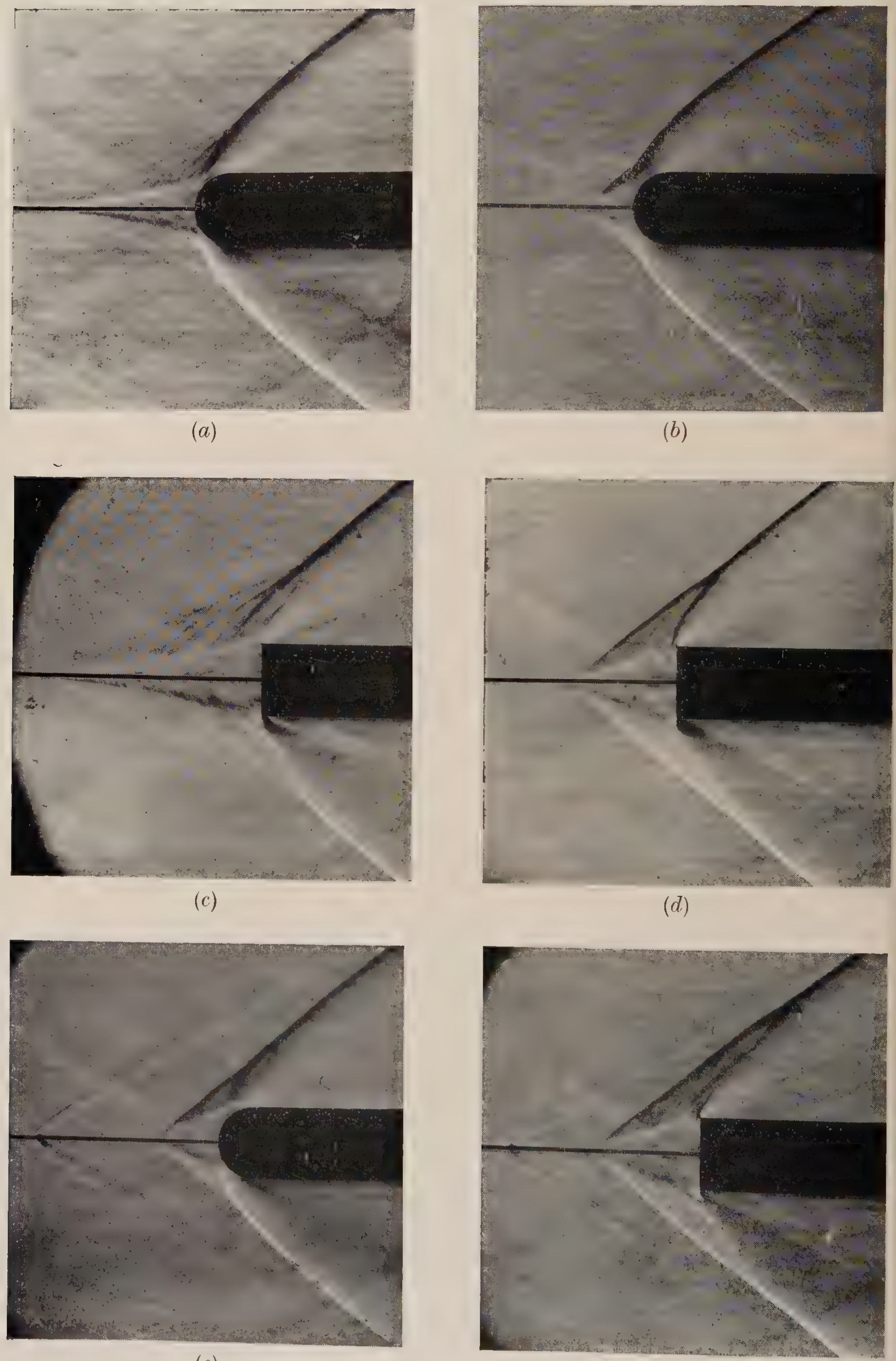

(a) (b)

(c) (d)

(e) (f)

Fig. 6

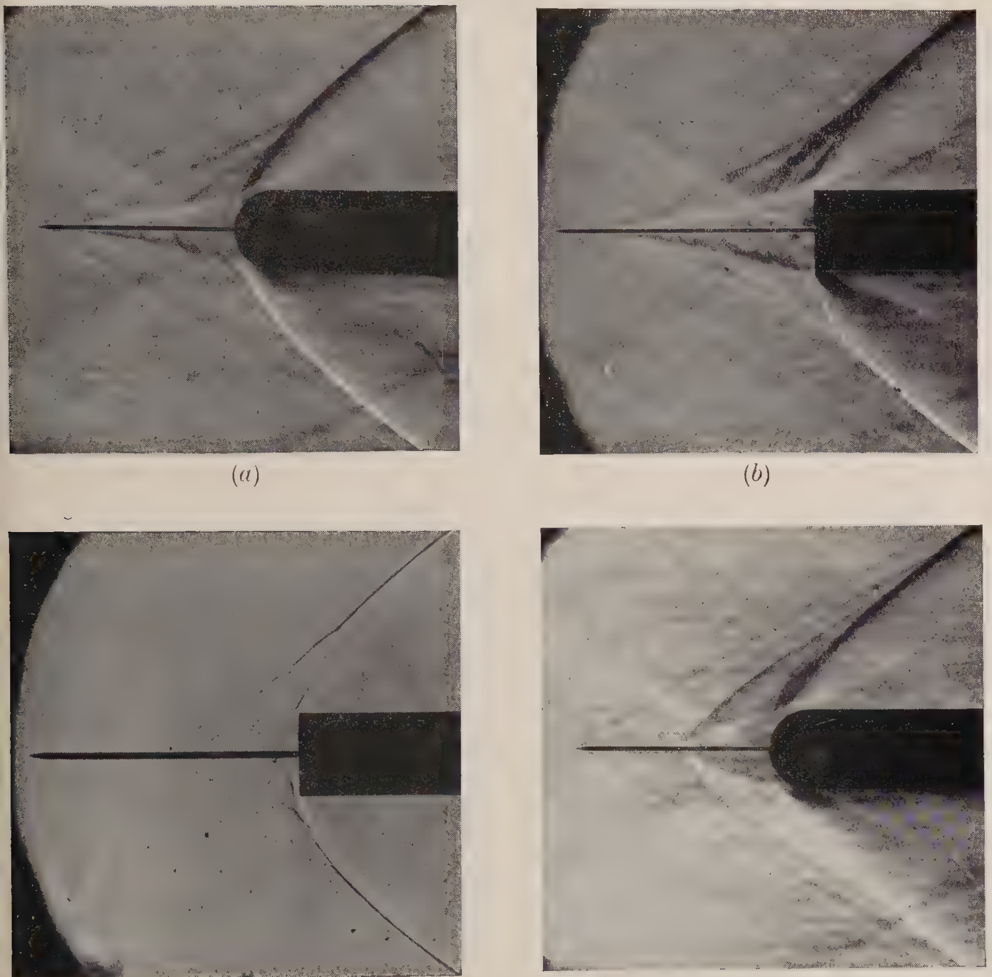

(a) (b)

(c) (d)

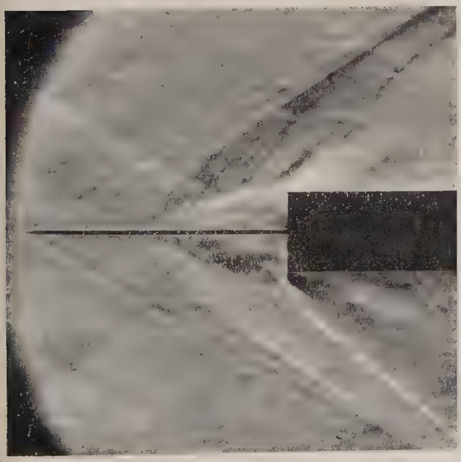

(e)

Fig. 8

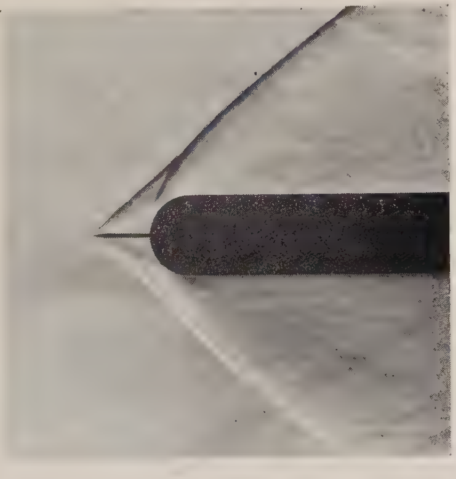

Fig. 12

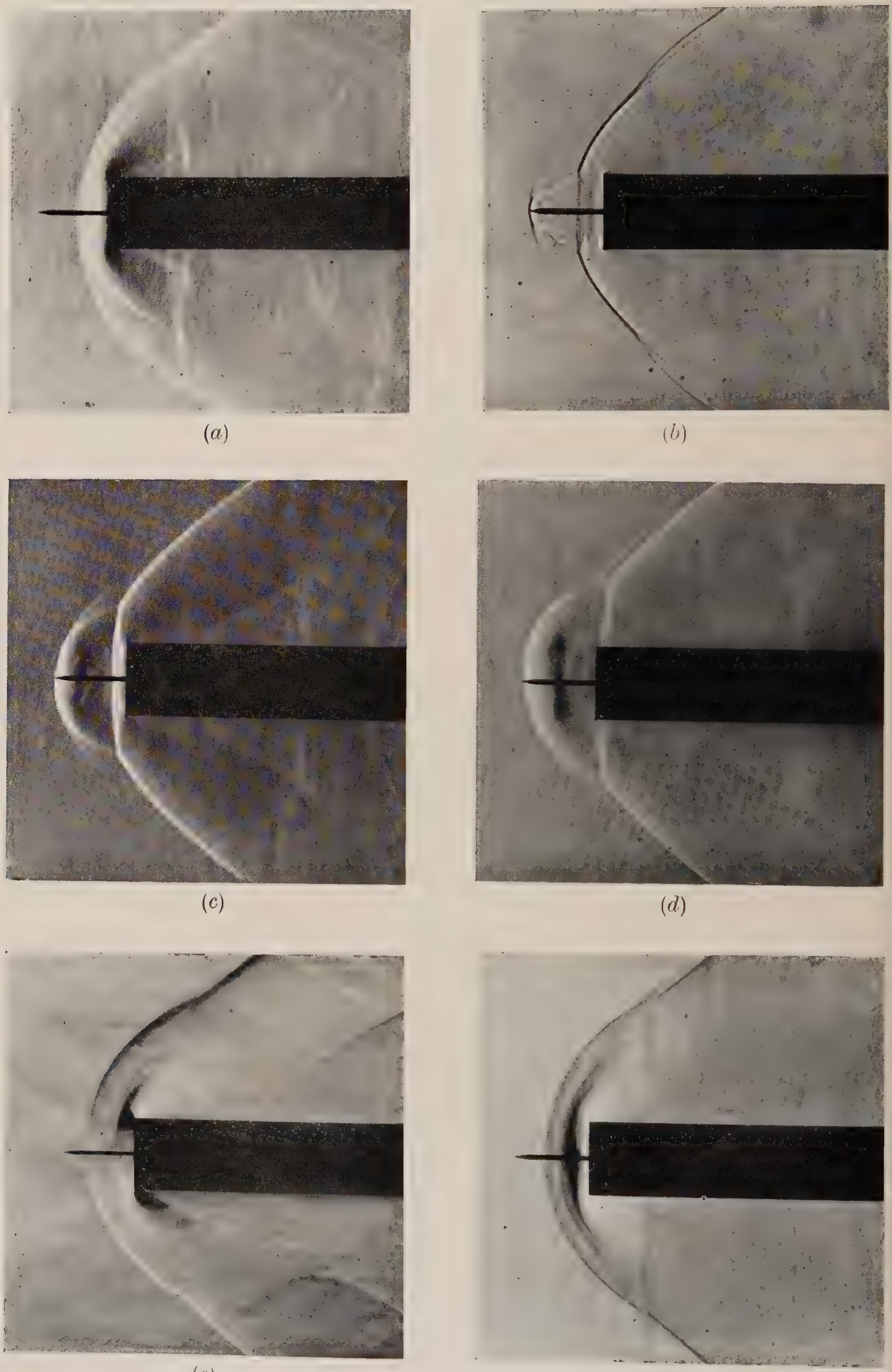

(a) (b)

(c) (d)

(e) (f)

Fig. 13

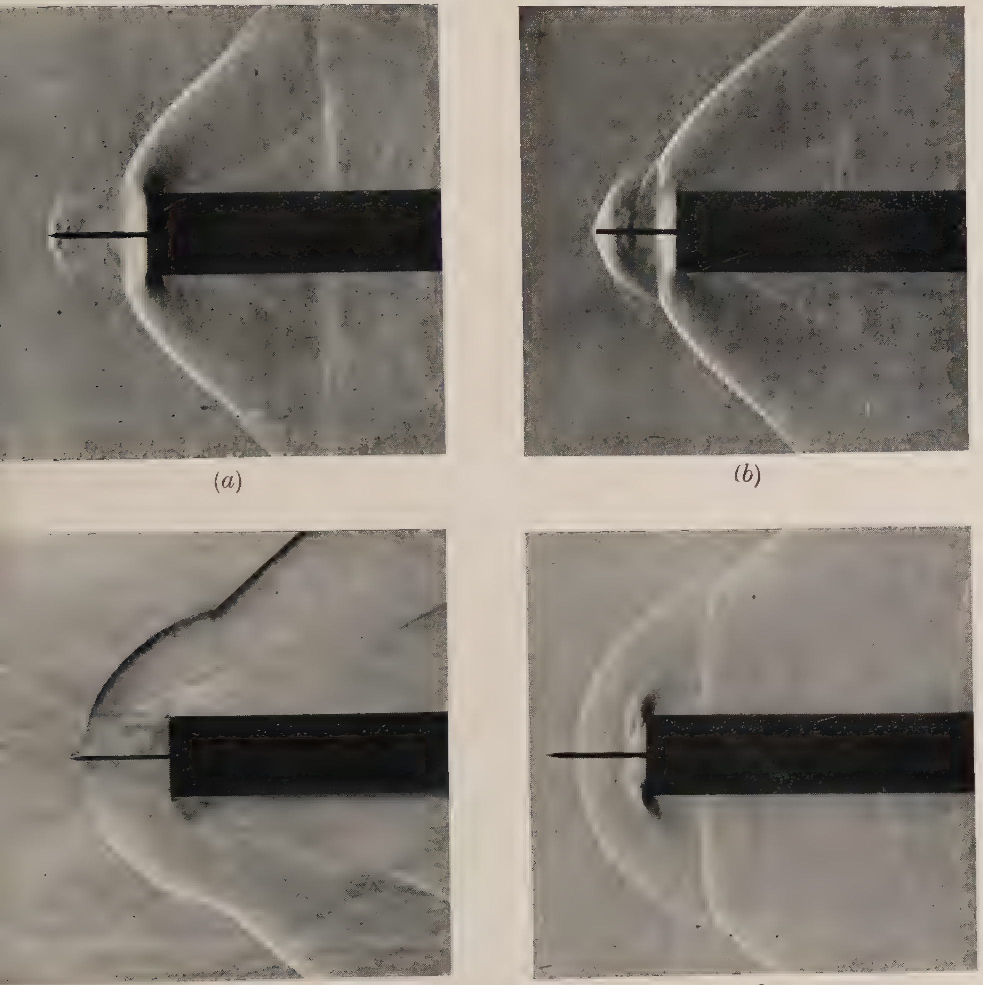

(*a*) (*b*)

(*c*) (*d*)

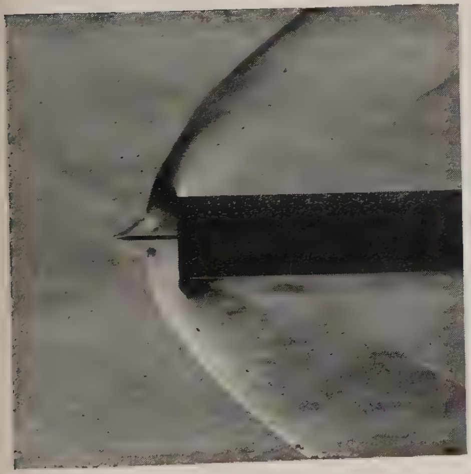

(*e*)

Fig. 11

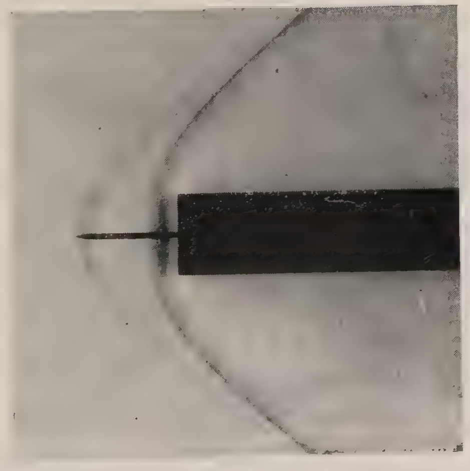

Fig. 15

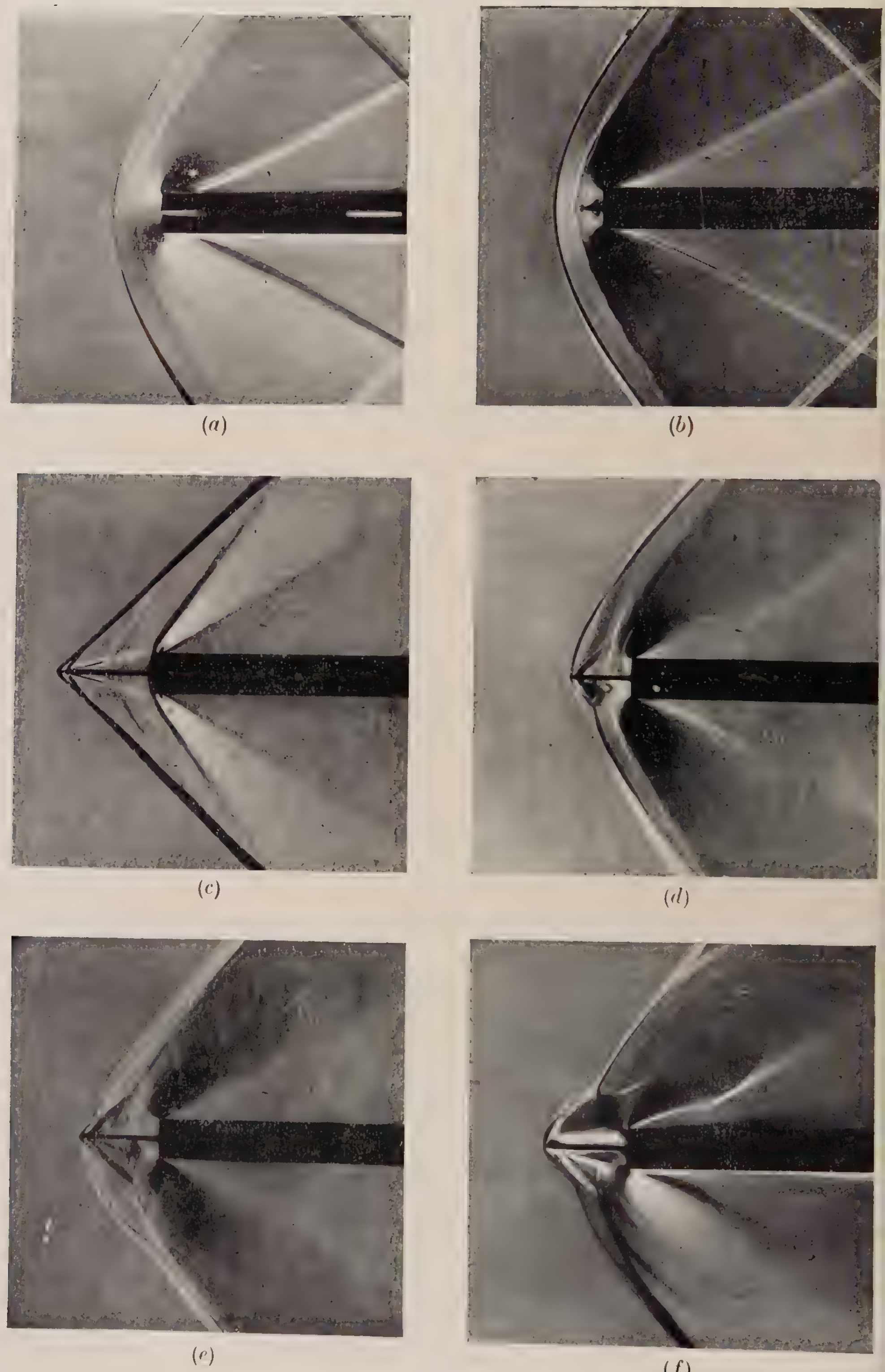

(a) (b)

(c) (d)

(e) (f)

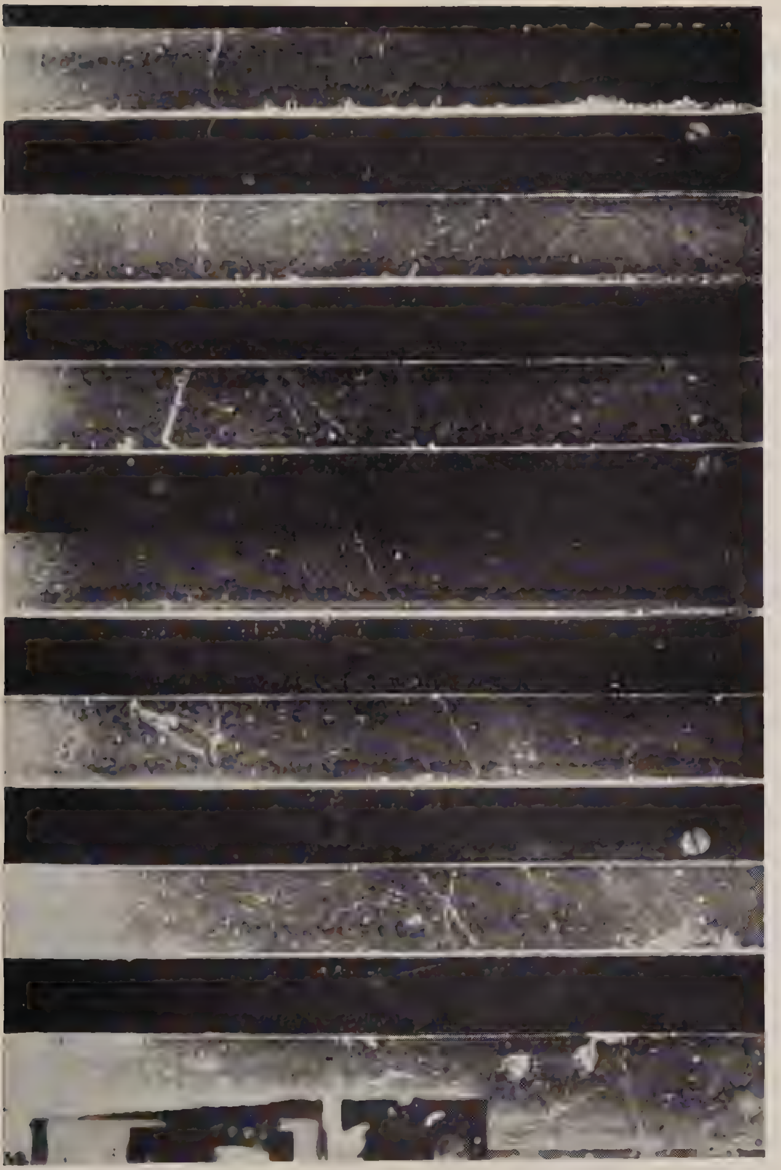

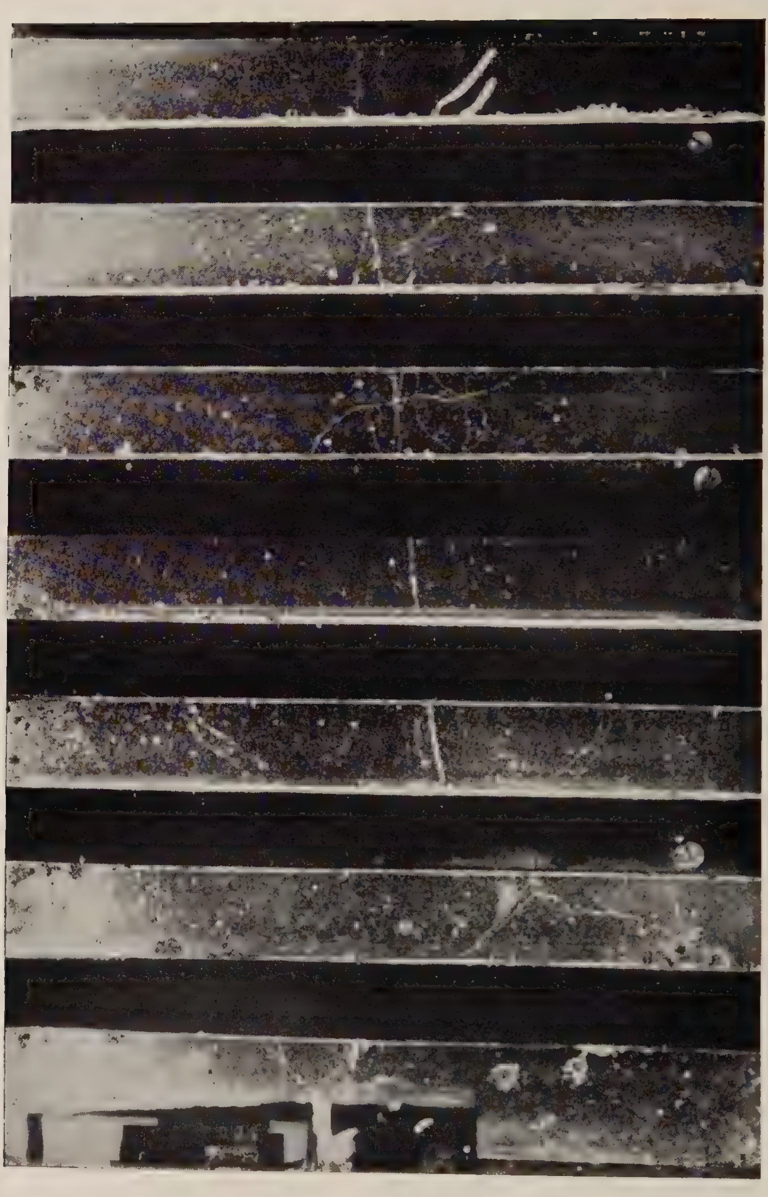

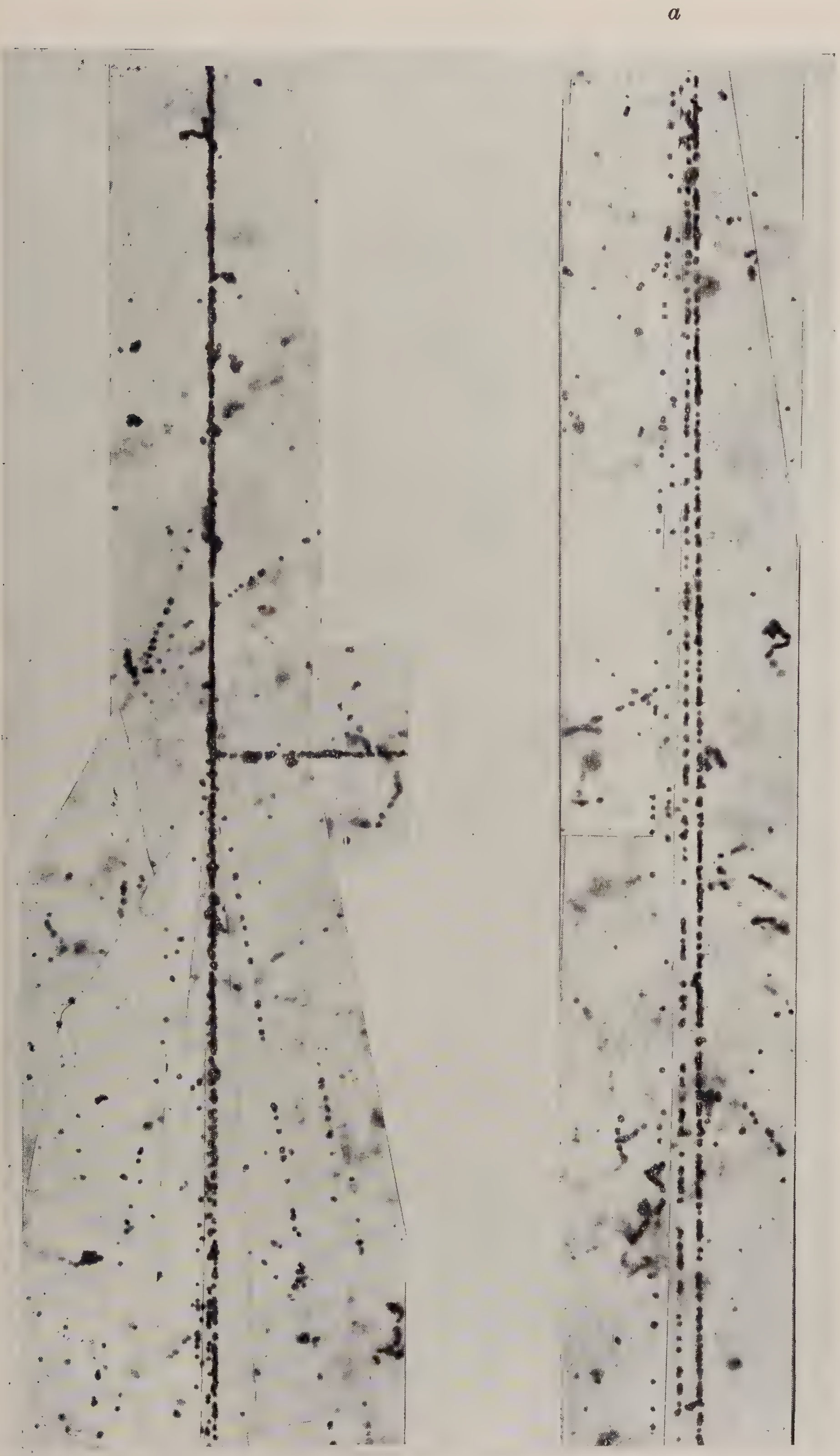
a

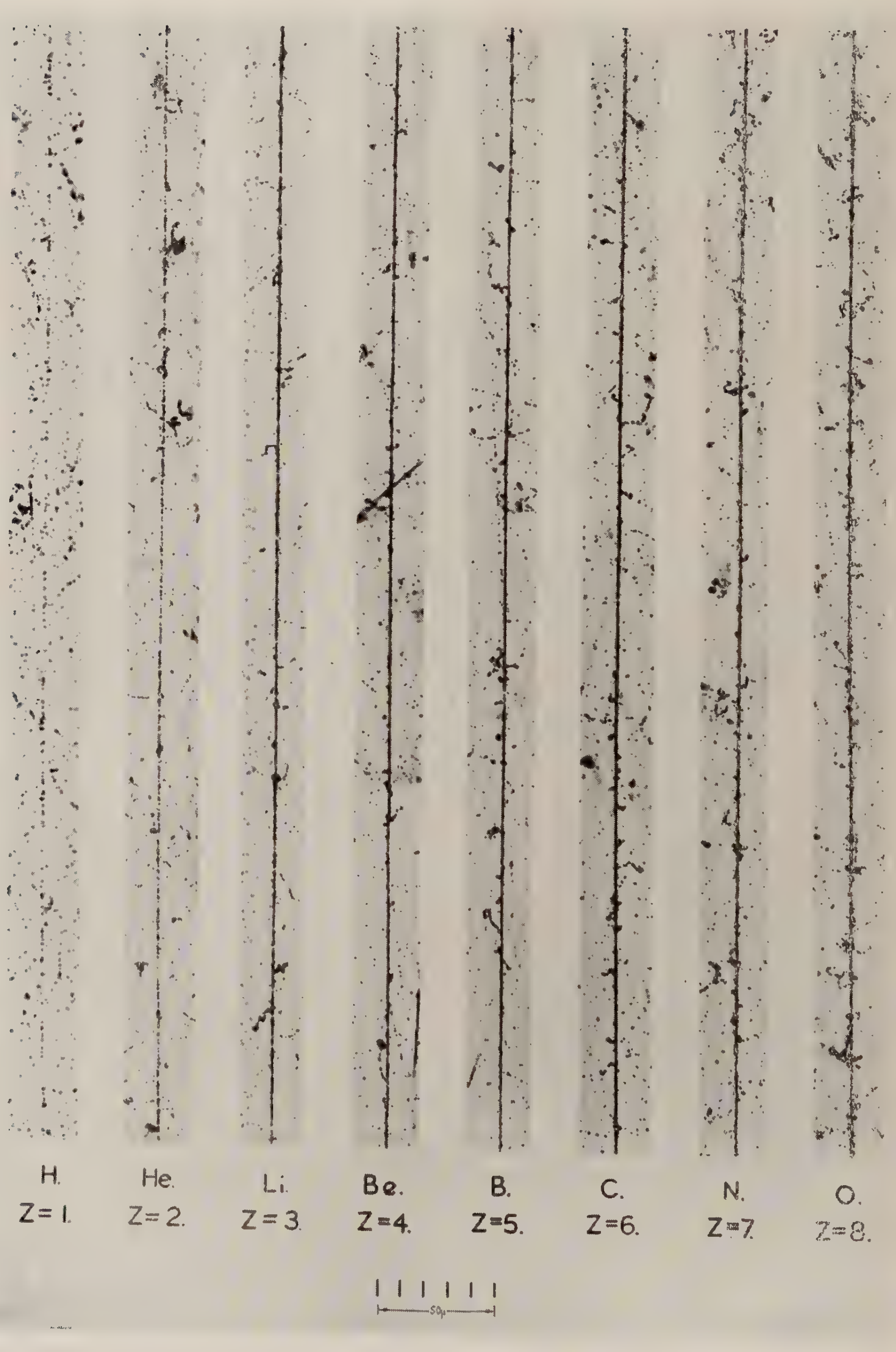
H.
Z = 1.
He.
Z = 2.
Li.
Z = 3.
Be.
Z = 4.
B.
Z = 5.
C.
Z = 6.
N.
Z = 7.
O.
Z = 8.
50μ

Ne.
Z=10.
Na.
Z=11.
Mg.
Z=12.
Si.
Z=14.
Ca.
Z=20.
Ti.
Z=22.
Fe.
Z=26.
50μ

*a*

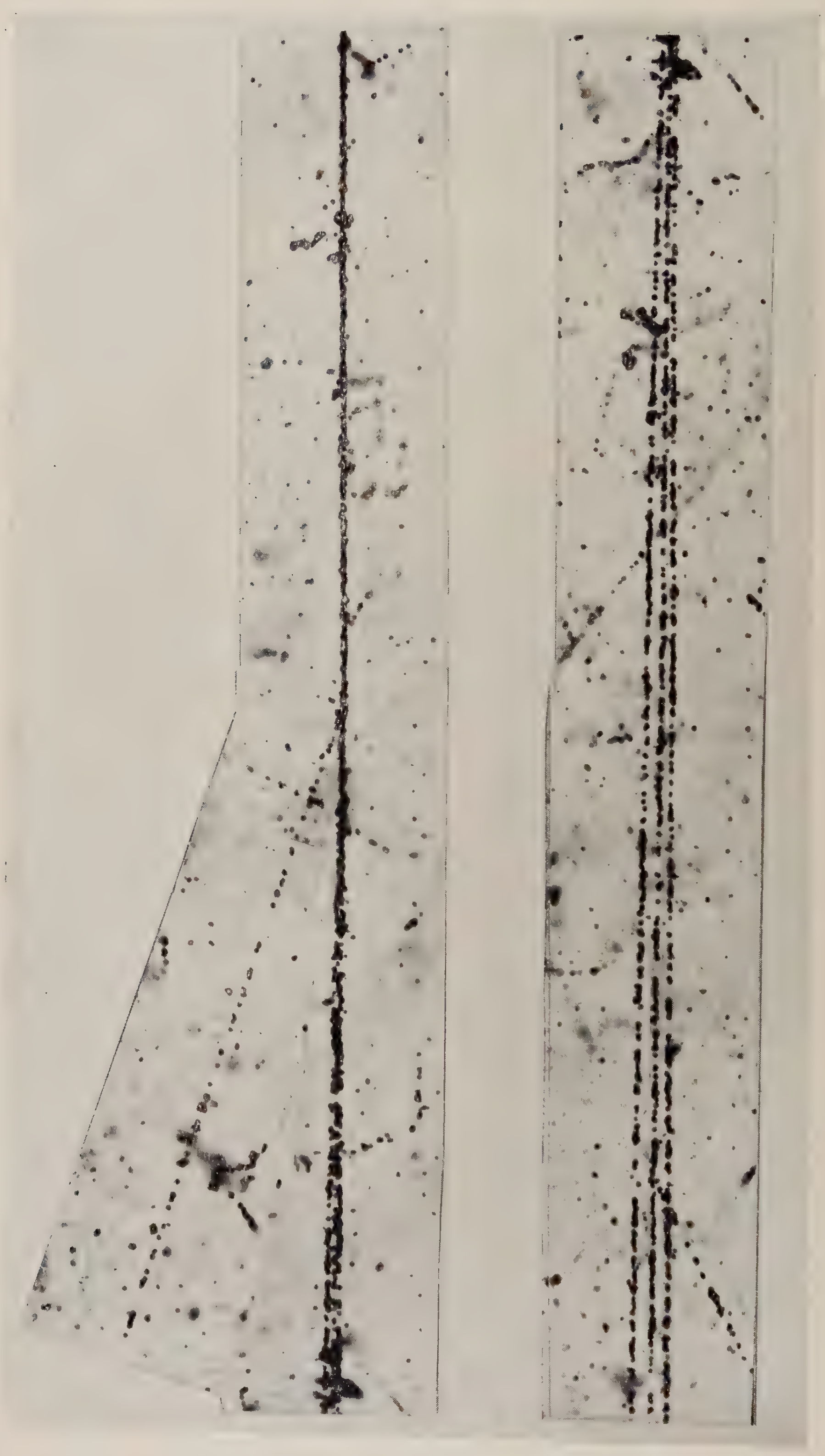

R. R. DANIEL *et al.* Phil. Mag. Ser. 7, Vol. 43, Pl. XLVIII.

$0+28p$
$E_p \sim 3000$ Bev

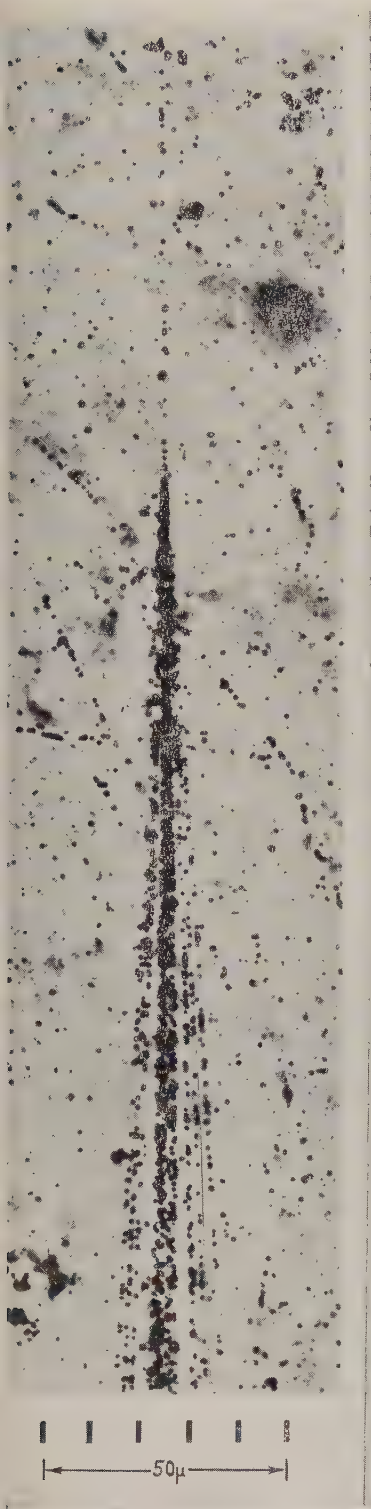

(a)

$1+9p$
$E_p \sim 1000$ Bev

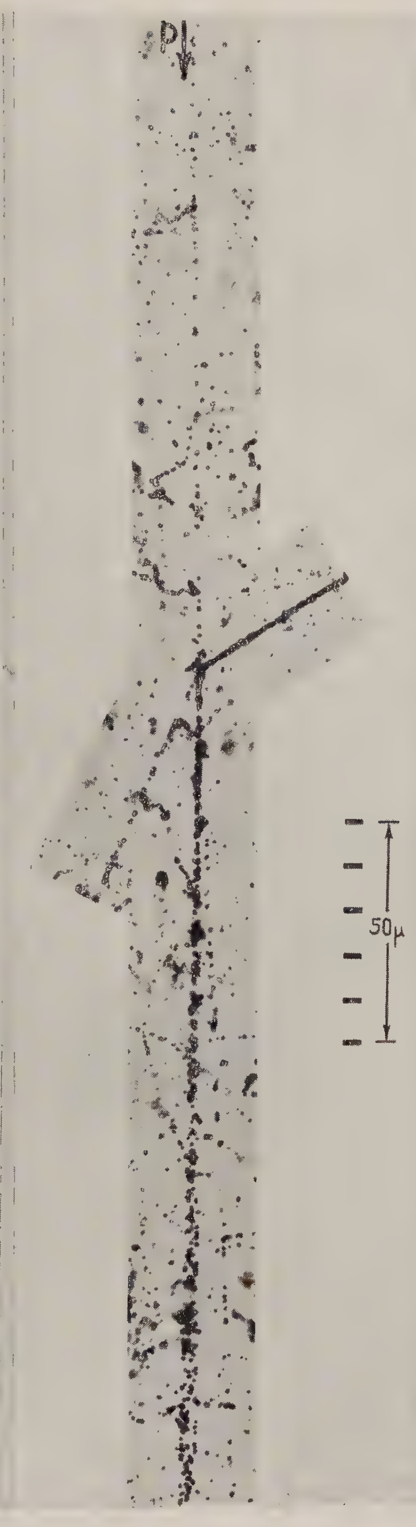

(b)

$0+4p$
$E_p \sim 2000$ Bev

$7+13p$

(c)

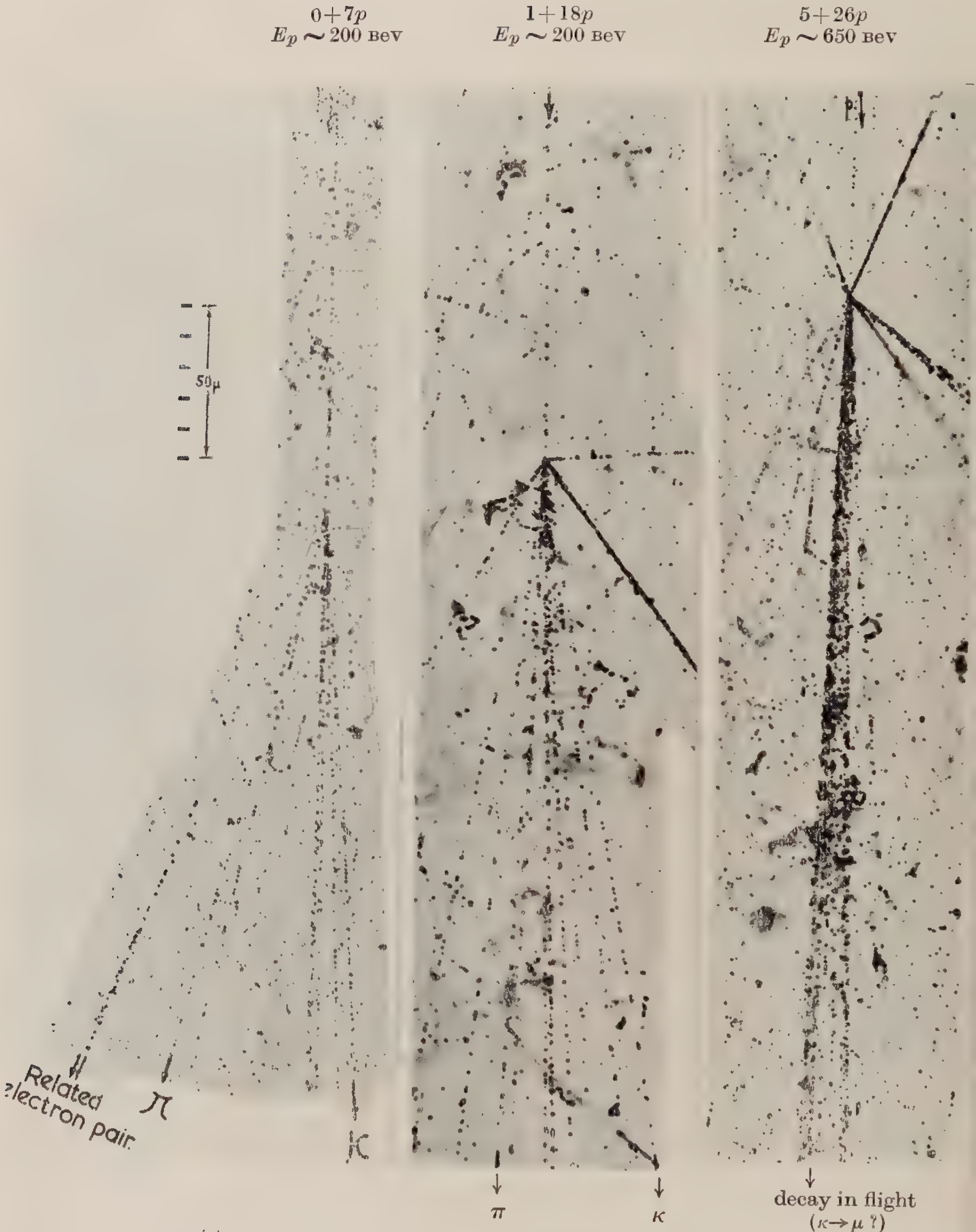

$0+7p$
$E_p \sim 200$ BeV

$1+18p$
$E_p \sim 200$ BeV

$5+26p$
$E_p \sim 650$ BeV

(*a*) (*b*) (*c*)

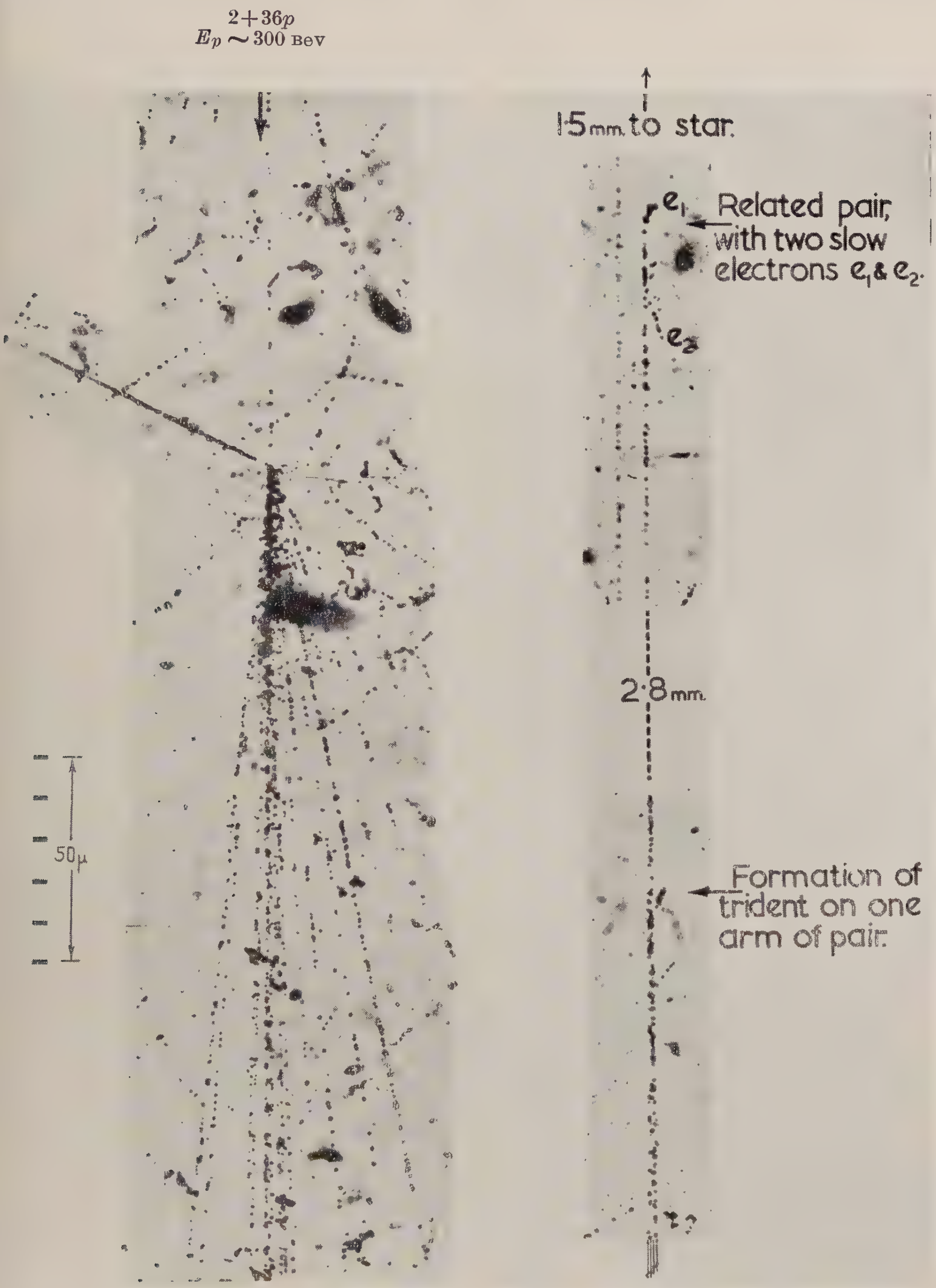
2+36p
E_p ~ 300 Bev
50μ
1·5 mm. to star.
e₁
Related pair, with two slow electrons e₁ & e₂.
e₂
2·8 mm.
Formation of trident on one arm of pair.

$3+36\alpha$
$E_p \sim 400$ BeV/nucleon

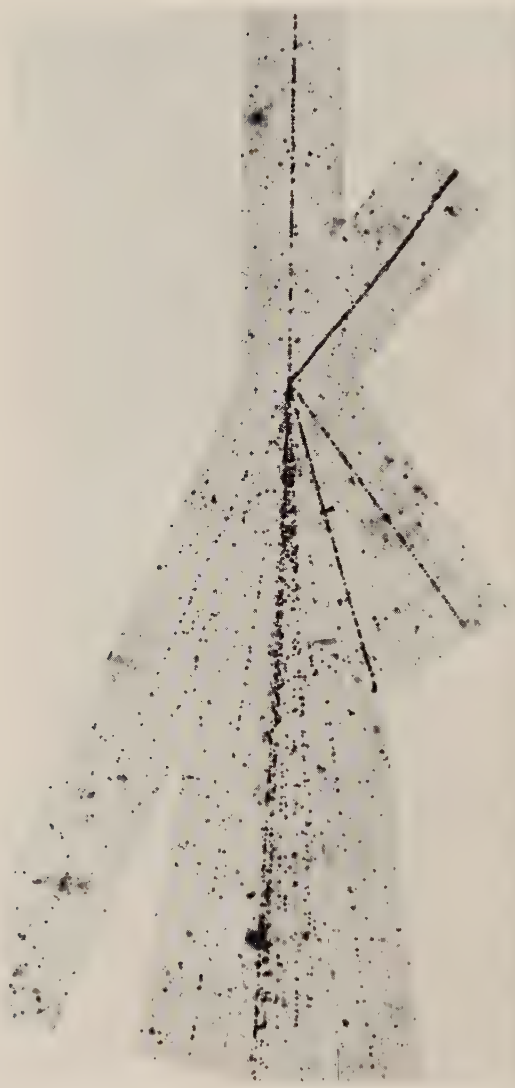

(*a*)

$4+50\alpha$
$E_p \sim 800$ BeV/nucleon

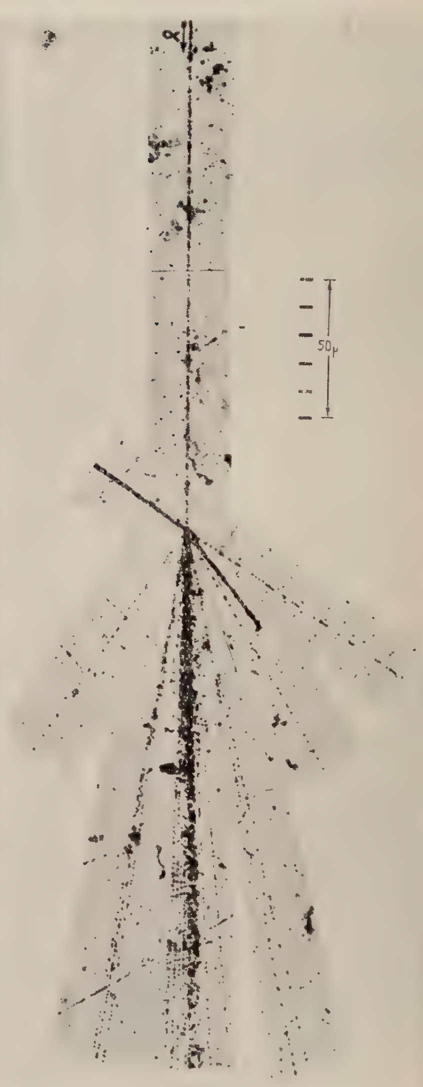

(*b*)

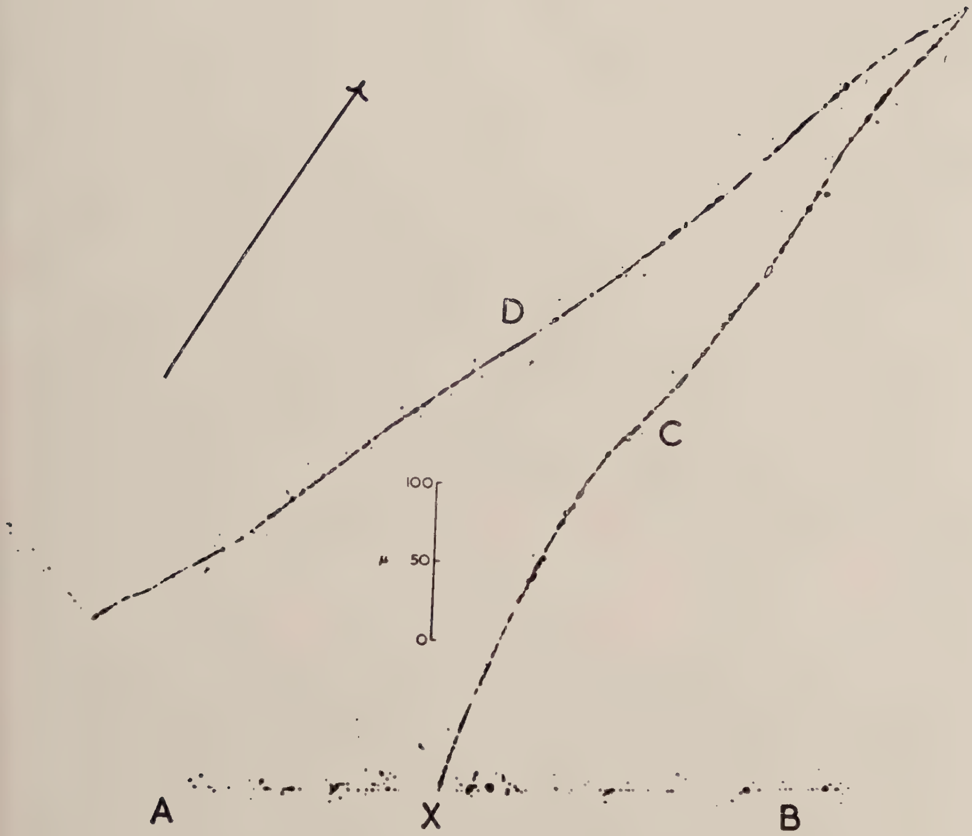

Example of multiple meson production with hydrogen as target nucleus (Observer, Mrs. J. Muirhead). The arrow points in the vertical direction from air to ground.

Fig. 1

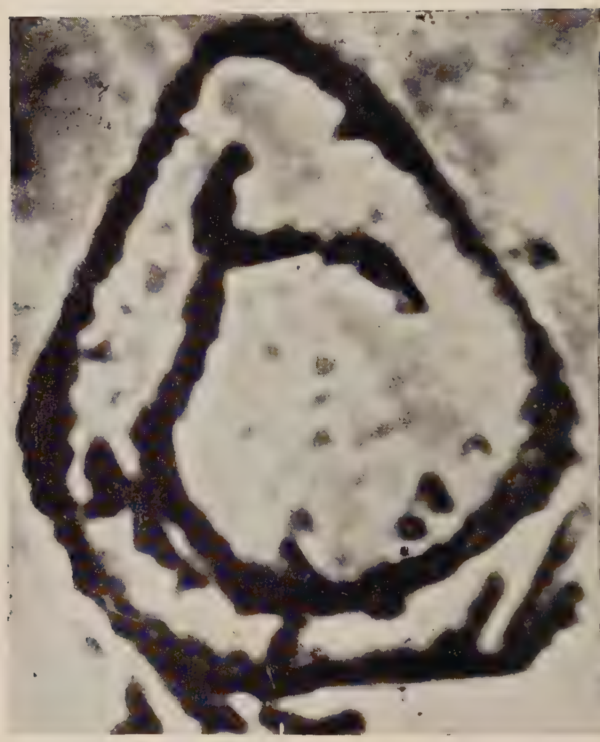

×5400

Fig. 2

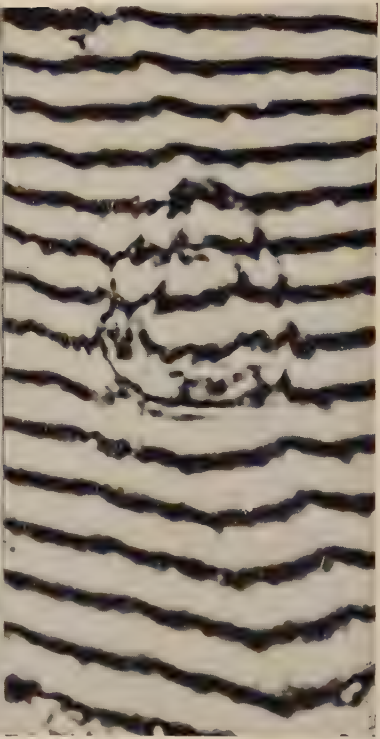

×1600

Fig. 3

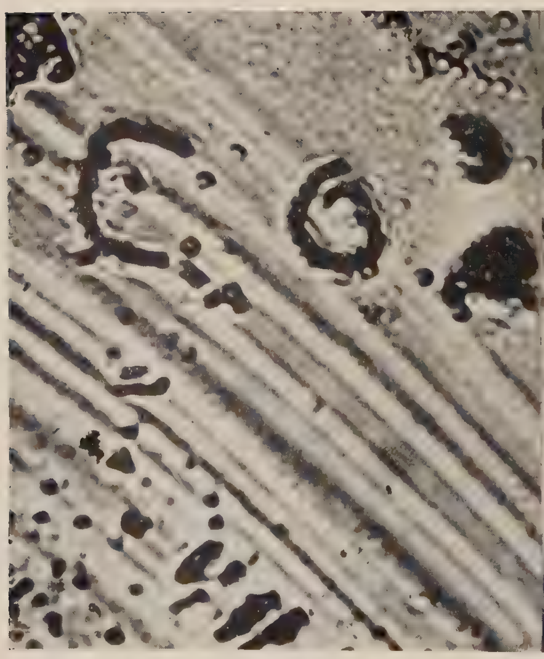

×1250

Fig. 4

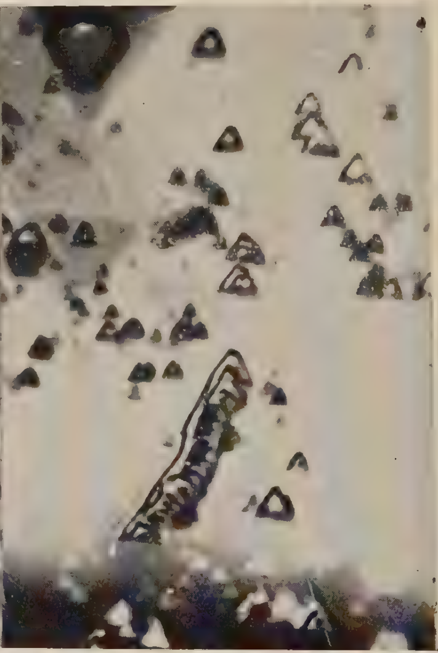

×1200

Suppose that the temperature of the fluid is well below the Boyle inversion temperature. Then for values of $\rho$ which satisfy $1+2\epsilon B\rho<0$, where $B$ is the second virial coefficient, the denominator of the integrand has at least two real zeros. Let these zeros be at $u=\pm u_0$ and let the zeros of $1-\sigma\beta(u)$ in the upper half-plane be at $u=u_s$.

It is convenient to take the contour of integration along the real axis and above the singularities at $u=\pm u_0$. To evaluate the integral it must be split into two parts :

$$\frac{\epsilon}{2\iota\sqrt{(2\pi)}}\left[\int_{-\infty}^{+\infty}\frac{u\beta(u)}{1-\sigma\beta(u)}\exp(\iota ru)\,du-\int_{-\infty}^{+\infty}\frac{u\beta(u)}{1-\sigma\beta(u)}\exp(-\iota ru)\,du\right].$$

If $r>0$ and $|u\beta(u)|\to 0$ uniformly as $|u|\to\infty$, then the first of these two contour integrals may be evaluated by closing the contour by a semicircle in the upper half-plane, and the second by a semicircle in the lower half-plane. The integrals cannot both be evaluated by means of the same closed contour since $\sin ru$ is not uniformly bounded in either the upper or the lower half-plane. Using the residue theorem, it can be readily established that a solution of the linearized integral equation is

$$rf(r)=-\epsilon r\,.\,\alpha(r)-\frac{\epsilon\sqrt{(2\pi)}}{\sigma^2}\left[\frac{u_0}{\beta'(u_0)}\cos ru_0+\sum_s\frac{u_s}{\beta'(u_s)}\exp(\iota ru_s)\right], \qquad (2)$$

where the only assumption is that $\beta(u)=\beta(-u)$. The expression is real since the zeros of $1-\sigma\beta(u)$ must occur in conjugate pairs.

This expression is a solution of the linearized integral equation,

$$rf(r)=2\pi\rho\int_0^{\infty}\int_{-s}^{+s}(t+r)[f(t+r)+\epsilon\alpha(t+r)]dt\,.\,\epsilon s\alpha(s)\,ds \quad . \quad . \quad . \quad (3)$$

and any other solution may be obtained from it by the addition of terms of the form $A\sin ru_s$. Since the complex roots give rise to terms which are not bounded, the only arbitrariness in the solution lies in the possible addition of a term $A\sin ru_0$.

The solution (2) may be compared with the expression given by Green which excludes the term in $\cos ru_0$. This extra term must be included if the integral equation is to be satisfied, and it implies that the asymptotic behaviour of the radial distribution function is of the form

$$g(r)\sim 1-\frac{\epsilon\sqrt{(2\pi)}}{\sigma^2}\,\frac{u_0}{\beta'(u_0)}\,\frac{\cos ru_0}{r}$$

which does not satisfy Green's boundary condition

$$g(r)-1=0\{r^{-(3+\delta)}\}.$$

Such behaviour is not, however, physically impossible. It implies that on average the number of molecules in a spherical shell of radius $r$ and thickness $dr$ with a given molecule at the centre is given by

$$\rho 4\pi r^2\,dr\left(1-\frac{\epsilon\sqrt{(2\pi)}}{\sigma^2}\,\frac{u_0}{\beta'(u_0)}\,\frac{\cos ru_0}{r}\right)$$

when $r$ is large.

Now the oscillatory term represents the number of molecules in the shell in excess of the macroscopic average, and although this excess does not tend to zero for large $r$, the relative excess does become negligible, and it is only this which has a physical significance.

It is therefore suggested that the existence of a slowly decaying wave is a characteristic of the radial distribution function in the liquid state. If this is correct, then it follows that the x-ray scattering intensity, which is closely related to the radial distribution function, becomes infinite at a certain small angle. This is not impossible for the effect would be completely masked by the un-scattered beam of x-rays.

This suggestion is not contradicted by the work of Fournet (1949, 1951) who has used the solution of Green in considering the scattered x-rays. However, the extra term, which Fournet introduces into the intensity when discussing the x-rays scattered by a liquid phase, must be discarded if the integral eqn. (3) is to be satisfied, and the same expression for the intensity must be used in both the liquid and gaseous phases, the difference in the intensities being accounted for by the difference in densities.

### REFERENCES

FOURNET, G., 1949, *Comptes Rendus*, **228,** 1801 ; 1951, *Acta Cryst.*, **4,** 293.
GREEN, H. S., 1947, *Proc. Roy. Soc.* A, **189,** 103.
RODRIGUEZ, A. E., 1949, *Proc. Roy. Soc.* A, **196,** 73.

---

## *Etch Spirals on a Diamond Octahedron Face*

By S. TOLANSKY and M. OMAR
Royal Holloway College, Englefield Green*

[Received May 15, 1952]

IT has long been known that etch pits appear on the octahedron faces of diamonds when treated at high temperature (900° C) with potassium nitrate and sodium carbonate (e.g. Fersmann and Goldschmidt 1911, Williams 1932). Since it was anticipated that the onset of etching might well be seen at an earlier stage by using interferometry, experiments have been carried out on the etching of diamonds at a much lower temperature and this brief note reports preliminary observations obtained at 525° C.

In conformity with early observations large numbers of very small oriented triangular etch pits have been observed but, in addition, features have appeared of some considerable interest in connection with the recent theories of crystallographic growth by the mechanism of spiral dislocations. From the considerable mass of data obtained the following are typical.

---

* Communicated by the Authors.

It has been found that the onset of etching in many cases takes on a spiral form, sometimes simple, sometimes complex. These spirals are rarely more than one turn. Figure 1 (figs. 1–4, Plate LIII) is a typical case. We show this here with a good deal of empty magnification (×5 400 on the original, before reproduction) in order to make clearer the fact that the spiral consists of a chain of triangular etch pits, and furthermore the spiral does not close up although it branches as it progresses. The central first turn is distinctly hexagonal. Figure 2 (×1 600) is an interference picture taken by means of a thin film technique especially developed for the purpose of enabling interferometry at high magnifications to be conducted. This is obtained at the expense of fringe width which, although not comparable to that obtainable by the best multiple beam methods, yet suffices to give useful information. It is seen, for example, that the fringes kink on passing over the arms of the spiral and measurement reveals that the approximate depth is some 700 Å and is, moreover, reasonably uniform in both arms.

Figure 3 (×1 250) shows another typical spiral with a complete turn and one with an incomplete turn. It should be noted that the spirals vary in character. Some form an outline which is oriented and in the characteristic triangle shape associated with the ultimate familiar etch pits, others appear which are more nearly circular, and still others in which the outline approximates to a hexagonal character. Such indeed is partially noticeable in figs. 1 and 3.

In all cases the spirals appear to consist of chains of contiguous small triangular etch pits all oriented in the same direction. These appear occasionally in roughly straight-line chain form as shown in fig. 4 at ×1 200 which reveals more clearly the nature of the contiguous chains which in some cases ultimately become spirals.

Figure 4, it should be noted, is an interference picture taken by a thin film interference technique, specially designed to heighten contrast and with this technique details which are a small fraction of a light wave in depth can be revealed with high contrast. This thin film technique employs white light interference and involves very sensitive colour changes.

It may be noted that *no* growth spirals were detected on the diamond before etching, although sought for by interference methods. It is possible that these etch spirals in fact have developed on what were originally invisible growth spirals but we have no evidence to substantiate this. The point at issue is that in any case the anticipated height of a diamond growth spiral, if present, would probably be too small to be detectable by interferometry.

The density of these etch spirals per unit of area is relatively quite low on the surfaces etched at 525° C.

## REFERENCES

FERSMANN, A. v., and GOLDSCHMIDT, V., 1911, *Der Diamant*, Heidelberg.
WILLIAMS, A. F., 1932, *The Genesis of Diamond*, London.

# LXXVII. *Notices of New Books and Periodicals received*

*Atomic Physics.* By MAX BORN. Fifth Edition. (Blackie and Son.) Price 35*s*.

PROFESSOR BORN'S *Atomic Physics* has been of value to honours students and others for some years ; while the text has given a clear and readable introduction to the subject, the appendices have shown how many of the more important formulae are derived.

The fifth edition contains many additions, including a chapter on nuclear physics, and a section on the density of the electron cloud and Thomas-Fermi model of the atom. The book has been brought up to date in both content and detail, and the new edition is therefore most welcome. W. M. G.

*Heat and Thermodynamics.* By M. W. ZERMANSKY. An intermediate textbook for students of Physics, Chemistry and Engineering. Third Edition. (McGraw Hill Publishing Company Ltd., London, 1951.) [Pp.465.] Price 42*s*. 6*d*.

THIS British reissue of the third edition (1951) of this well-known textbook will be welcomed by both students and teachers of thermodynamics. It will be sufficient to mention a few of its advantages : equally careful treatment of both foundations and many applications, stressing the range of applicability of thermodynamics ; inclusion of numerous numerical data, examples and diagrams, all of them using the most recent data available ; treatment of modern methods of measuring thermodynamic quantities, and of producing low temperatures. The third edition has been considerably extended, some of the main changes being the insertion of numerous new figures and problems, and of a chapter of 45 pages on the physics of very low temperatures, which gives a very readable account of the thermodynamics of supraconductors and of liquid and solid helium.

In a further edition, which certainly will become necessary, the concept of a phase transition of the second order could be made more intelligible to the reader by treating a simple model of such a transition (for instance, the vaporization of a given mass of liquid in a constant volume) and by showing that at least one ' internal parameter ' with a *limited* range of variation must exist. A. S.

*Experimental Spectroscopy.* By R. A. SAWYER. [Pp. 358.] Second Edition. (Chapman and Hall Ltd.) Price 30*s*. net.

IN this new edition the chapters on Apparatus and Methods of Infrared Spectroscopy, The Spectroscopy of the Vacuum Ultraviolet, and Spectrochemical Analysis have been extensively revised. The text generally has been brought up to date and references are given to recent work. This excellent book can be recommended to all interested in the subject. L. J. G.

---

[*The Editors do not hold themselves responsible for the views expressed by their correspondents.*]